THE UNIVERSITY OF CHICAGO

TOWARD A DEEPER UNDERSTANDING AND APPRECIATION OF
STRESS-INDUCED BIOMOLECULAR CONDENSATION

A DISSERTATION SUBMITTED TO
THE FACULTY OF THE DIVISION OF THE BIOLOGICAL SCIENCES
AND THE PRITZKER SCHOOL OF MEDICINE
IN CANDIDACY FOR THE DEGREE OF
DOCTOR OF PHILOSOPHY

GRADUATE PROGRAM IN BIOCHEMISTRY AND MOLECULAR BIOPHYSICS

BY
CAITLIN JOY WONG HICKERNELL

CHICAGO, ILLINOIS
AUGUST 2024

To Mom, Dad, and John. To the struggling and doubting versions of myself, past and future. Soli Deo Gloria.

He also asked, "What else is the Kingdom of God like? It is like the yeast a woman used in making bread. Even though she put only a little yeast in three measures of flour, it permeated every part of the dough." Luke 13:20-21 (NLT)

TABLE OF CONTENTS

LIST OF FIGURES

LIST OF TABLES

ACKNOWLEDGMENTS

I have many people to thank for supporting me in this graduate school journey.

- Firstly, thank you to Allan for being a great advisor. I have grown immensely as a scholar and a scientist through your investment in me, and I do not like to consider alternate timelines where I ended up elsewhere. Thank you for holding me to the highest standards while simultaneously mentoring with utmost patience and always cheering me on when I hit, as you call them, "the valleys of death". I will always have a version of you in my head telling me to check my dashes.

- Thank you to my thesis committee members: Drs. David Pincus, Mike Rust, and Joe Picirilli. I am grateful for the useful advice, helpful feedback, and consistent support I received in all my meetings with you.

Next, thank you to the whole Drummond Lab! Every iteration of lab members has been an influential part of my science journey. Listed in order of appearance: Chris Katanski, Cat Triandafillou, Haneul Yoo, Sammy Keyport Kik, Jared Bard, Hendrik Glauninger, Kyle Lin, Dana Christopher, Joshua Melamed, Leah Chaney, Estefania Cuevas-Zepeda, and Karen Velez. It has been an honor and privilege to do science together.

Some special acknowledgements:

- Haneul, thank you for being a great role model to me and a major reason why I joined the Drummond Lab. I want to be like you when I grow up!

- Sammy, thank you for always encouraging me to ask hard questions, planning the parties with me, and setting the standard of work-life balance. I think fondly on the past versions of ourselves that trauma bonded as we tried to figure out grad school, and I'm really proud of us.

A thanks and shout out to Hendrik and Jared, my collaborators and co-laborers: I am so grateful to have worked two of the best experimentalists and sharpest brains I know.

- Hendrik, thank you for always bringing the highest quality scientific discourse followed by the most absurd comic relief. I have thought more deeply and laughed more often because of you.

- Jared, thank you for being a great experimental mentor. You gave me so many of your hours: training me on techniques, talking through experimental plans, troubleshooting, answering my questions...I cannot repay them, so I will try to pay them forward. I know you are already a great PI.

- Kyle, thank you for being the best desk neighbor, coffee co-conspirator, sounding board, and supportive friend. I am very grateful for your positivity, listening ear, and way with memes. Without you, the lows would have been so much lower. Thanks for keeping the plants alive.

- To Dana and Josh, the future is truly yours. Thanks for keeping the lab young and fun.

- To Leah, Stef, and Karen, it's been fun fighting dragons with you.

I'm thankful that my years as a grad student have equally been filled with friends and family, who also deserve acknowledgement!

- Thank you to my dear friends: Andrew, Phillip, Caleb, Maggie, Emily, Kevin, Stephanie, Rachel, Sonia, Tiffany, Andy, Nathaniel, Christine, Krystle, Dayna, Lucy, Grace, Joyce, Rachel, Zoe, Christine. Grad school can be isolating, so I am overwhelmingly thankful for how you are all in my life and I in yours. You filled these years with good meals, deep conversations, movie nights, game nights, karaoke nights, video calls,

road trips, weddings, baby showers, and so much more. Thanks for checking in on me, cheering me on, and giving me something to look forward to every weekend. Sorry you probably didn't really know what I was working on this whole time, but thanks for asking anyway.

- Thank you to my GCF small group: Brian, Carolyn, Ahn, Andrew, Adam, Phillip, Ellen, Maggie, Lyndon, Caroline, Jeremiah, Thao, Trevor, Madeline, Michaela, Guillermo, Alec, Marie, Mercy, Nathaniel. I am most thankful for your consistency, but the lively conversations, prayer, and fun weeks are a plus.

- Thank you, Phillip, for answering all my stat and coding questions. You asked for a shout-out in my dissertation and so you received.

- Thank you, Andrew, for listening to so many of my early presentations and being so willing to talk about "my stuff" all the time. Your patience, nonjudgmental help, and sad coffee chats got me through the early years of grad school. My imposter syndrome would have been off the rails without you.

Finally, thank you to my family, my greatest supporters:

- Mom, Dad, Matthew, Jeremy, Auntie Elaine, Uncle Fred, Christine: Your unwavering love and support have been a constant source of strength for me throughout the past six years. Thank you for buying me meals, listening to my complaints, offering prayers, and just letting me be myself and not think about work when I was with you. I am deeply appreciative of all that you have given me during this time, and it's hard to express how much your support has fueled my work.

- To Mom and Dad, thank you for telling me you are proud of me, in so many ways, but especially in words.

- Finally, thank you, John. This space cannot contain all my love and gratitude for you. The PhD contained in this dissertation is the result of days when I'd walk out of GCIS and return home to you, sometimes on top of the world, sometimes exhausted or stressed about experiments. Thank you for always being there to receive me as I am, whether I needed to be cheered on or comforted. Thank you for the pep talks, thank you for sharing my joy and sadness, thank you for the boba and the laughter. I know this is my thing, but I wouldn't have finished it without you. You are the best partner in this journey, and I'm excited for more adventures together.

ABSTRACT

When cells experience stress, they undergo a number of dramatic intracellular molecular changes. One of these changes is the formation of biomolecular condensates, or clusters of mRNA and proteins. When these clusters are visible by microscopy, they are called "stress granules." Although these condensates have been observed for many years across many species, many questions remain. What exactly is the composition of a stress granule? What is the mechanism of formation? What, if any, is the function of stress granules? Are they an adaptive response by the cell? The field has not coalesced around answers to these fundamental questions, compelling further study.

This dissertation covers a review of stress granules, summarizing previous work and outlining the grand challenges in this area. Additionally, it includes a project on the stress-induced condensation of mRNA. During stress in yeast, we observed global, length-independent condensation of mRNA that seems to be regulated by a block in translation initiation. We also observed that stress-induced transcripts are excluded from condensates, driven by the timing of transcription. Finally, our data suggest the existence of small, sub-microscopic condensates that are not visible by standard microscopy. We propose a model where stress-induced mRNA condensation allows the cell to prioritize translation during stress, sequestering away old transcripts so the cell can focus on a stress-specific translational program. Lastly, this work includes a study on whether the stress-induced condensation behavior of poly-A binding protein 1 (Pab1) regulates the translation of stress transcripts during recovery from stress. We did not find data to support this model, leaving Pab1's adaptive condensation behavior as an open question.

As a whole, this work comments broadly on stress granules and specifically on how condensation does and does not contribute to the stress response in yeast. It also points toward future challenges and goals, such as a deeper understanding of the mechanism of

mRNA condensation and its precise adaptive role during stress.

CHAPTER 1

INTRODUCTION

Life does not always happen optimally; sometimes it is stressful. This is as true for humans as it is for the cells that make up human bodies and for single-celled organisms such as budding yeast, with whom we share some distant but common ancestor. That humans and yeast have survived so many years on the evolutionary tree implies not only the ability to thrive in hospitable environments, but also the ability to endure a range of inevitably inhospitable environments. For a cell with a dream of becoming two cells (Francois Jacob), the inability to physically leave an inhospitable environment requires some internal method of responding and adapting to stress.

Our ancestral cells were likely exposed to primordial stresses such as heat shock, starvation, osmotic stress, salt, and oxidative stress, leading to the development of a "stress response". This stress response describes a series of dramatic intracellular molecular changes that are strikingly different from the 'normal' state of an unstressed cell. Taking the model of yeast during heat shock, in contexts where budding yeast cells would grow rapidly, stressed cells do not grow and divide. Instead, there is a specific activation of heat shock genes, resulting in the transcriptional induction of a distinct set of genes [Ritossa, 1962]. Furthermore, translation, which typically occurs rapidly and robustly, is globally attenuated, except for the selective translation of stress genes [Storti et al., 1980, Lindquist, 1981]. Perhaps most intriguingly, proteins and mRNAs cluster together, forming large clumps that are not present during unstressed conditions [Kedersha et al., 1999, Storti et al., 1980].

Some of these molecular changes make intuitive sense, such as the induction of specialized stress transcripts. The formation of mRNA and protein clusters is much more mysterious. These clusters were historically interpreted as signs of cell damage, indicating the dysregulation of essential cellular processes. However, as outside observers of the process, it is difficult

to distinguish exactly what is happening in cells during stress. Are the responses indicative of downstream damage or are they an adaptive response to stress?

For example, consider the difference between sunburn and sweat. Both are downstream effects of sun exposure on a hot day. However, sweat represents an adaptive response: It helps to cool the body so it can better endure the heat. Although it deviates from the normal homeostasis of the body, sweat is ultimately beneficial rather than harmful. In contrast, sunburn is an example of damage resulting from stress. Sunburn is not beneficial and should be avoided due to its painful short-term and long-term consequences.

Historically, these clusters, or biomolecular condensates, have been thought to be more similar to sunburn. But what if biomolecular condensates are more like sweat, and are actually helping a cell survive and endure stress? Previous work in the Drummond lab has challenged the idea of biomolecular condensation as a deleterious response. Protein condensation was found to be reversible (efficiently by molecular chaperones) adaptive, and conserved [Wallace et al., 2015, Yoo et al., 2022, Riback et al., 2017, Keyport Kik et al., 2023].

Furthermore, the significance of these clusters has traditionally been assumed as a result of their appearance under a microscope. They are prominent, large, and brightly visible when fluorescently labeled. However, while these striking and large foci catch our eyes, does a cell 'see' them in the same way? It is entirely possible that adaptive responses could originate from small clusters of macromolecules, too small to be discerned by conventional microscopy. Visibility under a microscope may not be the phenotype selected for by evolutionary pressure.

The work described in the following pages contributes to the understanding of biomolecular condensation as an adaptive response orchestrated by cells. The majority focuses on how mRNA condenses during stress and its implications for cell survival during stress. Additionally, I describe a project that was attempting to definitively show a mechanism by which stress-induced condensation was helpful to cells. However, while the project did not yield

the anticipated results (the initial model was disproven without a counter-model to replace it), these findings can still enrich our understanding of biomolecular condensation, offering valuable insights into cellular adaptation under challenging conditions.

To conclude this introduction, stress-induced biomolecular condensation sits at a fascinating intersection, blending fundamental stress biology, newer concepts of biomolecular condensation, and evolutionary perspectives. While many fundamental molecular observations in cell stress were made in earlier, historic studies, the study of biomolecular condensation introduces new perspectives on the organization and localization of macromolecules within cells, providing new frameworks for understanding fundamental biological questions. Additionally, environmental cell stress reminds us that the external influences the internal, and that life is shaped and formed and changed by where it takes place.

CHAPTER 2

STRESSFUL STEPS: PROGRESS AND CHALLENGES IN UNDERSTANDING STRESS-INDUCED MRNA CONDENSATION AND ACCUMULATION IN STRESS GRANULES

This chapter has been adapted from Hendrik Glauninger, Caitlin J Wong Hickernell, Jared AM Bard, and D Allan Drummond. Molecular Cell, 2022.

2.1 Abstract

Stress-induced condensation of mRNA and protein into massive cytosolic clusters is conserved across eukaryotes. Known as stress granules when visible by imaging, these structures remarkably have no broadly accepted biological function, mechanism of formation or dispersal, or even molecular composition. As part of a larger surge of interest in biomolecular condensation, studies of stress granules and related RNA/protein condensates have increasingly probed the biochemical underpinnings of condensation. Here, we review open questions and recent advances, including the stages from initial condensate formation to accumulation in mature stress granules, mechanisms by which stress-induced condensates form and dissolve, and surprising twists in understanding the RNA components of stress granules and their role in condensation. We outline grand challenges in understanding stress-induced RNA condensation, centering on the unique and substantial barriers in the molecular study of cellular structures, such as stress granules, for which no biological function has been firmly established.
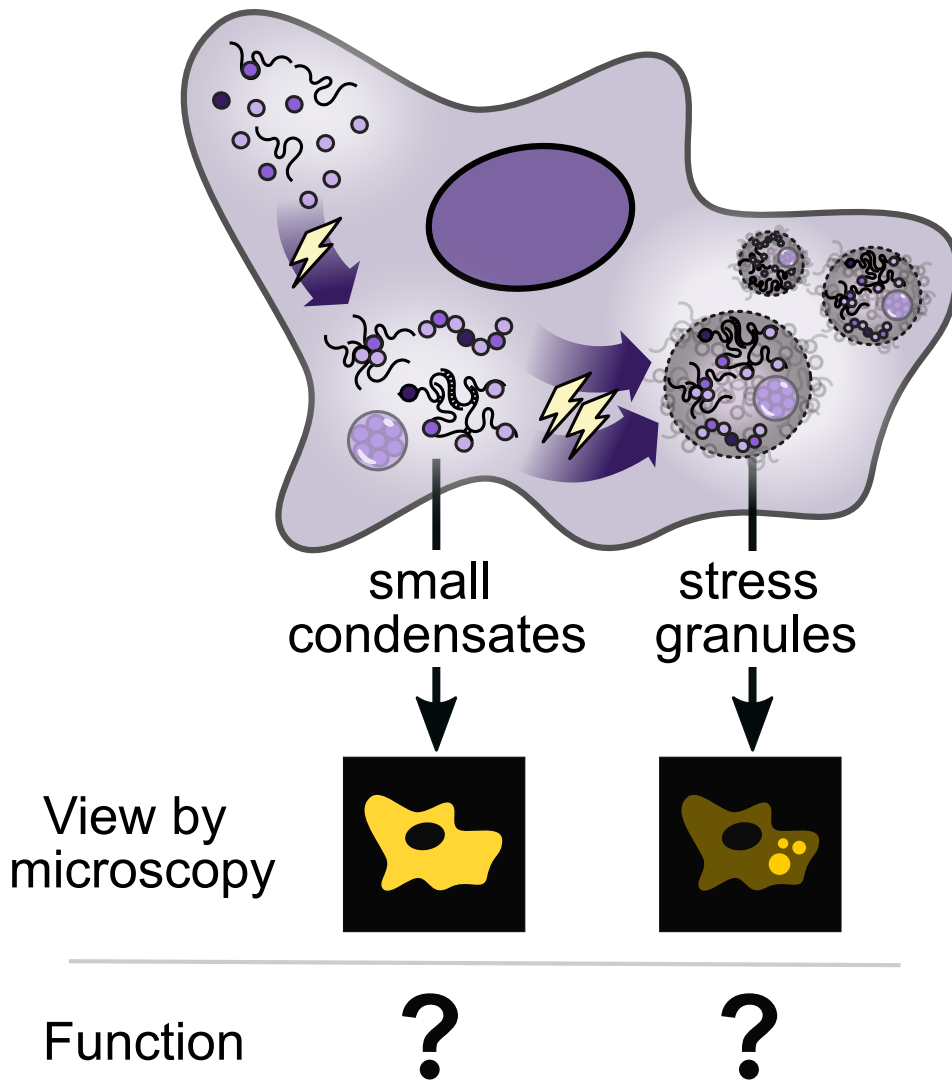
Figure 2.1: What is the function of stress-induced condensation?

2.2 Introduction

From humans and other vertebrates to single-celled yeasts, from plants to protozoa, the onset of primordial stresses such as heat shock, oxidizing agents, hypoxia, and starvation is rapidly followed by the intracellular condensation and accumulation of myriad proteins and mRNAs in cytosolic clusters [Cherkasov et al., 2013, Decker and Parker, 2012, Farny et al., 2009, Jain et al., 2016, Kedersha et al., 2000, 1999, Kramer et al., 2008, Nover et al., 1989, Wallace et al., 2015]. These enigmatic structures, called stress granules (SGs) when they grow large enough to resolve by microscopy, have become standard examples of so-called membraneless organelles alongside nucleoli, processing (P) bodies, paraspeckles, and others [Alberti and Carra, 2018, Boeynaems et al., 2018, Brangwynne, 2013, Gomes and Shorter, 2019, Guo and Shorter, 2015, Lyon et al., 2020, Mitrea and Kriwacki, 2016]. SGs and their condensed molecular precursors have become a nexus of extraordinary recent activity because of the involvement of protein and RNA liquid-liquid phase separation (LLPS) in their formation [Guillén-Boixet et al., 2020, Molliex et al., 2015, Riback et al., 2017, Sanders et al., 2020, Van Treeck and Parker, 2018, Wheeler et al., 2016, Yang et al., 2020] and hints that dysregulation of condensation and SG formation contribute to disease [Bosco et al., 2010, Patel et al., 2015].

Yet despite sustained and vigorous inquiry, a remarkable array of foundational questions remain unanswered. What do stress granules do, if anything? What are the functional consequences of condensation, and what functions do specific mechanisms of condensation, such as LLPS, carry out? (Throughout this review we explicitly intend "condensate" to be a catch-all term for membraneless clusters without any further stipulation as to their structure, process of formation, or adaptive significance (Box 1), largely following standard usage [Banani et al., 2017, Lyon et al., 2020]. What biological roles are played by molecular-level condensation events versus subsequent merging of these condensates into larger, microscopically visible

structures? How do condensation and accumulation occur, and are these processes mediated mainly by intrinsic molecular forces or extrinsic cellular machinery such as cytoskeleton-associated motors? To what extent are stress-triggered condensation and SG accumulation processes and participants conserved over evolutionary time?

Among the deepest challenges in studying stress granules is that, in the absence of molecular functions and cellular phenotypes, the phenomenon itself is operationally rather than biologically defined: a stress granule consists of anything which forms microscopically visible foci which colocalize with established SG markers (cf. Box 1. Although these structures have been hypothesized to play a variety of cellular roles, their function remains unclear [Buchan et al., 2011, Ivanov et al., 2019, Kedersha et al., 2002, Kedersha and Anderson, 2009, Kedersha et al., 2000]. That SGs are termed "membraneless organelles", where the latter word explicitly means a cellular structure that performs distinct functions, has served to create the unfortunate impression that this fundamental question has been answered.

This question of function applies not only to stress granules but also to the broader study of cytoplasmic ribonucleoprotein (RNP) foci including P-bodies, RNA transport granules, P-granules, and the nucleolus. In some cases, such as RNA transport granules in neurons, the question of function has been more directly addressed [Kiebler and Bassell, 2006, Pushpalatha and Besse, 2019]. However, in many cases, function is still presented as a model. P-bodies were long presumed to be sites of RNA degradation [Aizer et al., 2014, Franks and Lykke-Andersen, 2007, Sheth and Parker, 2003], but this model has been challenged [Eulalio et al., 2007, Hubstenberger et al., 2017]. Furthermore, work on G3BP1 aggregates in axons shows that condensates composed of canonical stress granule proteins may play a role under non-stress conditions, introducing basal stress granule-like condensates [Sahoo et al., 2018, 2020]. The questions and challenges regarding stress granules raised here apply to other biomolecular condensates, purported membraneless organelles, and contexts beyond cell stress.

As efforts to develop a parts list for SGs [Buchan et al., 2011, Cherkasov et al., 2015, 2013, Jain et al., 2016, Wallace et al., 2015] have proceeded alongside attempts to recapitulate in vitro certain molecular events such as stress-reactive condensation and RNA recruitment [Begovich and Wilhelm, 2020, Iserman et al., 2020, Riback et al., 2017, Van Treeck and Parker, 2018], evidence has emerged for multiple quasi-independent contributing pathways, multiple molecular stages, and multiple levels of organization in SGs and their precursors. This will serve as our jumping-off point. Given the multiple levels of molecular organization known to contribute to stress-induced RNA condensation, how do these levels interrelate, and at what level are adaptive features best understood?

Throughout this review, we intend for a larger question to lurk in the reader's mind. How can the characterization, interrogation, isolation, and reconstitution of stress-induced protein/RNA condensates and stress granules be effectively guided and evaluated in the absence of established functions, biological activities, or cellular phenotypes?

2.3 Multiple stages of stress-induced RNA condensation and stress granule formation

What is the relationship between protein/mRNA biomolecular condensation and stress granule formation? Although these processes are sometimes considered synonymous, and although how initial condensates accumulate in microscopically visible foci remains largely unknown, the existence of multiple stages in SG formation has long been understood (Figure 2.2). Existing models commonly reflect hierarchical organization in SGs, with some stable components ("core") surrounded by more dynamic components ("shell") [Jain et al., 2016, Wheeler et al., 2016], or nanoscopic "seeds" interacting and merging to form SGs [Padrón et al., 2019, Panas et al., 2016].

Evidence for these multiple stages comes from several independent sources. First, indi-
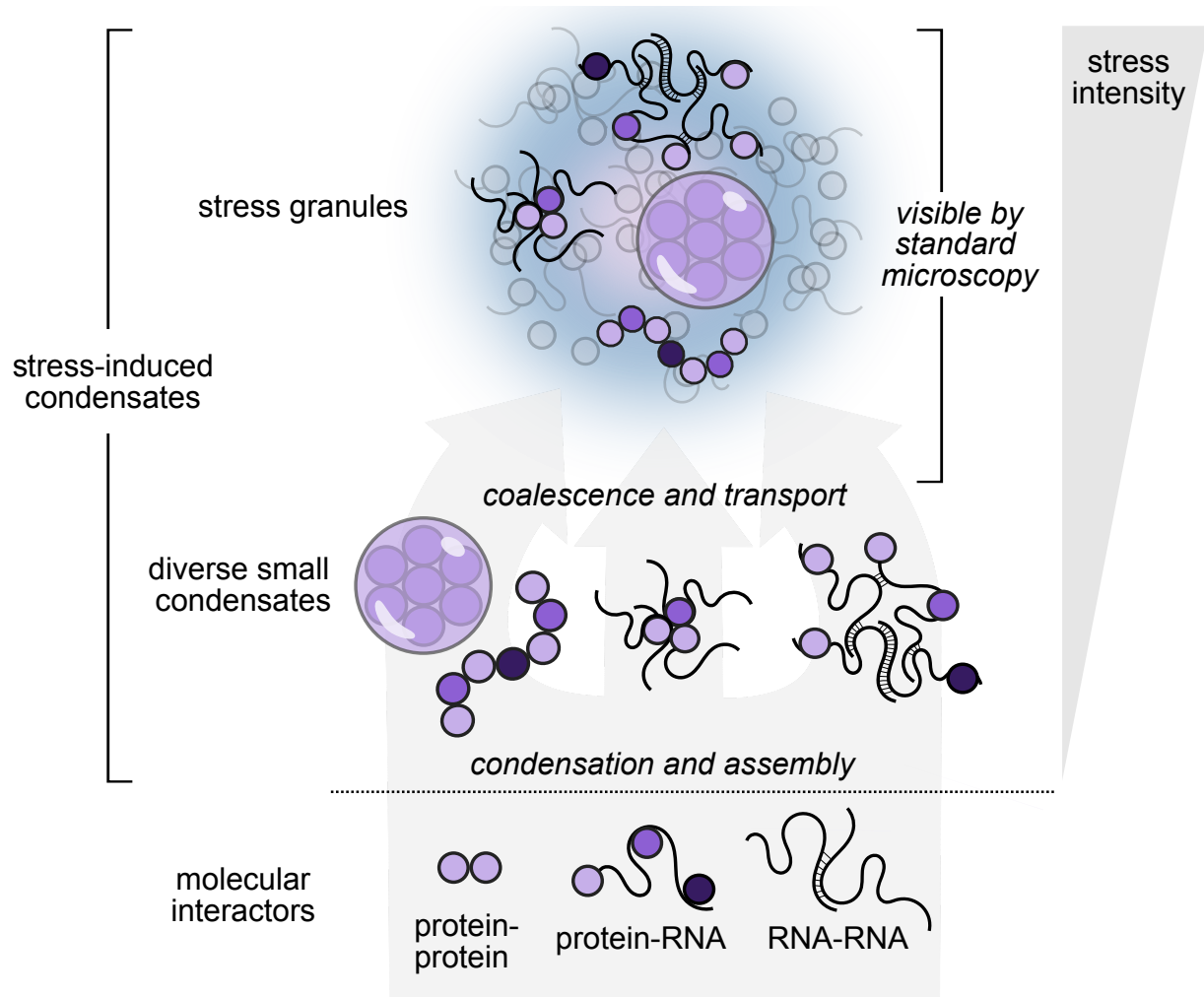
Figure 2.2: **Stress-triggered protein/mRNA condensation and stress granule formation occur in stages, depend on stress intensity and identity, and involve multiple types of molecular interactions.** Severe stress causes the accumulation of diverse small condensates into stress granules observable as cytosolic foci by standard microscopy.

vidual core markers for stress granules such as poly(A)-binding protein, G3BP, and Ded1 can be purified recombinantly and will autonomously condense in response to stress-associated physiological cues (e.g. heat shock, presence of long ribosome-free mRNA) in vitro [Guillén-Boixet et al., 2020]; [Iserman et al., 2020, Kroschwald et al., 2018, Riback et al., 2017, Yang et al., 2020]. These in vitro results suggest that condensation in vivo may not depend on interactions between a large set of SG components, at least at initial stages.

Second, although formation of canonical microscopically visible SGs can be blocked by translation elongation inhibitors [Kedersha et al., 2000, Nadezhdina et al., 2010, Namkoong et al., 2018, Wallace et al., 2015], the stress-triggered condensation, as measured by biochemical fractionation, of SG components such as poly(A)-binding protein proceeds virtually unaffected by such inhibition, indicating that accumulation of condensates into SGs is a separate step [Wallace et al., 2015]. This suggests that formation of canonical SGs involves cell-biological transport processes which bring multiple components together in the cytosol [Panas et al., 2016]. In support of this model, depolymerization of microtubules disrupts SG accumulation [Ivanov et al., 2003a,b]), and SGs tether to the endoplasmic reticulum and lysosomes using specific factors for intracellular transport [Liao et al., 2019]. Similarly, in contrast to in vitro ATP-independent condensation processes, ATP-driven mechanisms are required for SG formation in cells [Jain et al., 2016]. Transport and accumulation of small condensates and other components is a separate process from the initial condensation events which also accompany stress.

Finally, the appearance of canonical stress granules generally depends on stress intensity and duration, and in important cases, low levels of stress cause condensation of protein constituents but not their SG accumulation. For example, heat shock in budding yeast leads to biochemically detectable condensation of certain proteins after 8 minutes at 37 °C or 42 °C, and accumulation of certain proteins in cytosolic foci, but formation of classic SGs marked by poly(A)-binding protein requires pushing temperatures to 44–46 °C at this

timescale [Cherkasov et al., 2013, Wallace et al., 2015]. Limitations of imaging techniques may contribute to this discrepancy to some degree (see our discussion of grand challenges below), and exciting developments of improved microscopy-based methods—such as lattice light-sheet microscopy or fluorescence cross-correlation spectroscopy—may help minimize these concerns in the future [Guillén-Boixet et al., 2020, Peng et al., 2020]. But the differential accumulation of protein factors at different levels of stress intensity [Grousl et al., 2013]) rules out simplistic notions that, for example, stress granules are merely small at first and grow larger with intensifying stress. More evidence for an ordered assembly of stress granules comes from time-resolved proximity labeling experiments, which identified the interactome of the stress granule component eIF4A1 during heat shock of HEK293 cells [Padrón et al., 2019]. This study found that certain canonical stress granule components interacted with eIF4A1 before others. Thus, assembly proceeds in separable stages, ending with accumulation in large foci under severe stress.

The existence of assembly stages naturally raises the question: at what stages might specific functions be carried out? A deeper question haunting the field is: what do stress granules actually do?

2.4 Elusive functions of stress granules and stress-triggered RNA condensation

No commonly accepted function for stress granules yet exists. Many functions have been proposed, implicating stress granules in a range of roles, including sequestration of mRNAs and proteins; protection of mRNAs and proteins from degradation; promotion of enzymatic activities by increasing local concentration; minimization of cellular energy expenditure; and acting in translational quality control, signaling, and cargo delivery[Aronov et al., 2015, Buchan and Parker, 2009, Escalante and Gasch, 2021, Ivanov et al., 2019, Kedersha et al.,

2002, 2013, Mahboubi and Stochaj, 2017, Moon et al., 2020]. Stress granules have also been implicated in suppressing cell death by sequestering pro-apoptotic factors such as receptor of activated C kinase 1 (RACK1) [Arimoto et al., 2008, Tsai and Wei, 2010]. Similarly, a recent study found that stress granule formation suppressed pyroptosis, a form of cell death associated with inflammation, by sequestering the protein DEAD-box helicase 3 X-linked (DDX3X) [Samir et al., 2019]. However, the large variety of functions proposed for stress granules, combined with some conflicting findings, have made it difficult to form an overarching model of stress granule function [Mateju and Chao, 2022].

For instance, an oft-speculated function for RNA condensation is transiently protecting transcripts from degradation during stress [Hubstenberger et al., 2017, Moon et al., 2019, Sorenson and Bailey-Serres, 2014]), yet other work finds no effect on mRNA half-life following SG inhibition [Bley et al., 2015]. Another model holds that RNA condensation contributes to selective translation of non-condensed transcripts. Stress-induced transcripts are often translated in the midst of global translational shutoff. Some transcripts that are highly translated during stress, such as HSP70 and HSP90, do not associate with SGs, suggesting a connection between translation and escaping condensation [Kedersha and Anderson, 2002, Stöhr et al., 2006, Zid and O'Shea, 2014]. Certain translation initiation factors also condense, raising the possibility that a combination of protein and RNA sequestration can help promote selective translation during stress [Iserman et al., 2020, Wallace et al., 2015]. However, SGs are not required for global translational shutoff, so this selective translation would occur on top of a more dominant effect [Escalante and Gasch, 2021]. Additionally, translation has been observed inside SGs, complicating this model [Mateju et al., 2020].

A potential resolution to these conflicting results may be that particular functions are carried out by specific stages of organization. For example, stabilization of RNA by seques-tration can conceivably occur at the pre-microscopic condensate level whereas other proposed functions may require collection of components into a larger and more molecularly diverse
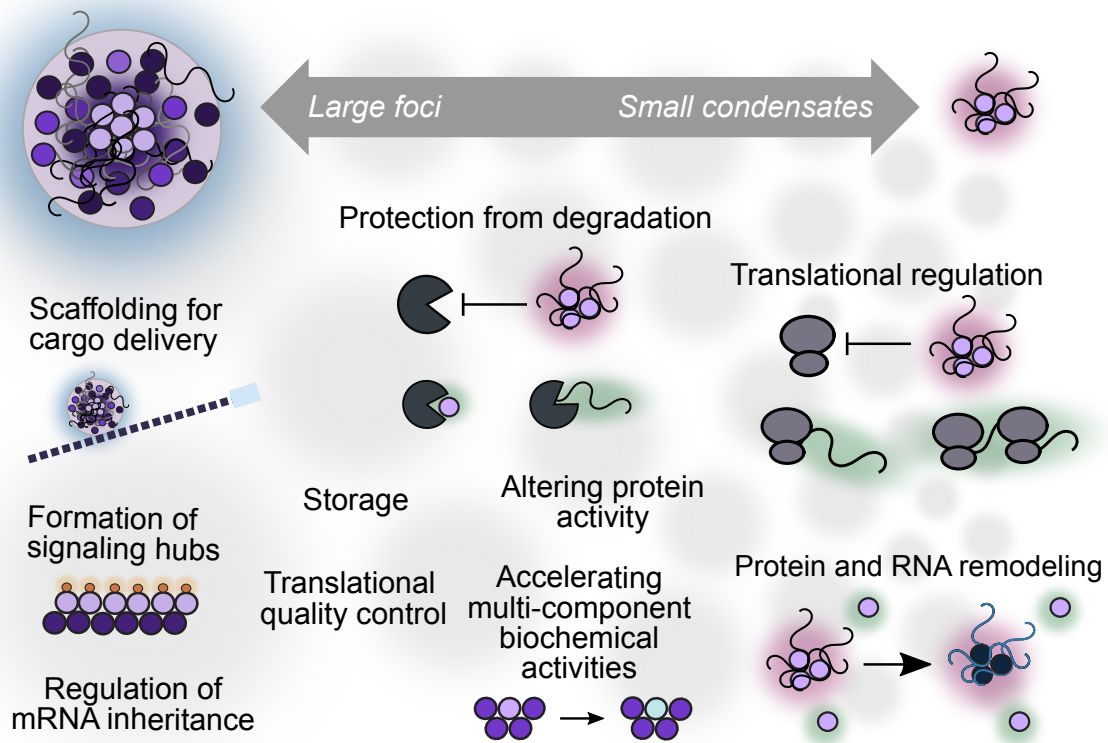
Figure 2.3: **Formation of canonical stress granules (visible by standard microscopy, composed of a large number of components) may not be required for many attributed functions.** Many roles could in principle be accomplished by small RNA/protein condensates consisting of a sharply restricted subset of components assembled into submicroscopic condensates. The diagram provides speculative positioning of functions on the size spectrum because strong hypotheses regarding which functions require large foci are lacking.

body (Figure 2.3. Hypothetically, a study in which perturbations block SG accumulation but not initial condensation, with no effect on RNA stabilization, would reach different conclusions than a study in which perturbations block both processes. An expanded understanding of assembly stages, a deepened grasp of the molecular drivers of these stages, and a widened array of perturbations capable of targeting specific stages and molecular determinants will be needed to sort out these questions.

Less discussed in the field are the issues inherent in studying biological phenomena whose functional contributions, if any, are unclear. Purification and reconstitution strategies, deprived of an activity-based standard for measuring success, must instead rely on morphological or compositional metrics whose relationship with biological function remains to be established [Begovich and Wilhelm, 2020, Freibaum et al., 2021]. The lack of functional insight is compounded by the remarkable lack of standard cellular phenotypes in the study of stress granules. Because not all of a given protein or RNA localizes to stress granules, determining a function must come from specifically perturbing condensation behavior without influencing activity, localization, or expression level. Even at the condensate level, phenotypes have been difficult to establish, although an allelic series of mutations which suppress poly(A)-binding protein's heat-triggered condensation in vitro and in vivo also suppress growth during heat stress [Riback et al., 2017]. The rarity of such phenotypes, particularly for stress granules, has led to a lingering question of whether SGs may often simply be byproducts of other cellular changes [Mateju and Chao, 2022].

2.5   Informing functions of stress-triggered condensation through the lens of disease

Some promising directions in uncovering stress granule function have come through study of disease contexts. Stress granules are induced by viral infection, where their formation has

14

been proposed to help restrict viral replication [Eiermann et al., 2020]. In fact, many viruses have developed strategies for preventing stress granule formation by, for instance, sequestering or cleaving key SG components [Katoh et al., 2013, White et al., 2007]. What function do stress granules serve that viruses are so intent on disrupting? One possibility is that stress granules could sequester viral RNA, similar to their proposed function in storing cellular mRNAs [Burgess and Mohr, 2018, Law et al., 2019]. However, as discussed above, it is difficult to conclude whether recruitment of viral RNA to SGs is required for proposed functions without mutations that specifically perturb SG formation while preserving separate molecular functions of SG components. One such perturbation comes from recent work showing that chikungunya virus promotes SG disassembly through the ADP-ribosylhydrolyase activity of nonstructual protein 3 (nsP3) [Abraham et al., 2018, Akhrymuk et al., 2018, Jayabalan et al., 2021].Removing this activity from nsP3 preserves SGs during infection, providing a manipulatable system for future studies of SG function without deletion of any host machinery.

The stressful environment inhabited by tumor—such as the nutrient deprivation, hypoxia, increased reactive oxygen species, and perturbed protein folding resulting from the dysregulation of metabolism and growth in malignancy—makes cancer biology a useful model for studying the functions of stress-induced condensation [Ackerman and Simon, 2014, Anderson et al., 2015, Clarke et al., 2014, Gorrini et al., 2013]. Moreover, certain chemotherapy drugs trigger cancer cells to form SGs, which are generally thought to be pro-survival, leading to condensation modulation as a potential target for therapeutics [Fournier et al., 2010, Gao et al., 2019, Kaehler et al., 2014]. In contrast, another chemotherapy agent, sodium selenite, triggers non-canonical SGs lacking certain components whose SG localization has been linked to cell survival. These non-canonical SGs have thus been suggested to be less functional in the stress response [Fujimura et al., 2012]. Additional work aimed at understanding the precise differences in stress-induced condensation between the considered pro-survival canonical

and the non-canonical SGs, at both the SG and pre-microscopic condensate level, will help inform the functions of condensation in response to stress and perhaps even inform the importance of its organization at the size/spatial levels.

Further underscoring the potential role of condensation in the pathogenesis of cancer, recent work studying myeloid malignancies has shown that specific driver mutations upregulate SG formation, which is linked to increased stress adaptation and cancer development [Biancon et al., 2022]. Additionally, work with disease mutations related to neurodegenerative diseases suggests a relationship between maladaptive protein aggregates and adaptive condensates like stress granules, suggesting that maladaptive aggregates may occur when stress granules are not properly disassembled [Gal et al., 2016, Gwon et al., 2021, Mackenzie et al., 2017]. Even so, our understanding of these maladaptive protein aggregates will be limited without a deeper understanding of the function of adaptive condensates. Without understanding the functions of stress-induced condensation, we can only speculate on the pathophysiology of persistent stress granules.

While many studies of stress granules focus on proteins which, when fluorescently tagged, are easily visible microscopically, RNA sits at the center of stress granule formation and function. We thus begin with a consideration of how our understanding of RNA's role has changed as new methods have come into use.

2.6   The role of RNA: old observations and emerging results

The accumulation of poly(A)-RNA is among the defining features of stress granules. Moreover, the role of mRNA in SG formation has long been known. Among the most crucial experiments is the demonstration that translational inhibition affects SG formation in a mechanistically specific way: elongation inhibitors such as cycloheximide and emetine, which freeze ribosomes on mRNA, block SG formation, whereas puromycin, which prematurely

terminates translation and frees mRNA of ribosomes, promotes SG formation [Bounedjah et al., 2014, Kedersha et al., 2000, Namkoong et al., 2018, Wallace et al., 2015]. Inhibition of transcription also inhibits SG formation [Bounedjah et al., 2014, Khong et al., 2017b]), further underscoring the role of RNA, at least at the accumulation stage.

But which RNAs? How does RNA contribute to condensation and SG formation? To what extent does RNA drive condensation or accumulation, and to what extent is it passively dragged along?

Early important results showed that prominent stress-induced mRNAs are selectively excluded from stress granules in both plant and mammalian cells [Kedersha and Anderson, 2002, Nover et al., 1989, Stöhr et al., 2006, Zid and O'Shea, 2014]. Because SGs are, by most metrics, accumulation sites for translationally repressed mRNAs, and because it is both biologically appealing and empirically established in some systems that stress-induced transcripts are well-translated [Preiss et al., 2003, Zid and O'Shea, 2014]), these early results placed stress granules at the center of translational regulation during stress.

But these foundational results have not survived into the recent era dominated by high-throughput studies, where transcriptome-scale effects can be observed. Modern studies do not find substantial depletion of stress-induced mRNAs from stress granules; instead, recent studies employing diverse approaches have converged on transcript length as the key correlate of mRNA recruitment to SGs. Messenger RNA length is the dominant correlate of their enrichment in the transcriptome associated with purified stress granule cores and stress-associated RNA granules [Khong et al., 2017b, Matheny et al., 2019, 2021, Namkoong et al., 2018]); in in vitro systems, increasing RNA length promotes RNA/protein phase separation organized by the stress-granule hub G3BP1 [Guillén-Boixet et al., 2020, Yang et al., 2020]); and single-molecule studies show that mRNA length correlates with the dwell-time of mRNAs on SGs and other condensed structures [Moon et al., 2019].

An increased concentration of ribosome-free mRNA following stress-induced translational

17

shutdown is considered the key trigger for SG formation [Hofmann et al., 2020]), and inhibition of translation initiation triggers condensation, such as in stress, eIF2α phosphorylation, or inhibition of the initiation factor eIF4A [Buchan et al., 2008, Iserman et al., 2020, Kedersha et al., 1999, Mazroui et al., 2006, Riback et al., 2017]. (Figure 2.4). This model is supported by several lines of evidence: 1) global translation initiation downregulation and subsequent polysome collapse is associated with RNA condensation during stress [Cherkasov et al., 2013]), 2) prevention of polysome collapse during stress blocks SG formation [Kedersha and Anderson, 2002]), 3) transfection of translationally arrested cells with free mRNA triggers SG formation [Bounedjah et al., 2014]), 4) inhibiting eIF4A, an essential translation initiation factor, promotes SG formation [Dang et al., 2006, Low et al., 2005, Mazroui et al., 2006, Tauber et al., 2020b]. Alongside these data, early and still-current alternative models in which RNA length plays a minimal role exist. For example, stalled preinitiation complexes (PICs) which accumulate during stress may in part form the core of SGs [Kedersha et al., 2002]) (Figure 2.4).

Beyond ribosome-free RNA, a role of RNA length makes intuitive biophysical sense, because the number of opportunities for either RNA-RNA or protein-RNA interactions—i.e., valence—naturally scales with length, all else equal [Jain and Vale, 2017]. Evidence for a role from RNA-RNA interactions is circumstantial, resting on partial recapitulation of some SG transcriptome features in vitro using only purified RNA [Van Treeck and Parker, 2018]), the dependence of in vitro phase separation on long, unfolded RNAs [Guillén-Boixet et al., 2020, Yang et al., 2020]), and RNA helicases [Tauber et al., 2020a]. Further discussion of the available evidence supporting the roles of RNA-RNA or protein-RNA interactions can be found in several informative reviews [Campos-Melo et al., 2021, Hofmann et al., 2020, Ripin and Parker, 2021, Van Treeck et al., 2018].

Even though a dominant role for RNA length is sensible biophysically, it is puzzling biologically. The overwhelming consensus holds that stress granules are accumulation sites
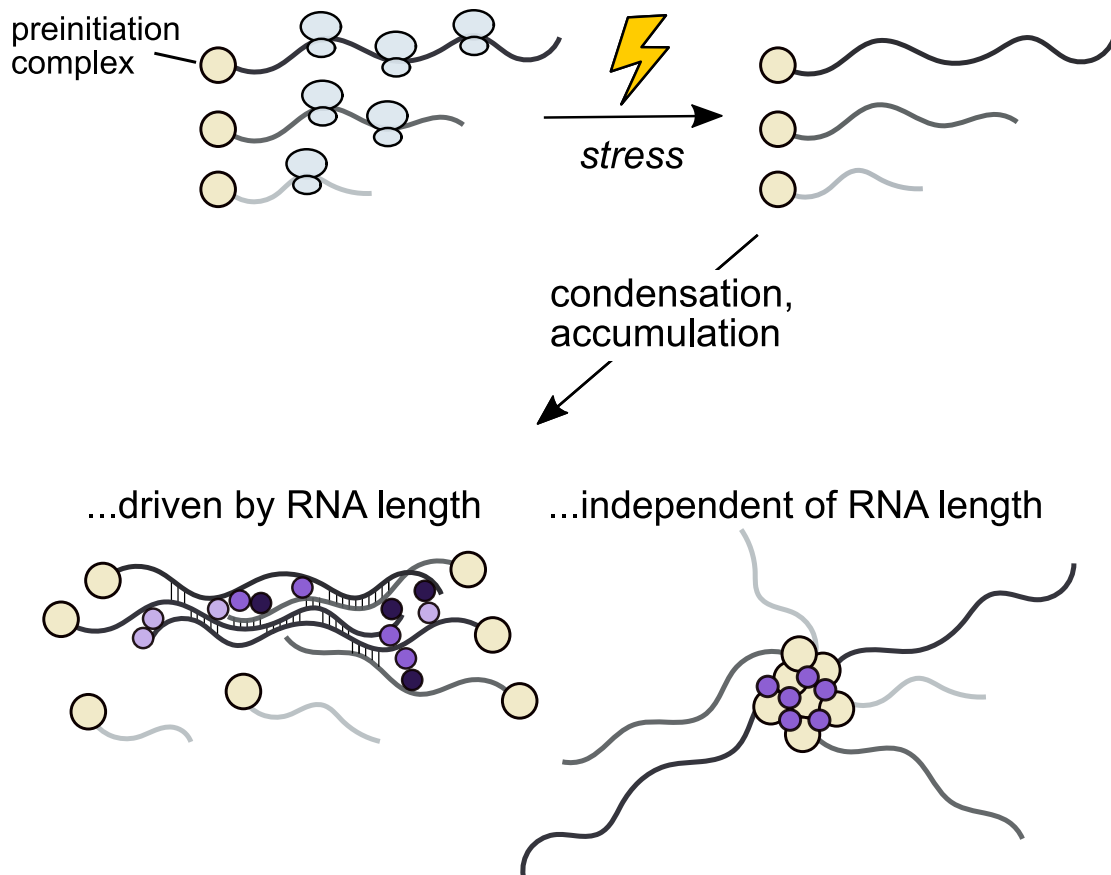
Figure 2.4: **The mechanisms of stress-triggered condensation and stress granule formation remain an area of active inquiry.** Treatments that inhibit translation initiation (often by phosphorylation of eIF2α, producing ribosome-free mRNA, cause stress granule formation in a wide range of systems and circumstances. Substantial recent work implicates long RNAs in condensation and formation of stress granules, a result which is biophysically plausible yet functionally puzzling.

for mRNA whose translation is suppressed during stress. Yet the length-driven model (and existing results supporting it) suggests that induction of long transcripts during stress would be futile for protein production, because long transcripts would be immediately recruited into translationally silent stress granules. However, while evidence that long transcripts are translationally silenced during stress, after their SG recruitment, is lacking, it has been hypothesized that shorter transcripts may be associated with rapid responses, which could help resolve the paradox [Lopes et al., 2021].

However, an important caveat is that mRNA length is also a natural confounding variable in experiments and analyses. Sedimentation by centrifugation is employed in most transcriptome-scale studies aimed at isolating SG-associated mRNAs, much as has been done in proteome-scale studies [Cherkasov et al., 2015, Jain et al., 2016, Wallace et al., 2015]. But unlike proteins, long RNAs, due to their size—an mRNA weighs roughly an order of magnitude more than the protein it encodes—will tend to sediment whether or not they are in a condensate. Consequently, comparing stress and non-stress conditions is crucial to determining the extra sedimentation due to stress. However, as others have pointed out [Namkoong et al., 2018]), the original study [Khong et al., 2017b]) reporting yeast and mammalian stress granule transcriptomes, and reporting the profound effect of length, did not include non-stress controls. Long RNAs may stick nonspecifically to affinity reagents in pulldowns due to their valence or increased structure [Samir et al., 2019]. Although subsequent controlled work in mammalian cells has confirmed the accumulation of longer RNAs in granules following ER or oxidative stress [Matheny et al., 2019, Namkoong et al., 2018]), the effects are more modest, and no non-stress control is yet available in yeast. Reduced translational efficiency (TE) has also been reported to be a major contributor to SG RNA accumulation. However, the two measures of TE used—codon optimality and ribosome density—have long been known to be inversely correlated with transcript length [Arava et al., 2005, Duret and Mouchiroud, 1999, Weinberg et al., 2016]), raising the question of whether

TE is a causal contributor to mRNA recruitment or a spurious correlation. Sedimentation-independent methods to examine recruitment of mRNAs, such as mRNA fluorescence in situ hybridization (FISH) in intact cells, have covered only a handful of targets [Khong et al., 2017b, Matheny et al., 2019]), reported only a modest SG recruitment effect from length, and concluded that "length, per se, is not the major driving force in SG enrichment" [Matheny et al., 2021]. Large-scale, well-controlled, systematic studies of the effect of length will be useful in resolving lingering uncertainty.

Given the sharp change in the apparent biology of RNA recruitment to SGs from early to present-day studies, the limited set of transcriptome-scale studies available at this writing, and the challenging nature of isolating molecular components of functionally ill-defined structures, the RNA components of stress-induced condensates and SGs will continue to be an area of intense investigation.

2.7   Mechanisms of dissolution

How do stress-induced RNA condensates dissolve after stress, as cells return to basal operations? Dissolution appears to be a regulated, controlled process that relies on specific proteins [Hofmann et al., 2020, Marmor-Kollet et al., 2020]. Proteins categorized as molecular chaperones and autophagic proteins have been implicated in SG dissolution, as have proteins associated with post-translational modifications (PTMs) such as sumoylation, ubiquitination, and phosphorylation [Buchan et al., 2013, Cherkasov et al., 2013, Gwon et al., 2021, Keiten-Schmitz et al., 2020, Marmor-Kollet et al., 2020, Maxwell et al., 2021, Shattuck et al., 2019, Yoo et al., 2022]. Work in yeast has revealed that heat-induced (42 ℃) protein aggregates are entirely reversible, which is incompatible with autophagy and suggests that different fates occur in different stresses [Wallace et al., 2015]. Recent work shows that molecular chaperones can dissolve stress-triggered protein condensates orders of magnitude more

efficiently than misfolded reporter proteins in vitro, suggesting that molecular chaperones may have evolved to interact with stress-induced condensates [Yoo et al., 2022]. Additionally, recent work in mammalian cells has shown that stress granules can be eliminated through either an autophagy-independent disassembly process or autophagy-dependent degradation, depending on the severity and acuteness of the initial stress [Gwon et al., 2021, Maxwell et al., 2021]. This work suggests that the disassembly of stress granules is related to the initial stress, suggesting that different methods of assembly may require different methods of disassembly.

The kinetics of stress granule dissolution may be tied to a functional role, such as translational control. If stress-induced condensates are sites of storage, the contents must be disassembled in a timely manner. It has been proposed that stress granules dissolve in discrete steps, where an initial shell is pulled away followed by a core, with particular proteins being recruited at distinct stages [Wheeler et al., 2016]. Proteins necessary for cell recovery from stress, such as translation initiation factors, may need to be dispersed earlier than other stress granule core proteins that are dissolved more slowly. In fact, proper disassembly of stress granules was shown to be required for recovering cellular activities, such as translation, after stress [Maxwell et al., 2021]. The dissolution of stress-induced condensates may be related to maladaptive insoluble protein aggregates that are often associated with diseases, motivating a further understanding of the mechanism and function of dissolution [Hofmann et al., 2020].

However, as the function of SGs remains unclear, the lack of functional assays demands careful experimental perturbations and cautious conclusions. For example, condensates that are no longer visible by microscopy may still occupy a conformation distinct from a monomeric form. New findings about the material state and assembly process of stress-induced condensates will illuminate the dissolution process, addressing questions such as whether the multiple steps of dissolution are equivalent to the stages of assembly or if a

change in material state may lead to a different dissolution process. On this front, the role of liquid-liquid phase separation in SG formation may have crucial consequences for how these structures dissolve.

2.8 Examining the role of liquid-liquid phase separation in stress-induced condensation

Liquid-liquid phase separation (LLPS) is a thermodynamically driven mechanism by which a solution of a compound demixes into a dilute and a dense phase above a certain critical concentration [Hyman et al., 2014]. A host of SG-associated proteins have been shown to undergo phase separation in vivo and in vitro [Guillén-Boixet et al., 2020, Iserman et al., 2020, Kroschwald et al., 2015, Molliex et al., 2015, Riback et al., 2017, Sanders et al., 2020, Yang et al., 2020]), and it is widely held that stress granule assembly is driven by LLPS (reviewed in [Hofmann et al., 2020]. Recent work has converged on G3BP as a central node in LLPS-driven SG formation [Guillén-Boixet et al., 2020, Sanders et al., 2020, Yang et al., 2020]), yet G3BP is dispensable for SG formation in response to certain stressors, such as heat and osmotic shock [Kedersha et al., 2016, Matheny et al., 2021]. Thus, G3BP-focused models of SG formation may overly simplify the complex process of stress-induced condensation.

Using LLPS as an assembly mechanism provides key advantages beneficial for responding to stress. The ultra-cooperativity of LLPS enables proteins to precisely sense and respond to small changes in their environments [Yoo et al., 2019]. For instance, in yeast Ded1 autonomously condenses in response to temperature stress. Ded1 from a cold-adapted yeast condenses at lower temperatures than that of S. cerevisiae, while Ded1 from a thermophilic yeast condenses at higher temperatures [Iserman et al., 2020]. This correlates with the fact that each yeast species has evolved to trigger its heat shock response relative to its

environmental niche. Other key advantages of LLPS include that it enables passive (energy-independent) cellular reorganization and that it is reversible. Following the removal of the stress stimulus, LLPS would no longer be energetically favored, and the system would spontaneously return to basal conditions.

Biomolecular condensation can result in the concentration of protein and RNA molecules into phases with a variety of material states. How could a condensate's material state—how liquid-like or solid-like it is—affect its function? More solid-like condensates have been linked to disease, as pathogenic mutations of certain condensing proteins such as FUS increase aging and a loss of liquid-like properties over time [Patel et al., 2015]. This thinking extends to RNA condensates as well, as it has been proposed that RNA helicases prevent RNA-RNA entanglement to maintain a liquid-like condensed state [Tauber et al., 2020b,a]. Further, the viscoelasticity of the nucleolus has been linked with enabling the vectorial release of properly folded ribosomes [Riback et al., 2022]. Yet, the material state of stress-induced condensates does not appear to be widely conserved across eukaryotes, which like other evolutionarily variable features would usually be taken as evidence that the material state is not central to function. For instance, yeast SGs are more solid-like than those of metazoa [Kroschwald et al., 2015]), although there are methodological caveats [Wheeler et al., 2016]. Reconstituted heat-induced condensates of the yeast SG protein Pab1 are solids [Riback et al., 2017]) which are not spontaneously reversible, even though these condensates are readily dispersed by endogenous molecular chaperones [Yoo et al., 2022]. Even within an organism, pH-induced condensates of the yeast SG protein Pub1 are more liquid-like than those induced by heat shock—and only the heat-induced condensates depend on chaperones [Kroschwald et al., 2018])—yet both conditions are thought to be physiologically relevant.

The apparent lack of conservation of the material state can be rationalized when we consider that a condensate's material state appears irrelevant for many of the functions ascribed to SGs. For example, if the role of stress-induced condensation is to temporarily

store housekeeping mRNA to enable the preferential translation of stress-response messages, how liquid-like the storage compartment is may be of minor importance. Additionally, if the function is to sequester certain proteins to perturb a given signaling pathway in the cytoplasm, the key feature is to deplete the protein from the dilute phase, and the liquidity of the dense phase is less relevant. On the other hand, if the material state is particularly relevant for the potential pathogenicity of condensates, then the evolutionary pressures on material state in different organisms may differ substantially even if SGs have a conserved cellular function.

2.9 Hazards in defining stress granule composition

Defining the composition of stress granules is complicated by a number of factors, even setting aside the existential problem of what constitutes a biologically important structure in the absence of well-established functions and phenotypes. Nevertheless, the obvious consistency and evolutionary conservation of the accumulation of some proteins and RNAs into large foci has led to a sustained effort to identify lists of molecular components involved in the lifecycle of stress granules. Individual mRNAs and proteins can be localized to microscopically visible foci of stress granule markers [Cherkasov et al., 2015, Khong et al., 2017b, Mateju et al., 2020, Moon et al., 2019, 2020, Wallace et al., 2015, Wilbertz et al., 2019]. On a larger scale, the stress granule interactome has been defined using a variety of techniques, many of which rely on using individual stress granule components, such as poly(A)-binding protein, G3BP1, TIA1, and eIF4A, as bait proteins and then assessing the mRNAs and proteins which interact with that bait. The interactors have been identified through immunoprecipitations, purification of particles containing a bait fused to a fluorescent protein, and by biotin proximity labeling [Hubstenberger et al., 2017, Khong et al., 2017b, Namkoong et al., 2018, Padrón et al., 2019, Somasekharan et al., 2020]. Additionally, proximity label-

ing methods have found similar interactomes between stress granule proteins prior to stress and during stress [Markmiller et al., 2018, Youn et al., 2018]. This may indicate that SGs are mainly stabilized by enhancements of basal interactions, or that the interactions which distinguish SGs are labile or refractive to these methods.
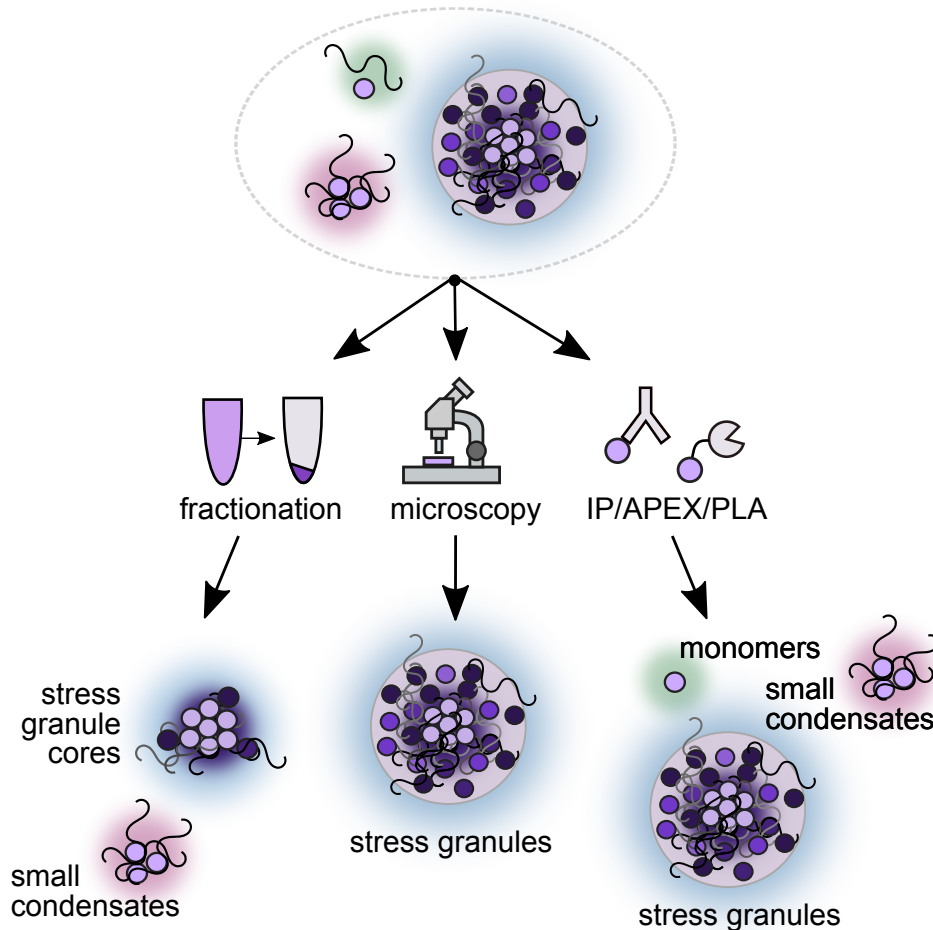
Figure 2.5: **Different methods used to probe stress-induced condensation capture and report on different stages of stress-induced condensation and stress granule formation, providing complementary information**

The different levels of organization in stress-triggered condensation and SG formation, along with diverse methods whose relative accuracy can be difficult to establish given the ill-defined nature of the target, combine to create a challenging experimental landscape

26

(Figure 2.5). Unlike a membrane-bound mitochondrion or a relatively compositionally stable ribosome, stress-induced condensates and stress granules lack features which might simplify their description.

A hallmark of biomolecular condensation is that many of the components of the condensate individually associate through weak, dynamic interactions [Alberti and Hyman, 2021]. No biologically clear cutoff for interaction strength exists, making it unclear how to decide if a given component is part of the structure or not. For instance, many transcripts have been observed to associate only briefly with stress granule proteins [Wilbertz et al., 2019]. How long must an mRNA reside at a stress granule to be considered a component? Additionally, consistent but weak associations may be lost during the isolation steps necessary for sequencing, mass spectrometry, or other biochemical methods. Perhaps certain molecular components form a scaffold to which client proteins are recruited [Campos-Melo et al., 2021, Shiina, 2019, Zhang et al., 2019]. Differences in interaction strength may reveal biologically important differences; for example, major molecular chaperones associate with stress granules by colocalization [Cherkasov et al., 2013]), but do not co-fractionate with stress-triggered condensates [Wallace et al., 2015]. Should such chaperones be considered a component of stress granules, merely associates, or something else? Here again, functional assays would sharpen these distinctions in crucial ways.

Because stress granules are operationally defined as microscopic foci marked by specific proteins, the definition of the structure is unfortunately entwined with technical limitations and with compositional preconceptions. Failure to observe foci microscopically, for example at low levels of stress, are consistent with two distinct biological possibilities: the absence of condensates entirely, or the formation of structures below the diffraction limit which still retain key properties of larger condensates [Guzikowski et al., 2019]. Likewise, failure to observe colocalization with a specific marker molecule may reflect legitimate biological variation either in the marker itself or in the structure being marked.

27

Finally, the composition of stress granules is not static, but depends on the nature of the stress and also changes over time [Aulas et al., 2017, Buchan et al., 2011, Padrón et al., 2019, Reineke and Neilson, 2019, Zhang et al., 2019]. Cells have evolved a variety of strategies to deal with changing environments. In the face of brief stresses, it may be advantageous to store transcripts until the stress has passed, allowing for a faster restoration of growth, whereas prolonged stress may necessitate more drastic reprogramming of cellular processes [Arribere et al., 2011]. Consequently, deciding whether a molecular species is or is not a part of the stress granule transcriptome/proteome, reducing the problem to a yes or no, may obscure more biology than it illuminates.

2.10   Grand challenges in studying stress-induced protein/mRNA condensation

As is now apparent, stress granules and their molecular precursors represent an exemplary system in which field-level challenges find crisp expression. Here we identify grand challenges in the study of these structures [Grousl et al., 2009, Wallace et al., 2015, Yang et al., 2014].

The first central challenge is to identify the functions of stress-induced condensates and SGs, and determine how these functions are executed. Of particular importance is the identification of fitness-related cellular phenotypes. The near-total reliance on molecular or imaging phenotypes, in the absence of function- and fitness-related phenotypes (growth, survival, differentiation, activity), has become tolerated in ways that may hinder progress. For example, given that canonical stress granules only become microscopically visible during severe stress in some important cases [Grousl et al., 2009, Wallace et al., 2015]), the reliance on microscopic methods may blind us to wide swaths of functional phenomena. In addition, the identification of a cellular phenotype would make it possible to design genetic screens that search for factors that are not just involved in focus formation but are integral to SG
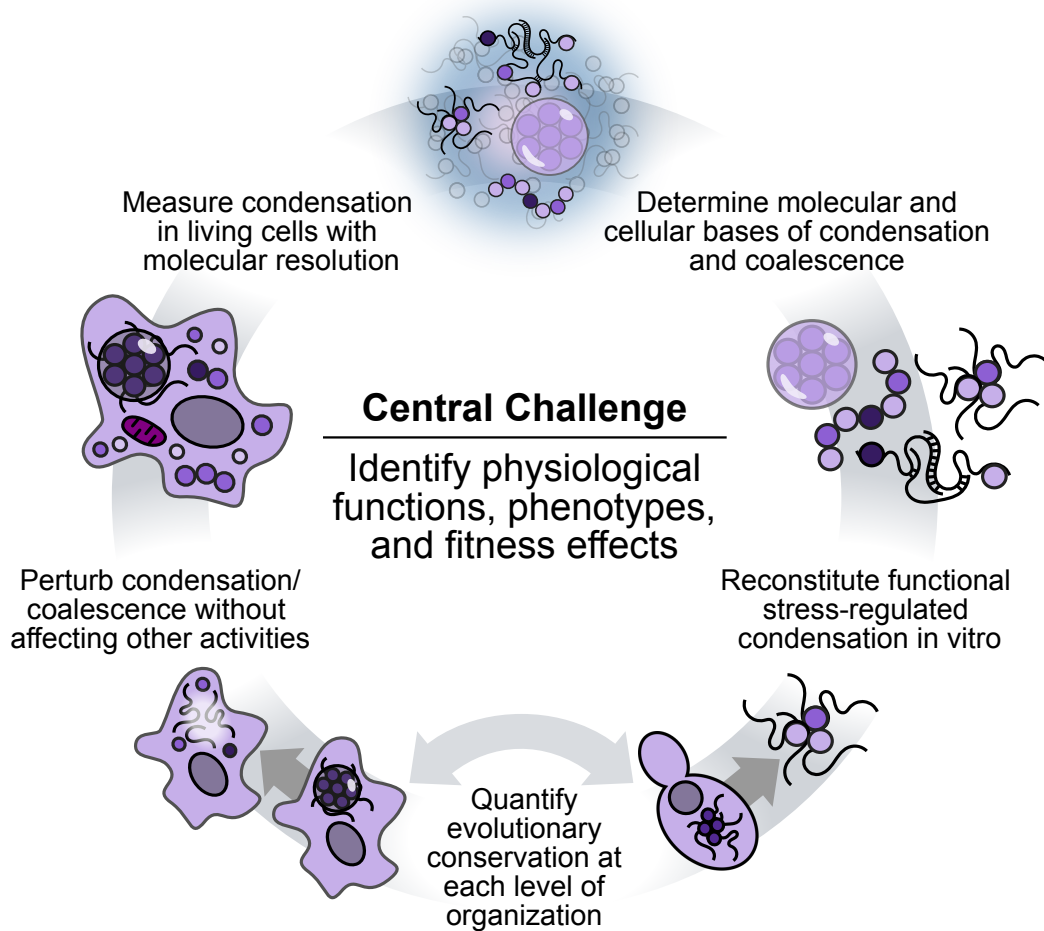
Figure 2.6: **Grand challenges in the study of stress granules and stress-induced condensation**

function [Yang et al., 2014].

Similarly, the use of inducers which robustly and reliably produce stress granules but are of uncertain physiological relevance, such as the broadly popular sodium arsenite, may have hidden disadvantages. If cells have not evolved to respond to a trigger, the cellular response is likely to lack organizational and molecular features which characterize responses to more physiological triggers such as heat, hypoxia, and osmotic shock [Grousl et al., 2009]. Even for these stresses, intensities which exceed physiological levels are in routine experimental use. Moreover, to validate a potent inducer such as sodium arsenite phenotypically against physiological inducers remains challenging until a phenotype or function of physiological stress granules is itself firmly established. Surmounting this central functional challenge will require sustained searches, a focus on physiology to match the extraordinary attention given to biophysics, and perhaps new thinking to identify a set of standardized phenotypes for functional studies.

Surrounding this central challenge lurk many other intertwined grand challenges. Some are well-established: determining the molecular bases of condensation and accumulation, and measuring molecular-scale condensation in living cells. Success on the latter would allow us, for the first time, to observe all the stages of stress-triggered condensation in vivo, even under mild stress conditions where large canonical SGs do not form.

In attempting to discern the molecular determinants of condensation and SG formation, less discussed is the crucial difficulty—another grand challenge—of perturbing these phenomena cleanly, that is, without disrupting other activities. By analogy, study of an enzyme might involve, in order of decreasing disruption, a gene knockout, a temperature-sensitive mutation, a catalytic mutation, or development of a specific and reversible inhibitor. Despite considerable strides in this direction for SGs (including screens for gene knockouts which disrupt SGs), at this juncture the search for clean perturbations remains almost entirely open [Yang et al., 2014].

In the absence of defined functions, another clear grand challenge looms: biochemical reconstitution of SG activities and functions. Reconstitution demonstrates the sufficiency of specific molecules and conditions to recapitulate cellular behavior. At present, all efforts have necessarily focused on reconstitution of traits without any unambiguous link to cellular fitness or adaptive function. Our situation in the stress granule field is remarkably different from historical efforts to purify specific biochemical fractions or molecules which could recapitulate an observed cellular activity [Grousl et al., 2009].

Finally, the evolutionary conservation of stress granules provides powerful motivation for their study. But to what extent are they conserved? To what degree are the following conserved: specific components and stages; molecular determinants such as domains; biophysical forces; formation and dispersal pathways; regulators; and ultimate functions? Answering these questions would meet our final grand challenge. Serious efforts to use evolutionary approaches, and to move beyond a handful of model organisms, has the potential to dramatically accelerate progress in our understanding of these enigmatic structures and processes. To the extent that SGs are not merely reliable side-effects of some other biological process, consistent contributions to cellular and organismal fitness will be the decisive factors in their preservation across the tree of life.

These grand challenges underscore that the field of stress granule biology is at a pivotal point. As we approach the 40-year mark since stress granules were first observed in tomato plants, we are due to move toward a deeper understanding of stress granules. Armed with clearly defined challenges, we can tackle the fundamental unknowns that still remain. Massive parallel surges in our understanding of composition and assembly mechanisms, both cell-biologically and biophysically, appear poised to drive a positive feedback loop of research integrating studies of assembly at multiple biological scales, mechanistic studies of the impact of condensation on mRNA lifecycles, and finally the fitness advantages that stress-induced condensation imparts [Nover et al., 1983].

CHAPTER 3

TRANSCRIPTOME-WIDE MRNA CONDENSATION PRECEDES STRESS GRANULE FORMATION AND EXCLUDES STRESS-INDUCED TRANSCRIPTS

This chapter has been adapted from Hendrik Glauninger, Jared AM Bard, Caitlin J Wong Hickernell, et al. 2024. I performed all microscopy experiments and image analysis, collaborated with the depletion experiments, polysomes profiles, and translation assays. Initial Sed-Seq experiments were done by Edward Wallace, HG did the HAC1/GCN4/hairpin work,

3.1 Abstract

Stress-induced condensation of mRNA and proteins into stress granules is conserved across eukaryotes, yet the function, formation mechanisms, and relation to well-studied conserved transcriptional responses remain largely unresolved. Stress-induced exposure of ribosome-free mRNA following translational shutoff is thought to cause condensation by allowing new multivalent RNA-dependent interactions, with RNA length and associated interaction capacity driving increased condensation. Here we show that, in striking contrast, virtually all mRNA species condense in response to multiple unrelated stresses in budding yeast, length plays a minor role, and instead, stress-induced transcripts are preferentially excluded from condensates, enabling their selective translation. Using both endogenous genes and reporter constructs, we show that translation initiation blockade, rather than resulting ribosome-free RNA, causes condensation. These translation initiation-inhibited condensates (TIICs) are biochemically detectable even when stress granules, defined as microscopically visible foci, are absent or blocked. TIICs occur in unstressed yeast cells, and, during stress,

grow before the appearance of visible stress granules. Stress-induced transcripts are excluded from TIICs primarily due to the timing of their expression, rather than their sequence features. Together, our results reveal a simple system by which cells redirect translational activity to newly synthesized transcripts during stress, with broad implications for cellular regulation in changing conditions.

3.2   Introduction

Cells must respond to changing environments to survive and thrive. When faced with a broad range of sudden maladaptive environmental changes—stresses—eukaryotic cells down-regulate translation, induce stress-responsive transcriptional programs, and form cytosolic clusters of proteins and mRNA. When microscopically visible as foci colocalized with markers such as poly(A)-binding protein, these clusters are called stress granules (SGs) [Cherkasov et al., 2013, Farny et al., 2009, Hoyle et al., 2007, Khong et al., 2017b, Nover et al., 1989, Protter and Parker, 2016, Riback et al., 2017], structures which are conserved across eukaryotes, yet still poorly understood. SGs are complex examples of biomolecular condensates, membraneless structures without defined stoichiometry which form by a range of processes and which concentrate specific types of biomolecules [Banani et al., 2017, Mittag and Pappu, 2022]. What precisely are stress granules composed of? How do they form and dissolve? What is their function, if any? What is the relationship between stress granule formation and the accompanying transcriptional and translational responses? All these questions remain active areas of inquiry.

Early work in multiple systems established that what are now recognized as stress granules recruit multiple RNA-binding proteins and translation initiation factors, along with pre-stress mRNA, yet exclude nascent mRNA produced during stress [Collier et al., 1988, Kedersha et al., 1999]. In mammalian cells, exclusion of two specific stress-induced heat shock

protein mRNAs from SGs, HSP70 and HSP90 [Kedersha et al., 2002, Stöhr et al., 2006] along with nonspecific recruitment of untranslated mRNA [Stöhr et al., 2006], matched prior work on heat shock granules in plants, which recruited mRNAs encoding housekeeping proteins but not those encoding newly synthesized heat shock proteins [Nover et al., 1989].

Translation initiation serves as a focus of stress-dependent translational regulation and plays a central role in SG formation. Several translation initiation factors themselves are classic markers for stress granules, apparently as part of stalled translation initiation complexes preceding assembly of the large ribosomal subunit (60S) at the start codon. A wide range of stresses, from starvation to heat shock to oxidative stress, trigger phosphorylation of initiation factor eIF2α and subsequent repression of initiation for most mRNAs, and also cause SG formation. In certain cases, such as for heat shock in mammalian cells, preventing eIF2α phosphorylation is sufficient to prevent SG formation [Farny et al., 2009]. However, heat shock triggers SG formation by an eIF2α-phosphorylation-independent pathway in budding yeast [Farny et al., 2009, Grousl et al., 2009], indicating that eIF2α phosphorylation is not itself the trigger for SGs.

Instead, subsequent ribosome run-off, polysome disassembly, and the exposure of ribosome-free mRNA which serves as a template for SG assembly links initiation inhibition to SG formation [Bounedjah et al., 2014, Kedersha et al., 1999]. Polysome disassembly has been called the "universal trigger" for SGs [Hofmann et al., 2020]. Consistent with the ribosome-free RNA template model, inhibitors of translation elongation which lock ribosomes on transcripts, such as cycloheximide (CHX) and emetine, inhibit SG formation, whereas an elongation inhibitor which causes ribosome release, puromycin, promotes SG formation [Bounedjah et al., 2014, Kedersha et al., 2000].

Recent work has provided extraordinary evidence, and a deeper biophysical foundation, consistent with a central role of ribosome-free RNA in stress granule formation. Transcriptome-scale study of the mRNA components of stress granules in both yeast and mammalian cells

revealed that mRNA length is the overwhelming determinant of recruitment: long mRNAs accumulate in SGs, short mRNAs are excluded [Khong et al., 2017b, Matheny et al., 2019, 2021, Namkoong et al., 2018]. Long RNAs provide opportunities for multiple interactions necessary to form condensates—and thus for the multivalent interactions needed to drive biomolecular condensation, separation of a mixed solution of biomolecules into concentrated and dilute regions, now recognized as principle of cellular organization without membranes [Banani et al., 2017]. Increasing RNA length promotes RNA/protein phase separation in vitro by the stress-granule hub protein G3BP1 [Guillén-Boixet et al., 2020, Yang et al., 2020], and single-molecule studies show that mRNA length correlates with the dwell time of mRNAs on stress granules and other condensed structures [Moon et al., 2019].

Yet these transcriptome-scale findings are in conflict with early results showing selective exclusion of stress-induced mRNAs from stress granules, a phenomenon not reported and, we show, not present in recent studies. Beyond length, only pre-stress translation levels or related features like codon bias have been identified as major correlates of recruitment [Khong et al., 2017b]. Even this result is puzzling, given that SGs recruit nontranslating mRNAs after stress, not before stress, and yet no relationship between post-stress translation and SG recruitment has been reported to our knowledge. Meanwhile, stress-induced messages are translationally privileged during stress [Preiss et al., 2003], such that their recruitment to SGs—complex biomolecular condensates which concentrate nontranslating mRNA, among other defining features—would be paradoxical.

Finally, stress granules themselves have an unusual status as a biological phenomenon. With no associated function or phenotype for their specific disruption, they are presently defined solely by visual criteria, the presence of microscopically visible foci colocalizing with specific markers such as poly(A)-binding protein (Pab1 in budding yeast). Absence of foci is routinely interpreted as absence of stress granules. Yet biomolecular condensation of multiple RNA-binding SG components in vivo and in vitro in response to physiological stress condi-

35

tions has been demonstrated [Franzmann et al., 2018, Iserman et al., 2020, Kroschwald et al., 2018, Riback et al., 2017, Wallace et al., 2015], and blocking SG formation with cycloheximide does not block in vivo condensation of Pab1 [Wallace et al., 2015]. Mild stresses trigger condensation without SG formation [Grousl et al., 2013, Wallace et al., 2015]. These results collectively indicate that stress-induced protein condensation is a distinct phenomenon from SG formation. They support a model in which stages of condensation occur prior to, and whether or not, stress granules eventually appear [Glauninger et al., 2022]. Whether RNA undergoes similar pre-SG stages remains unknown.

Here, using biochemical fractionation by sedimentation and RNA sequencing (Sed-seq), we show that virtually all pre-stress transcripts condense during stress regardless of their lengths, even in the absence of visible stress granules. At the transcriptome scale, stress-induced transcripts escape condensation and are robustly translated, confirming early anecdotal reports and contrasting with recent high-throughput results. We discover that specific endogenous transcripts are condensed before stress, only to be released upon heat shock for translational activation. Condensation of mRNA appears to be a distinct precursor potentiating SG formation. Although the mRNA condensation response is distinct across stresses, a surprisingly simple explanation rationalizes the differences. Following stress exposure, newly transcribed transcripts escape condensation and are preferentially translated. Together, these results show that mRNA condensation occurs even basally outside of stress and is measurable before visible stress granules form, expanding the importance of understanding mRNA condensation for cellular physiology in and outside of stress.

3.3 Sed-seq enables measurement of transcriptome-scale mRNA condensation

We previously used biochemical fractionation via sedimentation to isolate stress-induced protein condensates during heat shock in budding yeast [Keyport Kik et al., 2023, Wallace et al., 2015]. To measure condensation of RNA, we coupled this sedimentation assay with RNA sequencing (Sed-seq) (Figure 3.1A). We collected and quantified transcript abundances in total, supernatant, and pellet fractions, and estimated the proportion of each gene's transcripts in the supernatant (pSup) using a Bayesian mixture model [Wallace et al., 2015] validated by qPCR (Figure S1A). We included the chelating agent EDTA to disassemble polysomes which would otherwise sediment along with condensed mRNAs [Blobel, 1971, Nolan and Arnstein, 201969, Wallace et al., 2015]. Sed-seq does not by design enrich for mRNA association with a particular type of RNA granule, such as stress granules or processing bodies, enabling an unbiased measurement of stress-induced RNA condensation. Here we use the broad term condensation to describe molecules interacting to form denser structures, without any presumption of the precise nature or mechanism of formation of these structures.

We first used Sed-seq to examine mRNA condensation transcriptome-wide in unstressed conditions (30°C) and after short heat shocks at 42°C and 46°C; as expected, 46°C produced clear stress granules, visible as poly(A)+ RNA colocalized with foci of poly(A)-binding protein (Pab1), while the milder 42°C shock did not produce stress granules (Figure 3.1B). Sed-seq revealed large decreases in pSup across the transcriptome during heat shock, correlated with the intensity of the stress. Unlike stress-triggered protein condensation, which affects only a minority of the proteome [Walters et al., 2015], virtually all transcripts show substantial condensation after stress (Figure 3.1C). Similar to protein condensation [Grousl et al., 2009, Riback et al., 2017, Wallace et al., 2015], mRNA condensation occurs at 42°C

even when SGs are not apparent.
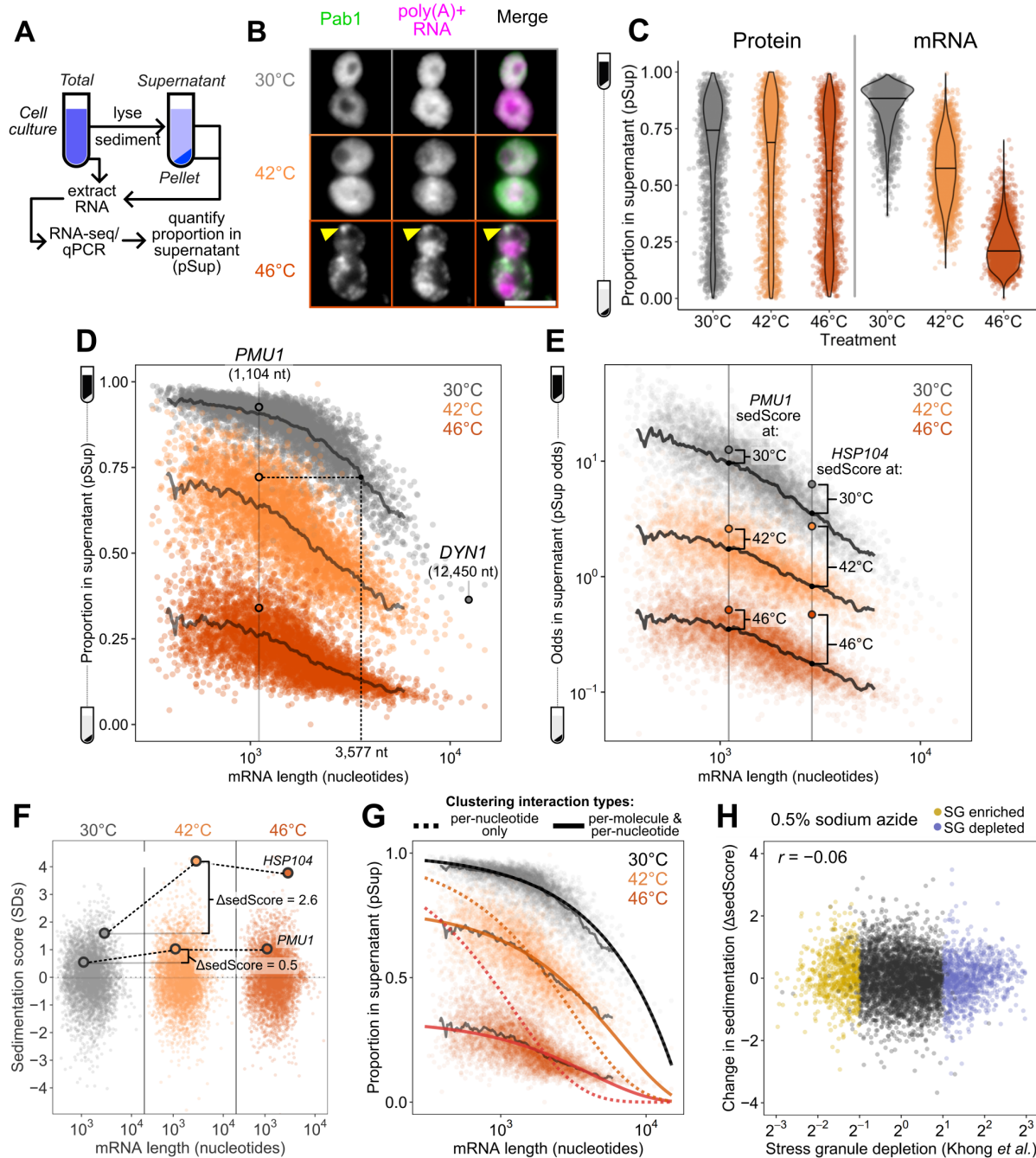
Figure 3.1: **Most transcripts condense during stress, even in the absence of stress granules.** (A) Analysis of mRNA condensation by sedimentation and RNA sequencing (Sedseq) enables calculation of mRNA proportion in the supernatant (pSup) across conditions. (B) 15 minutes of heat shock induces stress granule formation at 46°C but not at 42°C, as marked by poly(A)-binding protein (Pab1-HaloTag) and FISH against poly(A)+ RNA (scale bar = 5 µm).

Figure 3.1 *(previous page)*: (C) Unlike protein condensation, which affects only a small proportion of proteins (data from Wallace et al. Cell 2015), virtually all transcripts condense during stress, even when stress granules are not apparent. (D) Transcript pSup decreases with length in unstressed cells due to sedimentation of large monomeric mRNPs. pSup globally decreases with 10 minutes of heat shock, reflecting stress-induced condensation. (E) Sed-seq data allow quantification of key features: absolute sedimentation pSup, and relative sedimentation (sedScore), which controls for effects of long transcript sedimentation. sedScore is calculated on a log-odds scale to enable comparisons between low- and high-pSup transcripts. (F) Transcripts show substantial and different changes in relative condensation during stress. HSP104 mRNA increases 2.8 standard deviations in relative solubility (ΔsedScore = 2.6) while PMU1 mRNA changes little (ΔsedScore = 0.5). (G) A simple clustering model (see Supplementary Text) captures average pSup and stress-induced changes. Clustering must involve interactions independent of RNA length (e.g., between 5' or 3' ends) to fit the data. (H) Condensation measured by Sed-seq (ΔpSup, lower = more condensation) correlates negatively with previously reported stress granule depletion (lower = more condensation) (Khong et al. Mol Cell 2017).

Transcript length has been previously identified as the dominant determinant of mRNA recruitment to stress granules [Campos-Melo et al., 2021, Khong et al., 2017b, Van Treeck and Parker, 2018]. Such an effect seems intuitive because the likelihood of RNA-mediated molecular interactions naturally scales with length, consistent with the general importance of multivalency in biomolecular condensation [Banani et al., 2017]. In our data, long transcripts showed stronger sedimentation in all conditions, including when RNA was isolated from unstressed cells and when added, in purified form, to lysate (Figure 3.2B). We therefore sought to understand the origin of length-dependent sedimentation and its influence on downstream conclusions about the role of mRNA length and RNA-mediated multivalency in stress-triggered condensation. An extended treatment of our findings is provided in Supplementary Information, and we here focus on key insights, which differ markedly from conclusions of previous high-throughput studies.

Long transcripts—actually messenger ribonucleoprotein particles, or mRNPs—sediment when isolated from unstressed cells due to their mass (see Supplementary Text), without

any need to invoke condensation (Figure 3.1D). Consequently, a transcript's pSup is directly related to transcript length, whether or not that mRNA actually condenses. By spiking purified total mRNA from Schizosaccharomyces pombe into lysate from unstressed yeast cells, we verified that this length-dependence is recapitulated, and that this free mRNA largely remains soluble even when added to lysate from stressed cells in which most mRNA appears condensed (Figure 3.2B). The systematic relationship between pSup and mRNA length allows estimation of the size of stress-induced condensates in terms of the size of unstressed mRNPs with the same sedimentation behavior. For example, 1.1-kilobase PMU1 transcripts sediment after 42°C heat shock as if they were more than three times their size. After 46°C shock, they sediment as if more than ten times their unstressed size, with pSup lower than the heaviest detected mRNP in unstressed yeast, the 12.4-kilobase transcript encoding dynein (DYN1) (Figure 3.1D). These apparent several-fold changes in size are lower bounds (see Supplementary Text) and their magnitude justifies the provisional interpretation of sedimentation changes as cluster formation.

Several quantitative features can be extracted from Sed-seq data. We start by plotting pSup in log-odds space, log(Sup/Pellet), to prevent compression at very high or low pSup values (Figure 3.1E). We then calculate the relative pSup compared to the mean for similar-length transcripts, quantified as a Z score (sedScore) (Figure 3.2C). The sedScore measures differences in mRNP mass and potential condensation within conditions and removes the effect of length-based sedimentation (Figure 3.1F). Finally, we calculate the change in sedScore after stress (ΔsedScore), which reports on stress-induced changes in condensation (Figure 3.1F). We noted that certain transcripts showed significant changes in response to stress, such as the molecular-chaperone-encoding HSP104 mRNAs, which increase in relative solubility by more than 2.5 standard deviations upon 42°C shock (ΔsedScore = 2.8) while PMU1 mRNAs increase by an insignificant 0.5 standard deviations (ΔsedScore = 0.5) (Figure 3.1F).
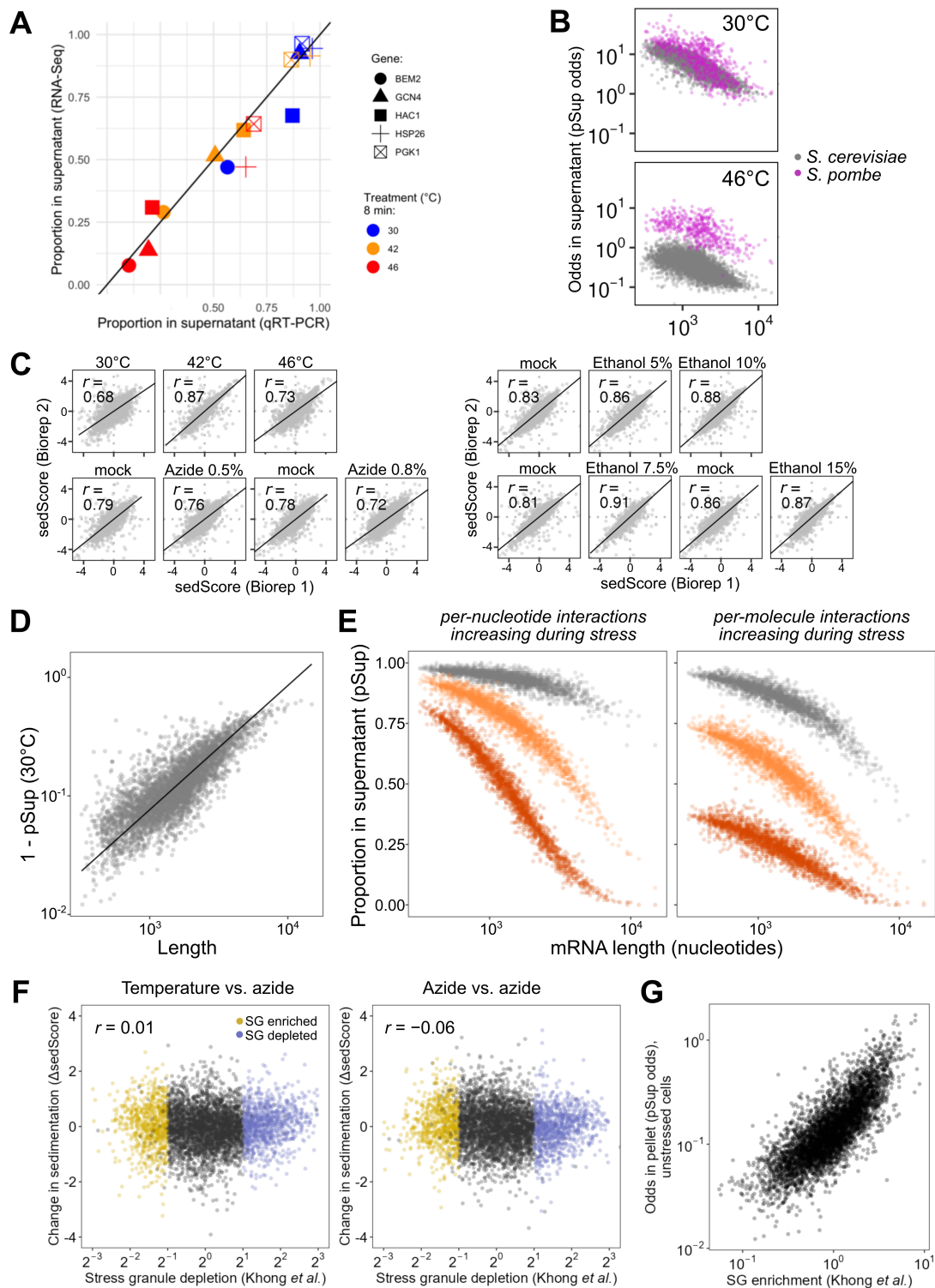
Figure 3.2: **Sed-seq captures previously unreported mRNA condensation largely driven by length-independent mechanisms.**

Figure 3.2 *(previous page)*: (A) The measurements of mRNA proportion in supernatant (pSup) from RNA sequencing match pSups calculated using spike-in-normalized abundances quantified by RT-qPCR. (B) Purified mRNA (S. pombe total RNA) spiked into lysate from unstressed yeast cells recapitulates length-dependent sedimentation of free mRNA, and remains largely free even when spiked into lysate from severely stressed yeast cells. (C) Across stresses, length-normalized sedimentation (sedScore) of biological replicates correlate well (r = Pearson correlation coefficient). (D) A simple model for the length-dependence of sedimentation for free mRNPs predicts a linear dependence between log(1-pSup) and log(length), which is observed (r = 0.81). (E) Simulations of mRNA clustering with only per-nucleotide (length-dependent) interactions permitted, at increasing rates of interaction, and simulations of mRNA clustering with only per-molecule (length-independent) interactions permitted, at increasing rates of interaction. (F) Negligible correlation (Pearson) is observed between reported depletion from azide-induced stress granules (Khong et al. 2017) and exclusion from stress-induced clusters (change in sedScore) after heat stress or azide stress. (G) Most of the variation in stress-granule depletion in a previous study can be explained by sedimentation of free mRNPs due to their length, and thus can be closely reproduced using only Sed-seq data from unstressed cells.

What interactions mediate condensation? A simple physics-derived model explains both the underlying length-dependence of pSup and the average increase in condensation across stresses (Figure 3.1G, Supplementary Text, Figure 3.2D,E). Two parameters govern condensation: the rate of interaction per nucleotide, and the rate of interaction per transcript. Per-nucleotide interactions model length-dependent interactions previously proposed to drive stress-granule recruitment, such as RNA-RNA interactions or interactions linked to RNA-binding proteins [Khong et al., 2017b, Matheny et al., 2021, Moon et al., 2020, Van Treeck and Parker, 2018]; per-transcript interactions model length-independent interactions, such as those involving the 5' cap or 3' end. This model fits sedimentation transcriptome-wide (Figure 3.1G, solid lines), estimating both per-nucleotide and per-transcript parameters as non-zero (p $< 2 \times 10^{-16}$). Importantly, length-independent interactions dominate the behavior of shorter mRNAs. Fitting average sedimentation with only per-nucleotide interactions dramatically underestimates the observed condensation of shorter mRNAs (Figure 3.1G, dotted lines). The median gene has transcript length 1,529 nt and more abundant mRNAs

are on average shorter. We conclude that stress-triggered condensation is inconsistent with interactions solely mediated by RNA-RNA interactions.

How does stress-induced condensation compare to previous reports of the stress-granule transcriptome [Khong et al., 2017b]? We initially compared ΔsedScore during heat stress to the reported stress-granule depletion based on pulldown and sequencing, and found that these measurements were uncorrelated (r = 0.01, Figure 3.2F). Because the previous study in yeast was done after 0.5% sodium azide treatment to induce stress granules, rather than heat shock, we treated cells with 0.5% azide and repeated Sed-seq. We found that the two measurements were slightly anticorrelated (r = -0.06, P $<$ (10^{-5}) (Figure 3.1H, Figure 3.2F). Because the previous study did not perform a non-stress control, we hypothesized that the inability to correct for length-based sedimentation created an artifactual enrichment for long transcripts. In support of this possibility, our Sed-seq results from unstressed cells reproduce the previously reported stress granule transcriptome to a high degree of accuracy (r = 0.8, Figure 3.2G). Whatever the reasons, Sed-seq produces results in sharp disagreement with previous work. We therefore asked whether meaningful biology might become apparent in these new data.
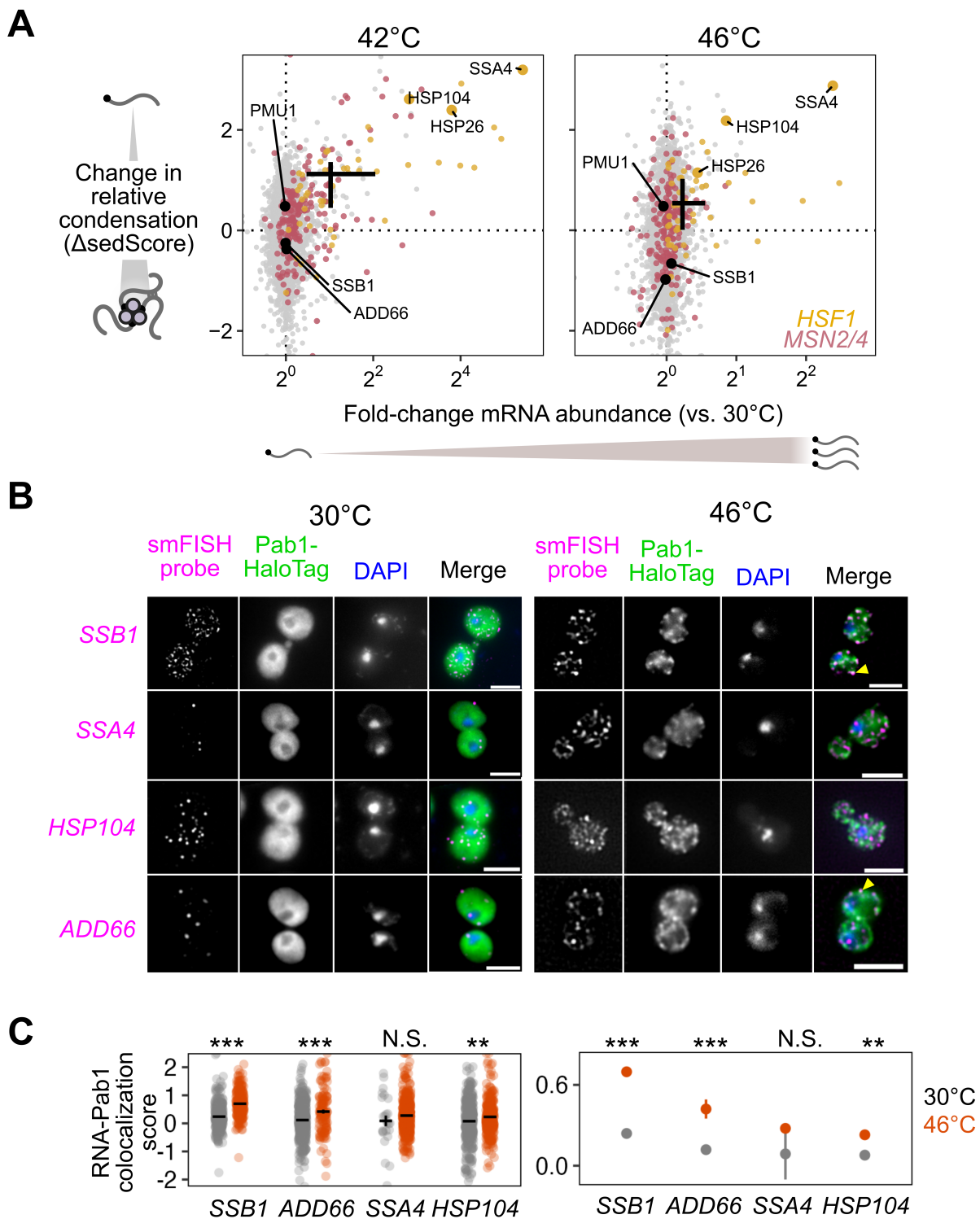
Figure 3.3: **Induced transcripts escape condensation during heat shock.**

Figure 3.3 *(previous page)*: (A) Comparison of mRNA abundance changes during heat shock reveals that transcript induction quantitatively predicts escape from condensation, regardless of the primary transcription factor driving induction. (B) smFISH of induced *(SSA4/HSP104)* and uninduced *(SSB1/ADD66)* transcripts confirms that induced mRNA are not localized to Pab1-HaloTag marked stress granules. Scale bars are 5 μm. (C) Colocalization was quantified by comparing the intensity of the Pab1 channel in regions with mRNA foci to random regions in each cell. The colocalization score is plotted per cell (left) or as the mean of all cells (right). (Wilcoxon rank sum test, N.S.: P $\geq$ 0.05; **: P < 0.01; ***: P < 0.001)

3.4 Stress-induced mRNAs escape condensation and are preferentially translated

The apparent escape of heat-shock-protein-encoding HSP104 transcripts from condensation during heat shock (Figure 3.1E,F) mirrors early reports of stress-induced transcript exclusion from stress granules [Collier et al., 1988, Kedersha et al., 2002, Stöhr et al., 2006]. With our transcriptome-scale data, we asked whether stress-induced transcripts were generally more likely to escape condensation. Indeed, genes regulated by the core heat shock response transcription factor Hsf1 strongly tend to escape condensation (ΔsedScore > 0) during heat shock (Figure **??**A, 3.4A,B, Wilcoxon rank sum test $P < 10^{-4}$). Escape is not specific to Hsf1 targets, as most genes whose abundance is up-regulated by stress also escape condensation, including targets of Msn2/4, another stress-activated transcription factor (Figure **??**A) [Solís et al., 2016]. We noted that the degree of induction correlated with the degree of escape, indicating that being regulated by stress-activated transcription factors was not the sole determinant of escape.

Stress-induced transcripts escape condensation even under conditions without apparent stress granules (e.g. 42°C). Are they also excluded from stress granules? To answer this question, we used single-molecule fluorescence in situ hybridization (smFISH)[Femino et al.,

1998] to examine the relative localization of transcripts to stress granules. We initially focused on two transcripts of nearly identical length, both encoding Hsp70 chaperones: *SSB1/2* transcripts, encoding a cytosolic Hsp70 species which is abundant in unstressed cells, and *SSA4*, encoding a stress-induced cytosolic Hsp70. We predicted that the induced *SSA4* transcripts would be excluded from stress granules. Consistent with our Sed-seq results, in 46°C heat-shocked cells, *SSB1/2* transcripts colocalized with stress granules marked by poly(A)-binding protein Pab1, while *SSA4* transcripts were largely excluded (Figure **??**B). We then picked another pair of transcripts (*HSP104* and *ADD66*) to test the other observation from our Sed-seq data: that length was not a determining factor in stress granule association or exclusion. Indeed, induced long *HSP104* transcripts were excluded, and uninduced short *ADD66* transcripts colocalized (Figure **??**B). In order to quantify this observation, we calculated the intensity of the Pab1 channel in regions with mRNA and compared that to random regions around each cell (Methods). Reflecting the extent of the colocalization between the mRNAs and stress granules, *SSB1* and *ADD66* containing regions are strongly enriched for Pab1 signal upon stress, while *SSA4* and *HSP104* are only slightly enriched (Figure **??**C). Together, Sed-seq and smFISH results form a consistent picture in which, regardless of length, stress-induced transcripts are excluded from condensates.

Is the escape of induced transcripts from condensation specific to heat shock? To answer this question, we carried out Sed-seq on cells exposed to different stresses: treatment with sodium azide (NaN_3), a standard trigger for stress granules [Buchan et al., 2011, Eiermann et al., 2022, Jain et al., 2016, Khong et al., 2017b], or with high concentrations of ethanol, a physiological condition for budding yeast which is also known to trigger granules 46 (Figure 3.5A). Following previous literature, we tracked SG formation using Pab1-GFP for heat shock and NaN_3 stress, and Pbp1-GFP for ethanol stress[Buchan et al., 2011, Kato et al., 2011, Wallace et al., 2015]. Across all three stresses, only severe stress triggered visible granule formation, while transcriptome-wide mRNA condensation was dose-dependent (Figure 3.5B).
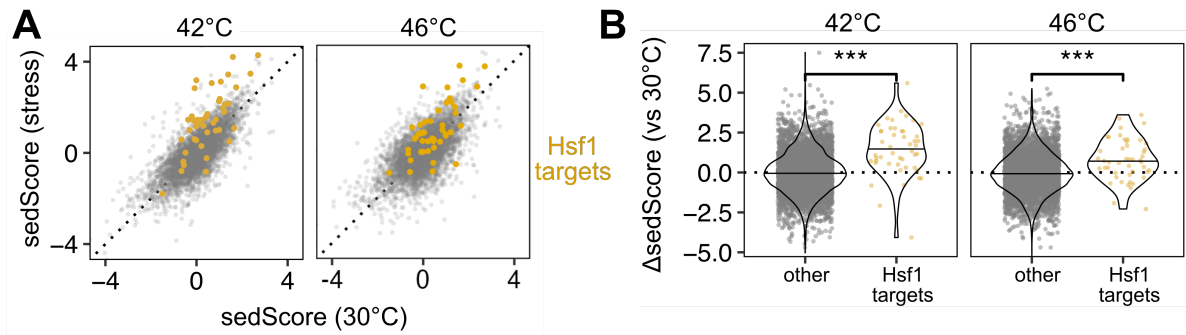
Figure 3.4: **sedScores during stress** (A) sedScores at 30°C largely match sedScores during heat shock, but the stress-induced regulon exhibits increased sedScores during stress reflecting escape from global condensation. (B) Hsf1-regulated transcripts have higher sedScores at both 42°C and 46°C compared with the rest of the transcriptome. (Wilcoxon rank sum test: *** = P < 0.001)

We find little evidence for increased stress-induced condensation of long transcripts for any of these stresses (Figure 3.6A).

Strikingly, stress-induced transcripts relatively escaped condensation across all three stresses (Figure 3.5C, S3C) as quantified by ΔsedScore. This result, now with transcript-specific precision, echoes early results showing exclusion of nascent transcripts from SGs [Collier et al., 1988, Kedersha et al., 1999]. In contrast, induced transcripts are not depleted from the previously reported SG transcriptome (Figure 3.6B)[Khong et al., 2017b]. Do the same transcripts escape mRNA condensation in response to different stresses? Comparison of the ΔsedScore's between stresses addresses this question. We compare the transcripts which are uniquely induced during heat shock, azide and ethanol stress, finding that a transcript generally escapes condensation if it is induced in that specific stress (Figure 3.6C). This is particularly apparent for the comparison between temperature and ethanol stresses.
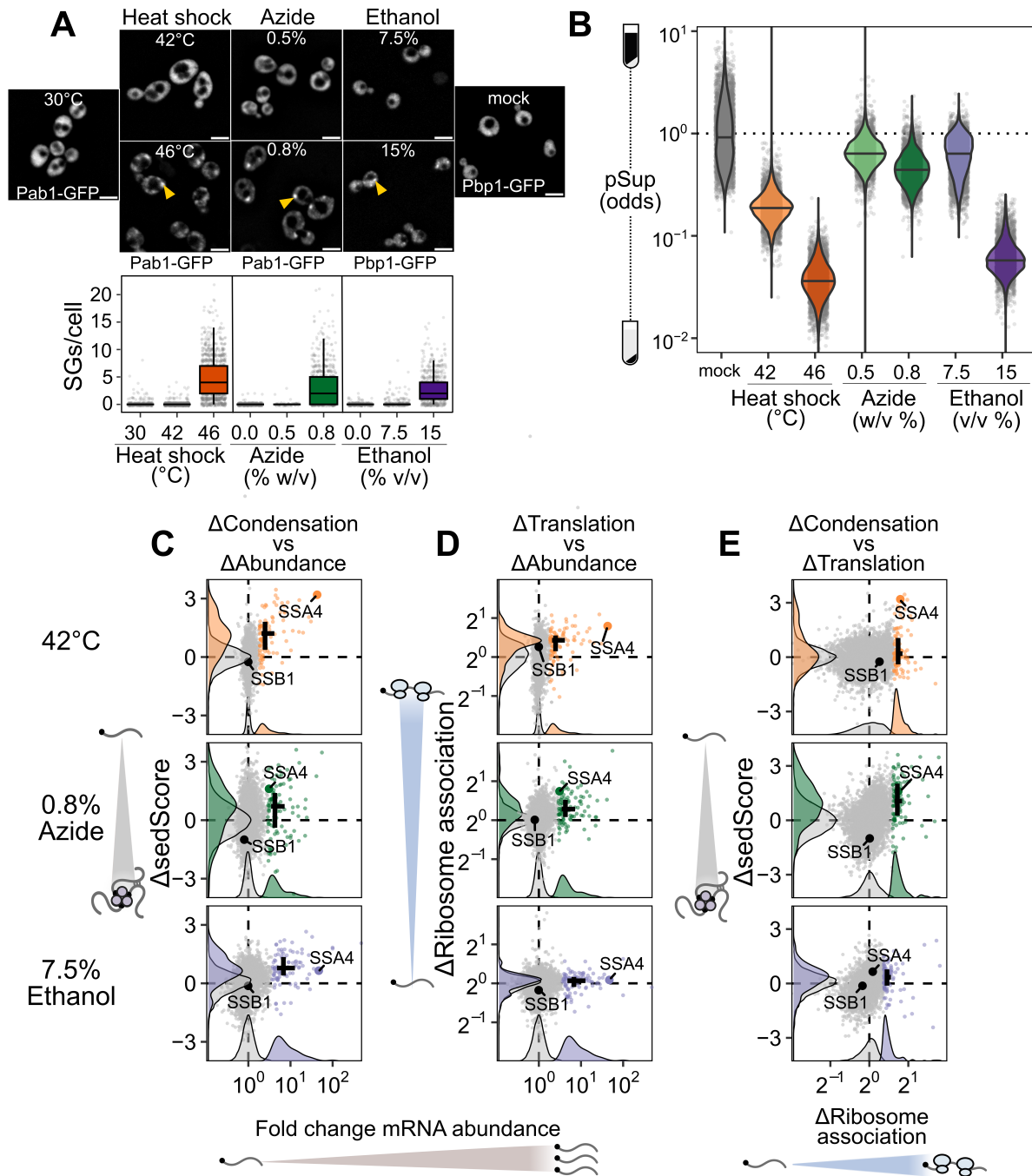
Figure 3.5: **Newly transcribed and well-translated mRNAs escape condensation across stresses.** (A) Severe, but not mild, stress induces visible SGs across multiple conditions. Scale bar is 5µm. (B) Both mild and severe stress induce transcriptome-wide sedimentation of mRNA, with the extent of pelleting correlating with the severity of the stress. (C) Across stresses, the most induced mRNA (top 100 induced transcripts are highlighted) escape from condensation.

49

Figure 3.5 *(previous page)*: (D) Polysome-seq was used to measure the stress-induced change in ribosome association (top 100 induced transcripts are highlighted). After heat shock and azide stress, the most induced transcripts also have increased relative translation. (E) Directly comparing changes in translation and sedimentation (top 100 translationally upregulated transcripts are highlighted) shows that well-translated messages during stress tend to escape condensation.

To what extent does mRNA translation correlate with escape from condensation? Because our results so clearly match early observations of untranslated-mRNA condensation and nascent-transcript escape, we measured mRNA-ribosome association transcriptome-wide by isolating and sequencing mRNA from polysome gradients, quantifying the stress-induced change in ribosome association on each transcript (Polysome-seq) [Arava et al., 2003]. In each of the three stresses, induced transcripts tended to be preferentially translated (Figure 3.5D, S3E). Similarly, preferentially translated transcripts tend to escape condensation (Figure 3.5E, S3F). Transcriptional induction, escape from condensation, and increased translation co-vary in each stress condition, indicating a functional role for condensation in translational repression of pre-existing transcripts. However, these results do not reveal the direction of causality.
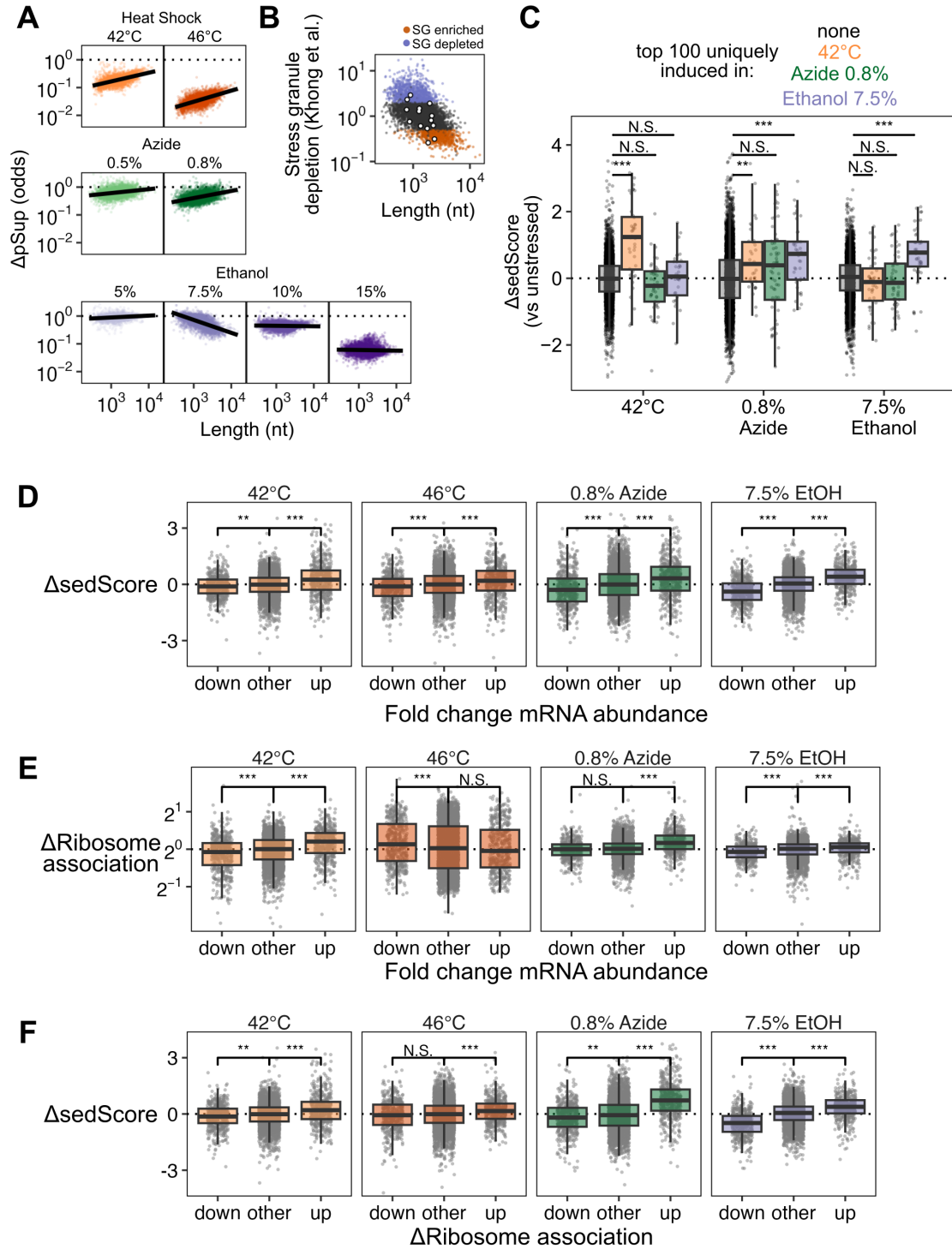
Figure 3.6: **Sed-seq analysis for other stresses.** (A) Length dependence of the change in sedimentation compared across stresses. In general, shorter transcripts increase in sedimentation more than long ones.

51

Figure 3.6 *(previous page)*: (B) Induced transcripts are not particularly depleted from stress granules based on data from Khong et al., 2017. Points in white are the top 1% of induced transcripts during azide stress. (C) The change in sedimentation of the top 100 uniquely induced transcripts across three stresses are compared. During heat shock and ethanol stress, only those transcripts which are specifically induced escape condensation. (D) Comparison of ΔsedScore grouped by the 10% most induced and repressed transcripts during stress. (E) Comparison of the change in ribosome association grouped by the 10% most induced and repressed transcripts during stress. (F) Comparison of ΔsedScore grouped by the top and bottom 10% transcripts with changing ribosome association during stress. (Wilcoxon rank sum with Bonferroni correction: N.S. $= P \geq 0.05$, ** $= P < 0.01$, *** $= P < 0.001$)

The observation that stress-induced transcripts escape condensation is consistent with a model in which newly produced transcripts are protected from condensation for some time during stress, regardless of their identity. This temporal escape model predicts transcript exclusion will correlate with the level of induction, which is directly related to the proportion of transcripts which are new during stress, assuming degradation can be neglected. A major alternative to the new-transcript model is that sequence-encoded mRNA features, such as structure or the presence of specific motifs or untranslated-region (UTR) binding sites, determine escape. This alternative model predicts that transcripts will escape condensation independent of induction level. Sed-seq data are consistent with the new-transcript model, showing escape from condensation strongly depends on induction level (Figure 3.5C, S3C). Even transcripts in the same regulons (Hsf1 and Msn2/4 during heat shock) show varying levels of escape dependent on their induction.

If timing of transcript production largely drives escape from condensation, then it should be possible to construct and express synthetic transcripts whose condensation is determined only by when their expression occurs. We built inducible reporters with regulatory regions (5' and 3' UTRs) from genes which are heat-induced (*HSP26*) and heat-insensitive (*PMU1*, whose condensation behavior follows the bulk pre-stress transcriptome). We chemically induced each reporter before and during heat shock, and measured their condensation behavior

via sedimentation with qPCR. Both reporters were uncondensed at 30°C, and condensed at 42°C and 46°C when expressed prior to heat shock. Both, however, showed substantially reduced condensation when newly expressed during heat shock (Figure 3.7A). These results provide further evidence that the timing of expression is a primary determinant of a transcript's condensation fate. Transcripts which are newly produced during stress will escape condensation to a significant degree, independent of their sequence features. On the other hand, transcripts produced before stress, even if they contain the sequence of a stress-induced gene such as *HSP26*, will nevertheless condense during stress.
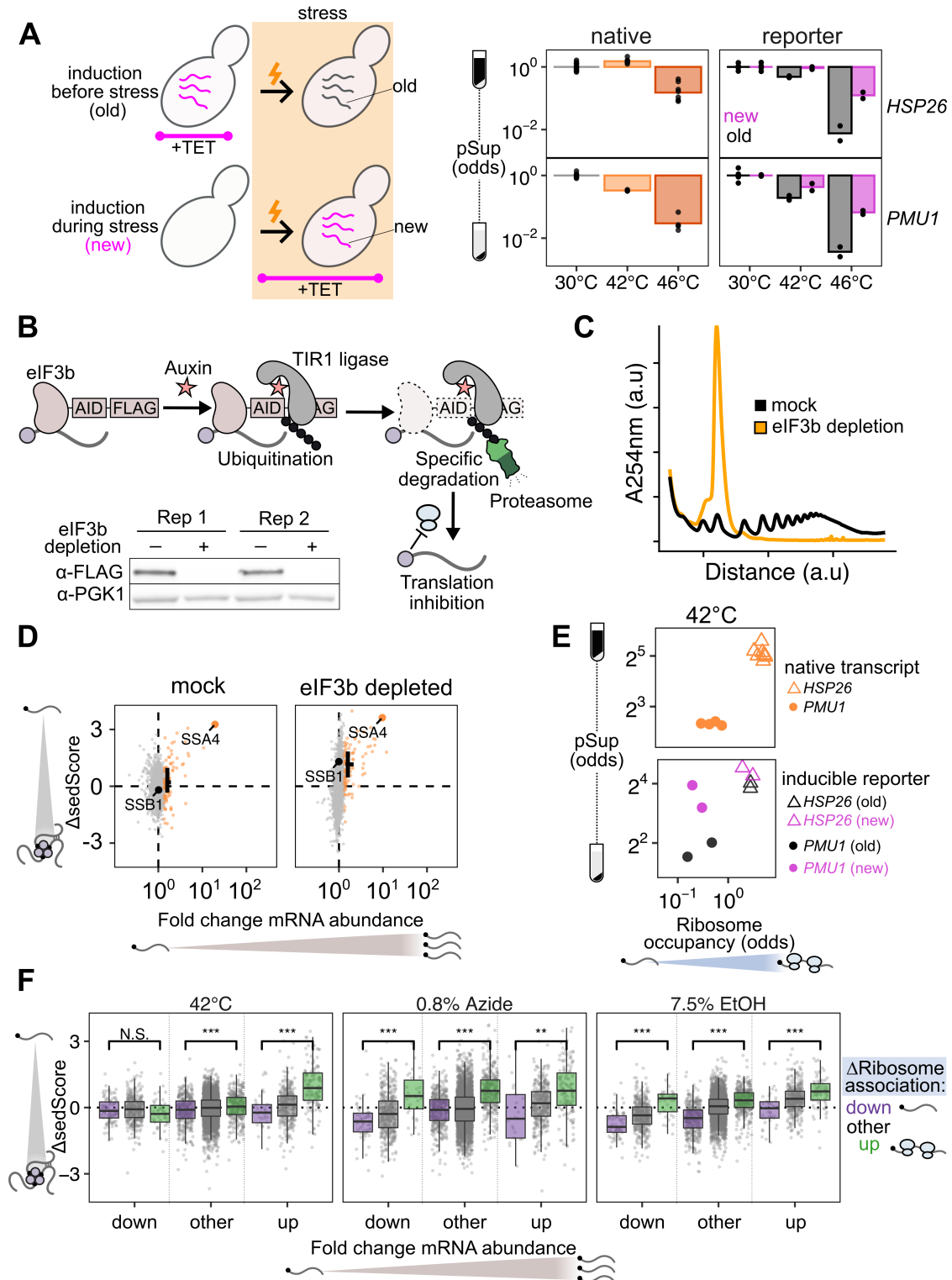
Figure 3.7: **Translation and induction are independently sufficient to promote escape from condensation.**

Figure 3.7 *(previous page)*: (A) pSup was measured by qPCR for inducible reporter transcripts with sequences derived from an induced transcript (*HSP26*) or an uninduced transcript (*PMU1*). Regardless of transcript sequence, "new" transcripts sediment less than "old" transcripts, showing that induction during stress is sufficient to drive escape from condensation. (B) The auxin-induced degradation system was used to deplete the translation initiation factor eIF3b. (C) Depletion of eIF3b led to translational collapse as measured by polysome profiles. (D) Even in the absence of translation initiation, stress-induced transcripts still escape condensation after 10 minutes of 42°C stress (highlighted: top 100 induced transcripts per condition). (E) The *HSP26*-derived reporter transcript is better translated than the *PMU1* reporter, as measured by qPCR analysis of ribosome association using sucrose cushions. Despite its poor translation, the newly induced *PMU1* reporter still relatively escapes condensation. (F) Analysis of data in Figure 3.5 dividing transcripts into the top 10% most up- or down-regulated transcripts by abundance and translation state. Translation is well correlated with escape from condensation across induction levels and stresses. (Wilcoxon rank sum test, N.S.: P $\geq$ 0.05; **: P $<$ 0.01; ***: P $<$ 0.001)

Given the clear relationship between transcript induction and escape from condensation, we sought to understand how translation fits into this model. First, we asked whether active translation is required for transcripts to escape condensation. We generated a strain of yeast with an auxin-inducible degron (AID) tag on the C-terminus of eIF3b, a subunit of the essential initiation factor eIF3 [Mendoza-Ochoa et al., 2019, Yesbolatova et al., 2020]. Western blotting confirmed successful degradation (Figure 3.7B), which resulted in profound reduction in global translation, as evidenced by polysome collapse (Figure 3.7C). We then performed Sed-seq on samples heat shocked after two hours of mock treatment or depletion of eIF3b. Even in cells with translation initiation blocked by eIF3b depletion, newly transcribed messages escape condensation, as highlighted with the black cross indicating the mean ΔsedScore of induced transcripts (Figure 3.7D). We conclude that escape from condensation by newly transcribed mRNAs can occur independent of their translational status.

Transcripts do not require active translation to escape condensation, but does their translational state affect how much they condense? To address this, we revisited the TET-inducible reporter system described above and determined the translational state of the re-

porter transcripts. We measured ribosome occupancy by spinning lysate through a sucrose cushion and quantifying the ribosome-free abundance in the supernatant and the ribosome-bound abundance in the pellet, after correcting for condensed mRNA which pellets even in EDTA buffer (Figure 3.8A-D). We found that, after 20 minutes of 42°C stress, the HSP26 reporter had high levels of ribosome occupancy while the PMU1 reporter had low ribosome occupancy regardless of whether the transcripts were new or old (Figure 3.7E). This translational difference matched the behavior of the native transcripts; native *HSP26* transcripts have a higher ribosome occupancy than native *PMU1* transcripts across conditions. Correspondingly, for both old and new transcripts, the well-translated *HSP26* reporter had a higher pSup than the poorly translated *PMU1* reporter at 42°C. This result is reflected in the transcriptome-wide data: across stresses, transcripts with increased translation were more likely to escape condensation than those with repressed translation (Figure 3.7F). This held true for the top 10% most-induced and top 10% most-repressed transcripts in ethanol and azide stresses, confirming that the influence of translation on condensation is layered on top of the newness of a transcript during stress. Although active translation is not required for a transcript to escape condensation, more translation can lead to more escape. This finding now invites the question: what is the fate of transcripts that are blocked in translation?

3.5 Translation inhibition-induced condensates (TIICs) of mRNAs precede stress granule formation and form in the absence of stress

To this point, we had focused on stress-induced condensates. However, in examining the transcriptome-scale data we noted that at both 30°C and 42°C there was a striking correlation (r = 0.49 and 0.51, respectively, $P < 10^{-6}$) between sedScore and transcript abundance (Figure 3.10A). That is, even in the absence of stress, abundant transcripts
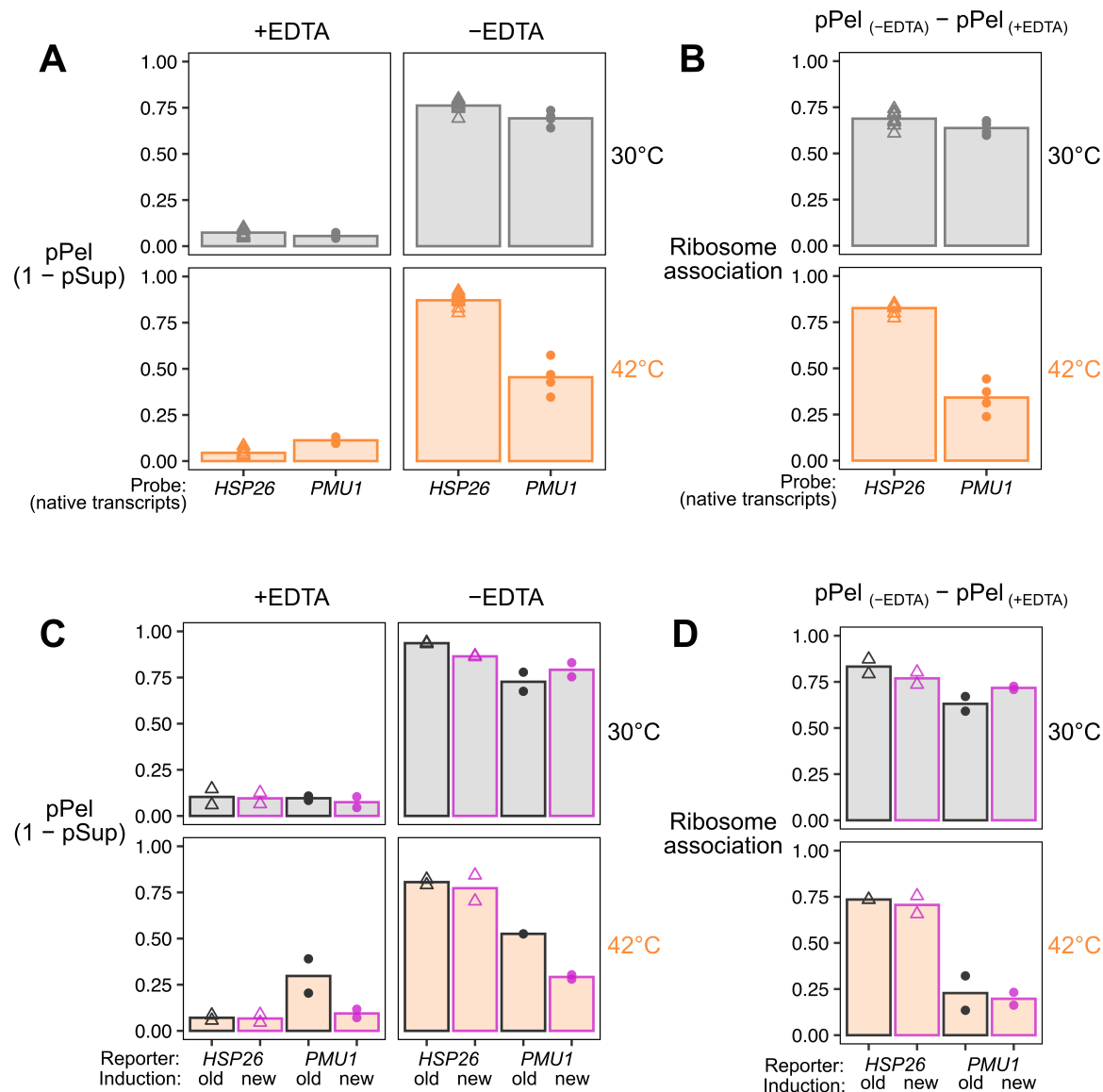
Figure 3.8: **Calculating ribosome association for translational reporters** (A) Cellular lysate from stressed (20 minutes at 42°C) or unstressed yeast was centrifuged through a 1M sucrose cushion with and without EDTA. The proportion of mRNA transcripts in the pellet was quantified with qPCR, normalized to spike-in RNA. (B) In the absence of EDTA, transcripts can pellet either because they are bound to ribosomes or because they are condensed, however ribosomes fall off transcripts in the presence of EDTA. Thus to calculate the ribosome occupancy, the pPel (+EDTA) is subtracted from the pPel (-EDTA). (C,D) The same samples as in (A) and (B), but tracking the abundance of the *HSP26* and *PMU1* reporters induced before stress (old) or after stress (new).

sediment less than rare transcripts. What could account for this observation? One feature of abundant transcripts is that they tend to be well-translated (Figure 3.10B). Indeed, the sedScores of transcripts during basal growth (at 30°C) showed an even stronger correlation with their translation state, as measured by ribosome occupancy—the fraction of an mRNA bound to at least one ribosome (Figure 3.9A, Spearman r = 0.66, P < 10^{-6}). To further test this result, we divided transcripts by the strength of the secondary structure in their 5' UTR, a feature known to predict the translation initiation efficiency of a transcript [Weinberg et al., 2016] (Figure 3.9A). Transcripts with the least and most predicted structure in their 5' UTR had, respectively, higher and lower sedScores than the bulk transcriptome. To explain this observation, we hypothesized that even during basal growth, poor translation initiation directly induces mRNA condensation which is observable in our sedimentation assay.
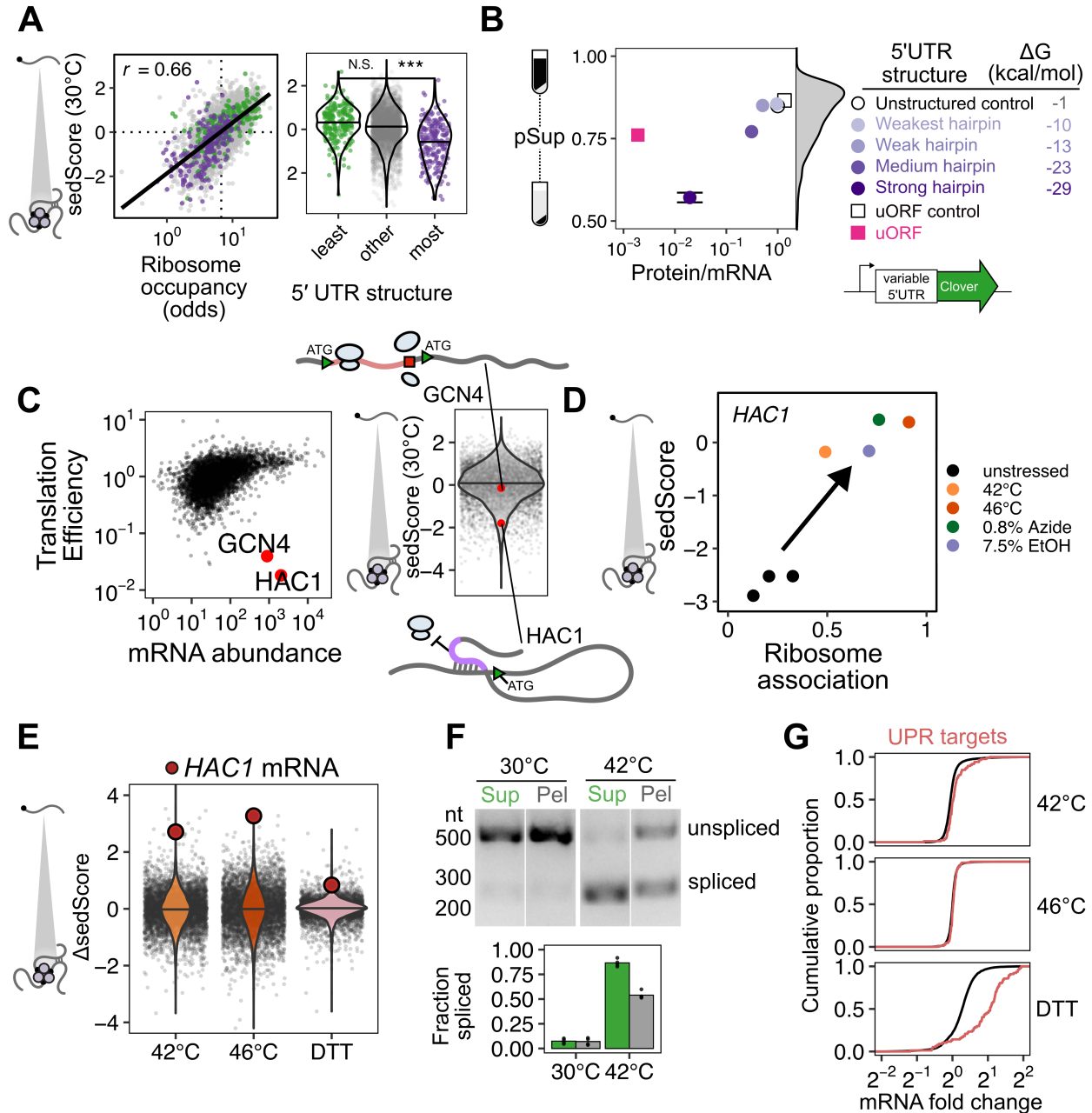
Figure 3.9: **Translation-initiation-inhibited condensates (TIICs) form in the absence of stress.** A) Left: Ribosome occupancy (fraction of a transcript bound to at least one ribosome) in unstressed cells correlates well with length-normalized sedimentation (sed-Score). Right: The amount of computationally predicted structure in the 5' UTR of transcripts predicts their sedScore. (B) Sedimentation reporters with variable strength 5' UTR hairpins or uORFs confirm the impact of translation initiation block on RNA condensation. Translation was quantified by the ratio of steady-state protein levels to mRNA abundance. Increased 5' UTR structure or the presence of a uORF leads to decreased translation and increased sedimentation.

Figure 3.9 *(previous page)*: ((C) *HAC1* and *GCN4* transcripts are both abundant and poorly translated, using data for translational efficiency from Weinberg et al. 2016. In unstressed cells, *HAC1* mRNA has a low sedScore while GCN4 mRNA exhibits nearly average sedimentation. (D) Across stresses, *HAC1* mRNA is translationally activated and also increases its relative sedimentation. (E) *HAC1* mRNA becomes less condensed during heat shock and DTT treatment. (F) 42°C treatment leads to splicing of *HAC1* mRNA as measured by RT-PCR, and the spliced form sediments less than the unspliced form. (G) UPR targets are slightly upregulated at 42°C and strongly upregulated in response to DTT treatment.

Accordingly, we asked whether we could recapitulate our in vivo observations of transcript-specific condensation using a series of synthetic mRNAs encoding the fluorescent protein Clover with progressively stronger translation initiation blocks created by hairpins in their 5' UTR [Weenink et al., 2018]. The hairpin series blocked translation initiation as measured by the ratio of fluorescence intensity to mRNA abundance, with more-stable hairpins more completely blocking translation (Figure 3.9B). As predicted, these constructs exhibited increased sedimentation which correlated with their translational efficiency (Figure 3.9B), demonstrating that in unstressed cells, a single species of translation initiation-inhibited mRNA forms sedimentable condensates.

Condensation of untranslated RNAs is consistent with a standard model for stress granule formation in which ribosome-free mRNA triggers condensation through RNA-mediated interactions [Guillén-Boixet et al., 2020, Hofmann et al., 2020, Sanders et al., 2020, Yang et al., 2020]. Are poorly translated transcripts condensing in unstressed cells because they lack ribosomes, or for some other reason? To investigate this further, we turned to a pair of exemplary endogenous transcripts. Among abundant transcripts in yeast—present in an estimated one copy or more per cell—two transcripts, *HAC1* and *GCN4*, stand out as being strongly translationally repressed in unstressed cells, either using translation efficiency data [Weinberg et al., 2016] (Figure 3.9C) or ribosome occupancy data reported here (Figure 3.10B). *HAC1* encodes the master regulator of the unfolded protein response (UPR)

while *GCN4* encodes the master regulator of the amino acid starvation response. *GCN4* has a length comparable to *HAC1* (1465 and 1197 nucleotides, respectively), and both are largely ribosome-free due to distinct mechanisms. Translation of upstream ORFs on the *GCN4* mRNA results in translation initiation but without translation of the main coding region[Hinnebusch, 2005], while RNA-RNA interactions within the *HAC1* mRNA block translation initiation[Cox and Walter, 1996].

However, the solubility of *GCN4* is typical for its length, whereas the solubility of *HAC1* is significantly lower than the mean of abundant transcripts (Figure 3.9C, S5C). *HAC1* transcripts sediment as if they were nearly four times the size of similar-length abundant mRNPs (Figure 3.10D), strongly hinting that condensation of multiple mRNPs, rather than merely additional mRNP mass, drives their sedimentation.
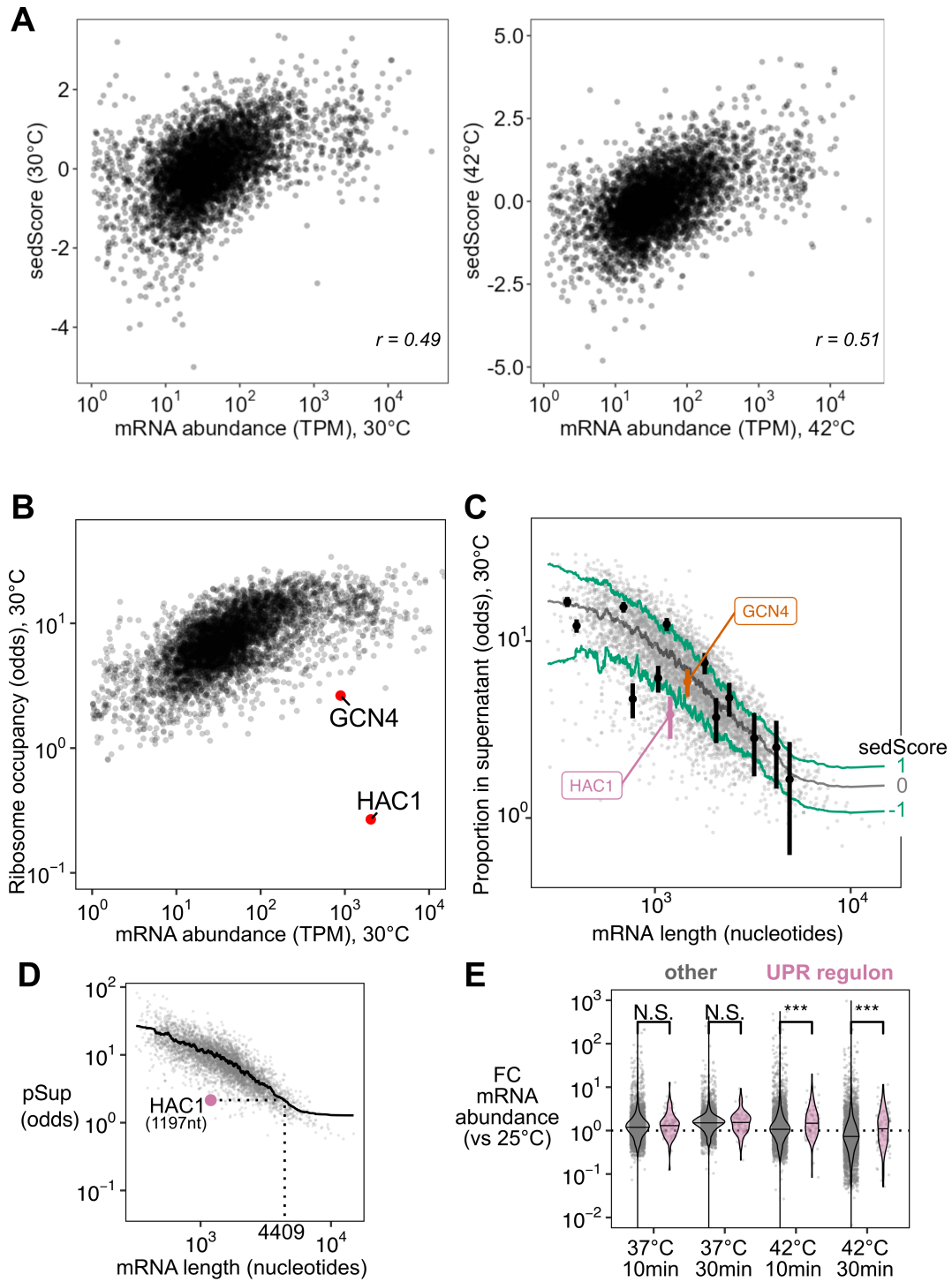
Figure 3.10: **SedScores at 30°C** (A) SedScores in unstressed (30°C) and stressed (42°C) cells correlate with mRNA abundance. Higher-expressed transcripts show lower levels of relative condensation (higher sedScores). Correlations shown are Spearman r, $P < 10^{-6}$.

Figure 3.10 *(previous page)*: (B) *HAC1* and *GCN4* transcripts stand out as being highly abundant but poorly translated, using ribosome occupancy data in unstressed cells reported in this manuscript. (C) *HAC1* has a consistently lower pSup (shown here in log-odds). Sedimentation data is from 7 different replicates of unstressed yeast with different hairpin reporters, as shown in Figure 3.9B. Each point represents the geometric mean of the transcript pSup across replicates. In addition to *HAC1* and *GCN4* transcripts, a random selection of genes are highlighted, with their standard error across replicates shown. Also shown is the pSup value corresponding to a sedScore of -1, 0, or 1 for each nucleotide length (see Methods). (D) *HAC1* mRNA sediments with a similar rate to transcripts that are 4x its length. (E) Reanalysis of Muhlhofer et al. 2020 RNA-seq data confirms that the UPR is upregulated after a 42°C stress but not a 37°C stress.

Consequently, ribosome-free mRNA, previously called the "universal trigger" of stress granule formation [Hofmann et al., 2020], cannot explain the sedimentation differences between *GCN4* and *HAC1*. Both species of transcripts are largely ribosome-free, yet only *HAC1* condenses. We replicated this difference with synthetic reporters that differed in their mechanisms of translation repression. A synthetic uORF construct built from the GCN4 5' UTR yielded substantially less condensation than the most stable hairpin construct, despite showing far stronger translational repression (Figure 3.9B). A control construct with five point mutations disrupting the start codon in each uORF[Mueller and Hinnebusch, 1986] promoted translation of the main open reading frame, as expected, and only modestly increased transcript solubility.

Together, these results form a coherent picture: a blockade in translation initiation, rather than the consequent exposure of ribosome-free mRNA, causes condensation affecting virtually the entire transcriptome under non-stress conditions. Because these non-stress condensates do not form microscopically visible foci and occur in the absence of stress, and thus are not stress granules, we refer to them as translation-initiation-inhibited condensates: TIICs ("ticks").

3.6 TIIC dissolution corresponds to translation initiation for UPR regulator *HAC1*

We noticed that *HAC1* mRNA, among the least-soluble transcripts in unstressed cells at 30°C (sedScore = -2.89), jumped by roughly three standard deviations in relative solubility upon a 10-minute heat shock at 42°C (ΔsedScore = 2.71) or 46°C (ΔsedScore = 3.27). The translation initiation inhibition of *HAC1* is relieved by mRNA splicing in the cytoplasm, leading to translation of the encoded *HAC1* transcription factor, its nuclear import, and subsequent UPR activation. This process was originally reported to be insensitive to heat stress using a 37°C shock [Cox and Walter, 1996]. Recently, a minor induction of *HAC1* splicing has been observed after hours of growth at 39°C [Hata et al., 2022]. The phenomena we observe above 42°C led us to hypothesize that this more robust heat shock caused dissolution of TIICs containing *HAC1* mRNA corresponding to relief of translation initiation inhibition by splicing. Indeed, across stresses, *HAC1* is both better translated and less condensed (Figure 3.9D). Multiple predictions follow: 1) *HAC1* TIIC dissolution should occur during activation by other UPR triggers; 2) *HAC1* should be spliced in response to the short heat shocks which trigger TIIC dissolution; 3) if *HAC1* mRNA is translated, the resulting *HAC1* transcription factor should drive transcription of UPR genes.

We tested each of these predictions in turn. First, we performed Sed-seq on cells treated with DTT, a standard UPR trigger. Confirming our prediction, *HAC1* mRNA showed among the strongest changes in relative solubility across the entire transcriptome upon DTT treatment (Figure 3.9E).

Second, we examined *HAC1* splicing in response to a 8-minute, 42°C heat shock. Before shock, *HAC1* mRNA was unspliced, running as a single large band. After shock, the spliced form of *HAC1* appeared as a smaller band (Figure 3.9F), confirming our second prediction. Under these conditions, *HAC1* is not completely spliced, which allowed us to make another

64

crucial observation: the spliced form of *HAC1* partitioned disproportionately into the soluble fraction relative to the unspliced form (Figure 3.9F), again consistent with *HAC1*'s formation of TIICs before stress and stress-induced dissolution.

Third, we looked for transcription of UPR genes at 42°C, as identified in Kimata et al 2006[Kimata et al., 2006]. We observed a slight but unmistakable induction after a 10-minute 42°C shock (Figure 3.9G, Wilcoxon rank sum test P $< 10^{-6}$). Based on this positive result, we predicted that other heat-shock data would show induction of the UPR at 42°C. Indeed, data from a systematic study of the heat shock response in budding yeast [Mühlhofer et al., 2019] revealed that UPR targets were not induced by a 37°C shock for 10 or 30 minutes (Wilcoxon test P values 0.15 and 0.70, respectively) as previously reported [Cox and Walter, 1996], but were significantly induced by 42°C shocks of 10 or 30 minutes (Wilcoxon test P values $< 10^{-3}$ in both cases) (Figure 3.10E).

Together, these results support a simple and previously unappreciated sequence of events during *HAC1* activation: *HAC1* mRNA, in TIICs before shock, decondenses and is spliced, permitting translation of the *HAC1* transcription factor protein which then drives UPR regulon transcription. Both DTT and short-term heat shock at 42°C produce this behavior.

Dissolution of *HAC1* TIICs and subsequent translation initiation at 42°C occurs while most other pre-stress transcripts experience the opposite effects, a blockade in translation initiation and formation of TIICs. The TIIC model predicts that globally blocking translation initiation, even in the absence of heat shock, should trigger transcriptome-wide mRNA condensation distinct from stress-granule formation. We therefore set out to test this prediction.

3.7 Blocking translation initiation at distinct steps causes mRNA condensation and implicates an upstream, competitive step

To block translation initiation at multiple steps, we generated different yeast strains with auxin-inducible degron (AID) tags on eight factors acting at multiple stages of initiation (Figure 3.11A,B) [Mendoza-Ochoa et al., 2019, Yesbolatova et al., 2020]. Western blotting confirmed successful translation initiation factor degradation (Figure 3.11C), which resulted in polysome collapse (Figure **??**A) and proteome-wide reduction in translation activity (Figure 3.11D, Figure **??**B–D).
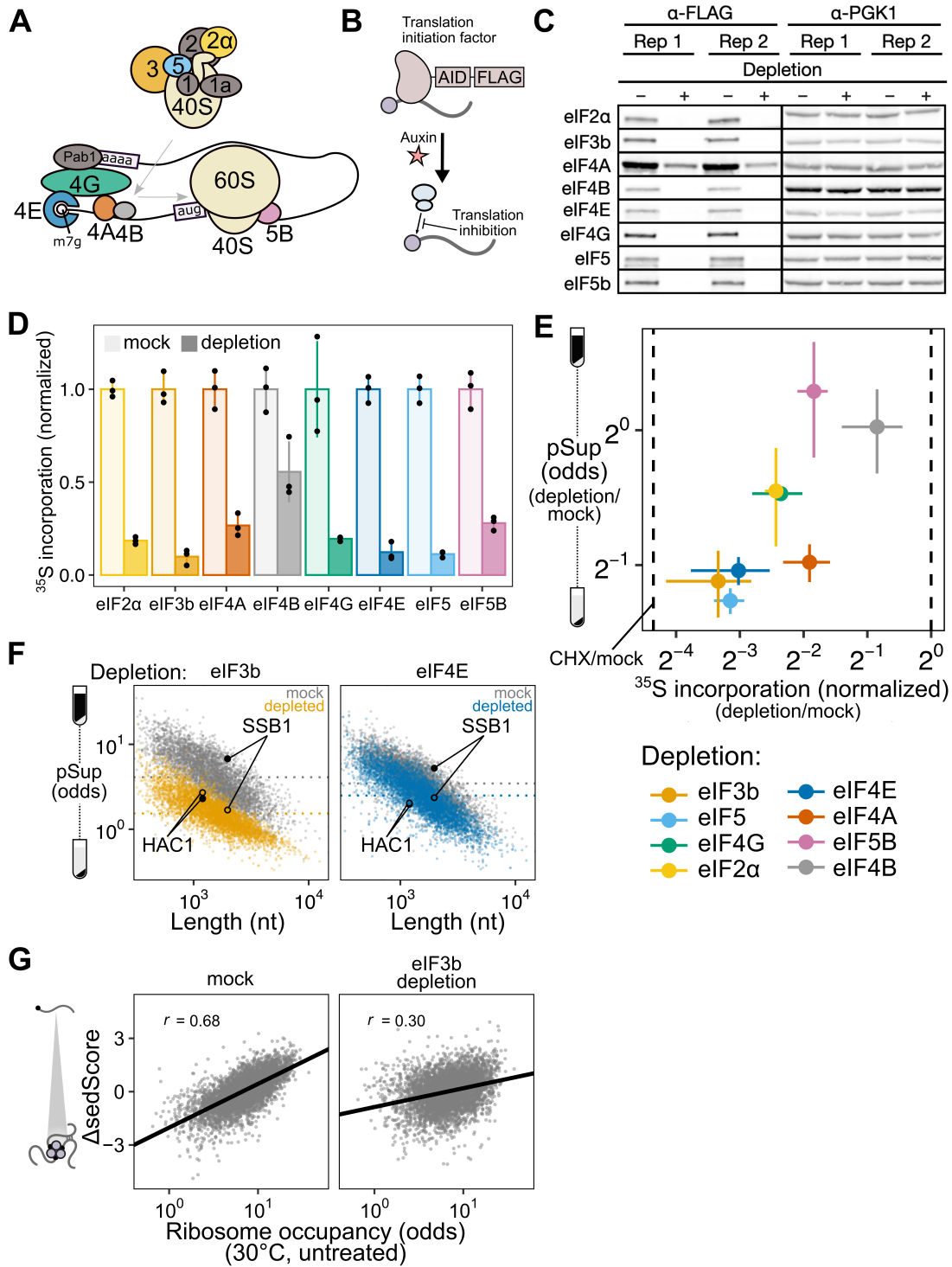
Figure 3.11: **Global translational initiation inhibition triggers transcriptome-wide TIICs.**

Figure 3.11 *(previous page)*: (A) Translation initiation factors involved in various steps of initiation were (B) depleted via the auxin-inducible degradation system. (C) Depletion for each factor was verified via western blot with Pgk1 used as a control. (D) The effect on global translation level caused by each initiation factor was tested by measuring the incorporation of radiolabeled amino acids. Each depletion caused a drop in translation to varying amounts. (E) The pSup of the *PGK1* and *BEM2* transcripts is strongly related to the amount of translation block caused by each initiation factor depletion, suggesting that none of these factors are essential for condensation. (F) Sed-seq was used after eIF3b and eIF4E depletion to measure global sedimentation. Depletion of both factors, and especially eIF3b, triggers global condensation—TIIC formation. (G) Left: The sedScore of transcripts correlates well with ribosome occupancy in the mock-treated sample, but this association is attenuated after eIF3b depletion.
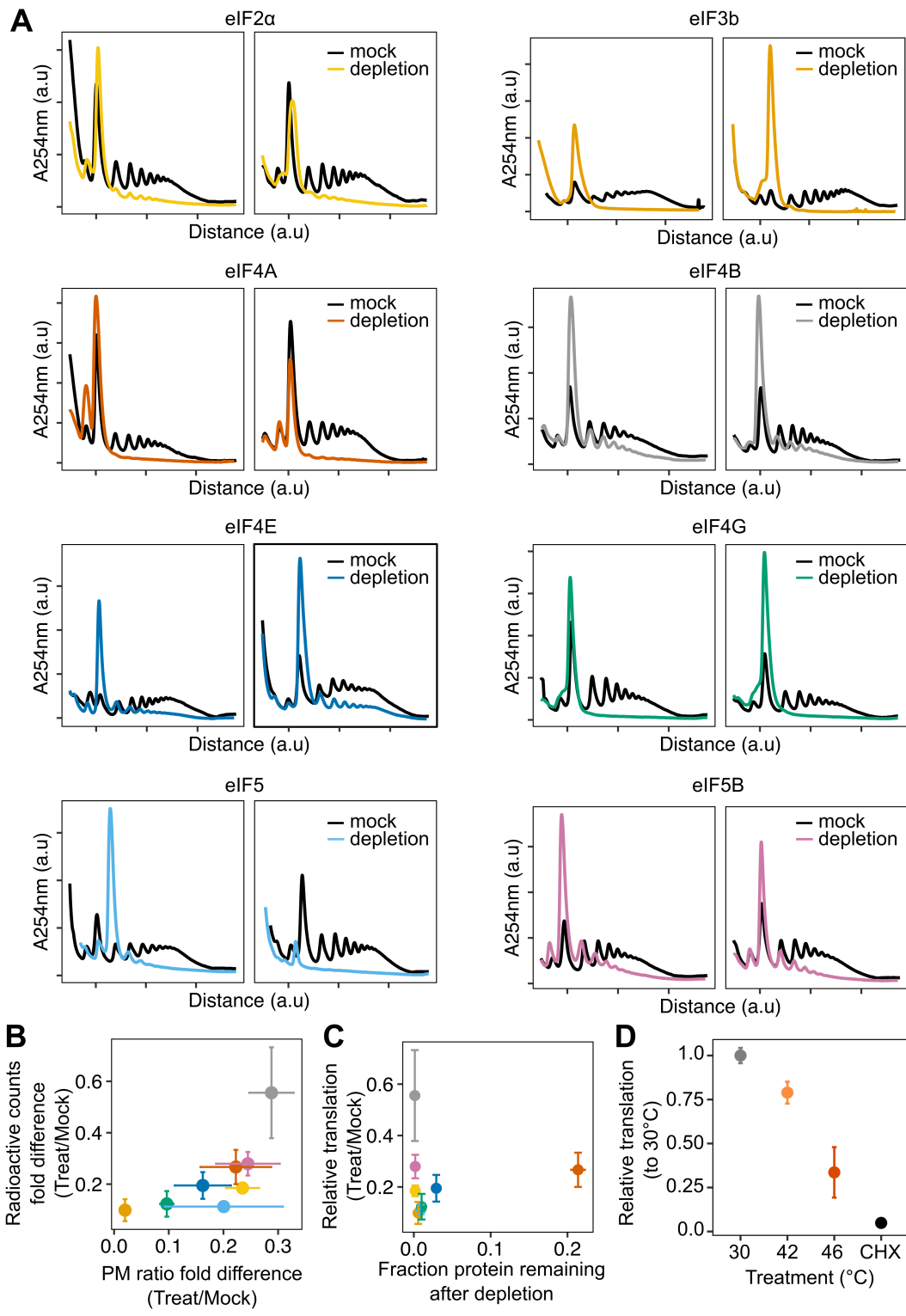
Figure 3.12: **Characterization of initiation factor-AID strains.**

Figure 3.12 *(previous page)*: (A) Polysome profiles of AID depletion strains. (B) Comparison of different measures of translation, including radiolabeled amino acid incorporation and polysome profiling. (C) Comparison of relative translation via radiolabeling versus the amount of each protein remaining after AID depletion. (D) Measures of relative translation via radiolabeled amino acid incorporation after 15 minutes of 30°C, 42°C, 46°C, or 100 µg/mL CHX.

We used qPCR to quantify the average pSup of two transcripts, *PGK1* and *BEM2*, following two hours of initiation factor depletion. As predicted, blocking initiation triggered mRNA condensation, with the degree of translation initiation block correlating with the extent of resulting mRNA condensation (Figure 3.11E). Depletion of eIF4B and eIF5B caused negligible condensation, but also had the smallest effect on translation. By contrast, eIF4A depletion caused particularly strong mRNA condensation, consistent with previous evidence showing that eIF4A inhibition can trigger SG formation [Mazroui et al., 2006, Tauber et al., 2020b].

How do initiation blocks affect condensation of individual transcript species? Our results above showed evidence for poorly initiated transcripts forming TIICs in unstressed cells, revealed by lower sedScore for transcripts with lower ribosome occupancy (Figure 3.9A). During global translation initiation block, we expect that all transcripts will form TIICs, leading to decreased pSups transcriptome-wide. To test this hypothesis, we performed Sed-seq on strains depleted for eIF4E, the mRNA cap-binding protein, and for eIF3b, the factor whose depletion led to the most severe block in translation. We observed transcriptome-scale mRNA condensation in both cases, to a profound degree after eIF3b depletion (Figure 3.11F). Because translationally repressed mRNAs already form TIICs in untreated cells, we predicted that they would show the smallest differences in sedimentation. Consistent with this prediction, initiation-inhibited *HAC1* mRNA showed almost no change after both depletions, whereas initiation-competent SSB1 mRNA showed marked changes, reflecting the

70

transcriptome average behavior (Figure 3.11F). Furthermore, reflecting the global conver-gence of sedimentation behavior during severe initiation block, the sedScores of transcripts in eIF3b-depleted cells are much less correlated with ribosome occupancy (Spearman r = 0.30) than the sedScores of transcripts in wild-type cells (Spearman r = 0.68) (Figure 3.11G).

Together, these results show that blocking translation initiation globally triggers global mRNA condensation and augments TIICs which are present in unstressed cells. We next sought to understand the relationship between TIICs, stress-induced mRNA condensation, and stress granules.

3.8   TIICs are stress-granule precursors

We counted stress granules before and after inhibiting translation initiation by eIF3b depletion, both in otherwise untreated and in heat-shocked cells (Figure 3.13A). Because automated counting scored some unstressed (30°C) cells as having multiple SGs, and all conditions show some degree of cell-to-cell variability, we scored populations of cells as SG-negative if the median number of SGs per cell was zero, and as SG-positive otherwise. Using this threshold, unstressed cells are SG-negative and cells shocked at 46°C are SG-positive (Figure 3.13A).
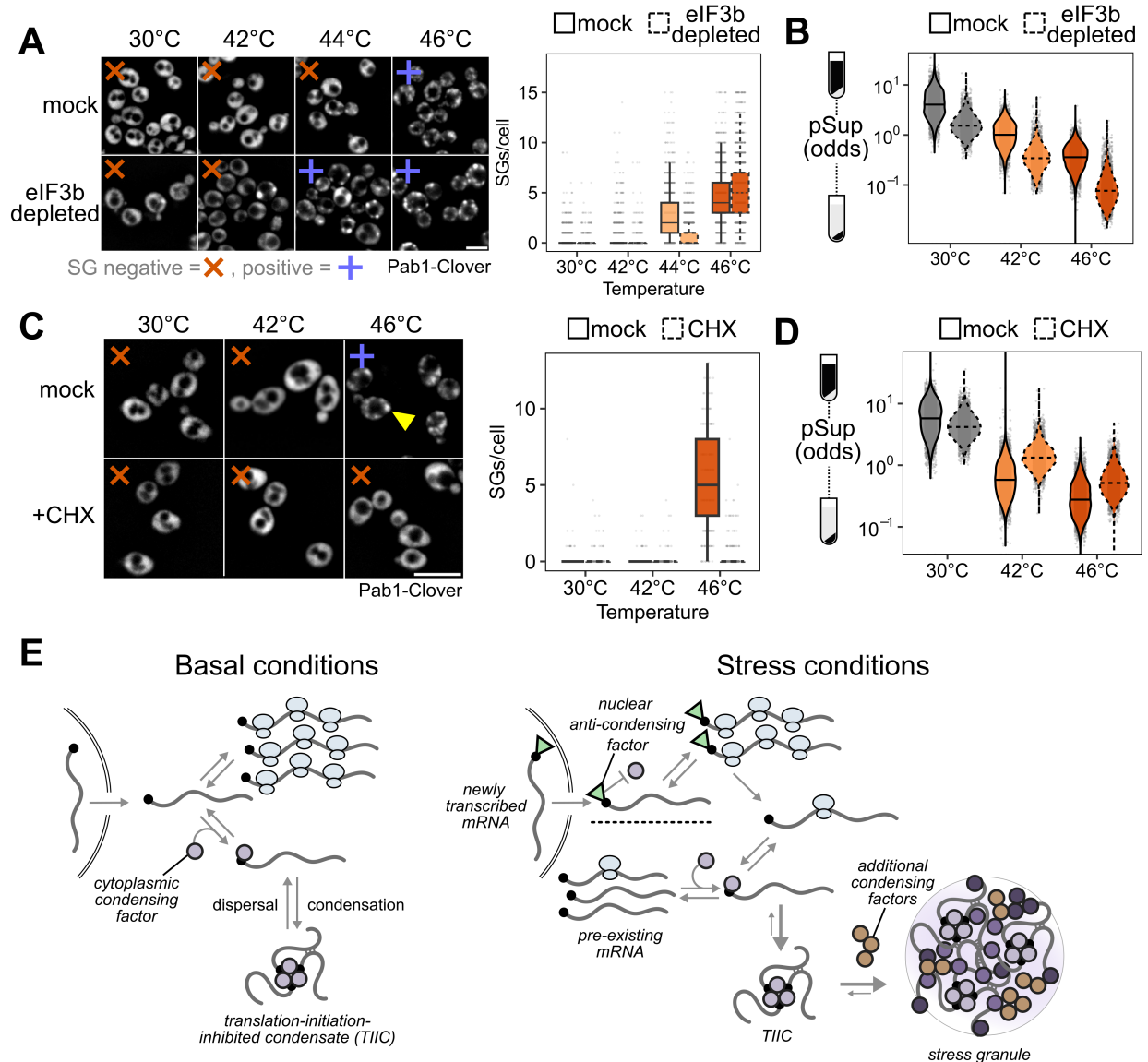
Figure 3.13: **TIIC formation precedes and potentiates stress-granule formation.**
(A) Stress granules are potentiated in eIF3b-depleted cells, as evidenced by the earlier appearance of stress granules compared to the mock treatment. Right: Quantification of the presence of stress granules in all conditions. (B) Sed-seq data comparing global condensation in eIF3b-depleted and mock cells after two hours of depletion followed by ten minutes of heat shock. eIF3b depletion triggers more RNA condensation at each temperature. (C) Ten minutes of cycloheximide (CHX) treatment prior to stress prevents visible stress granule formation. (D) CHX treatment inhibits, but does not prevent stress-induced RNA condensation.

72

Figure 3.13 *(previous page)*: (E) Model of the competition between translation initiation and TIIC formation during normal growth and stress. Well-translated transcripts are protected from condensation due to competition between translation initiation and TIIC formation. During stress, newly transcribed transcripts escape stress-induced condensation, likely due to a 5' bound protein or modification that inhibits condensation. Global inhibition of translation leads to transcriptome-wide TIIC formation. These TIICs are precursors of visible stress granules, whose formation involves additional stress-induced condensing factors.

After eIF3b depletion at 30°C, which causes substantial transcriptome-wide mRNA condensation (Figure 3.13B), cells are SG-negative (Figure 3.13A). We conclude that inhibiting translation initiation by eIF3b depletion causes TIIC formation but not SG formation, further confirming the distinction between TIICs and SGs.

Upon heat shock at 44°C, otherwise untreated cells are SG-negative, but when eIF3b is depleted, cells become SG-positive (Figure 3.13A). Thus, eIF3b depletion potentiates SG formation, strongly suggesting that TIICs are the building blocks for stress granules.

In every case, heat stress amplifies the mRNA condensation induced by translation initiation depletion. As we have already established above, this cannot be attributed to translation inhibition alone. Instead, the obvious hypothesis is that stress triggers additional condensation processes. While we do not yet know which molecules are responsible for this additional stress-induced mRNA condensation, multiple RNA-binding proteins have already been shown to autonomously sense heat shock and undergo condensation [Iserman et al., 2020, Krakowiak et al., 2018, Riback et al., 2017, Wallace et al., 2015].

As a final test of the provisional conclusion that TIICs are building blocks for stress granules, we asked how pharmacologically blocking SG formation affects mRNA condensation. Treatment with cycloheximide (CHX) prior to stress prevents stress granule formation[Mazroui et al., 2006, Wallace et al., 2015, Zhou et al., 2014], which we confirm—46°C heat-shocked cells are SG-positive, and 46°C heat-shocked cells pretreated with CHX are SG-negative (Figure 3.13C). There is a clear contrast between inhibiting translation initi-

ation (via depletion of eIF3b) and inhibiting translation elongation (via CHX): the former triggers SGs, while the latter prevents SGs.

However, CHX does not block mRNA condensation; stress-induced condensation is reduced, but remains substantial (Figure 3.13D). These results mirror those from studies of stress-induced protein condensation[Wallace et al., 2015]. We conclude that inhibiting SGs does not prevent mRNA condensation, consistent with our hypothesis that TI-ICs—condensed mRNAs—are precursors of stress granules.

3.9 Discussion

What is the physiological role of mRNA condensation in and outside of stress? Which mRNAs condense during stress, and why? What is the relationship between mRNA condensation, its functional causes and consequences, and stress granule formation?

We find that, across multiple stress conditions, virtually all preexisting mRNAs form translationally silent condensates to a degree which depends on stress intensity. At the same time, stress-induced transcripts escape condensation and are robustly translated. These results echo important early observations that stress granules exclude bulk nascent mRNA [Collier et al., 1988, Kedersha et al., 1999] and specific stress-induced heat shock protein transcripts [Kedersha et al., 2002, Stöhr et al., 2006]. Expanding and deepening these early results, our studies reveal that the timing of transcript production, rather than any particular transcript feature, is a primary determinant of escape from condensation; demonstrate the escape of dozens of stress-specific transcripts; and show that this escape from condensation guides selective translation. Still, a more fundamental result from our study, opening considerable new territory, is that stress granules per se play little if any role in these processes.

3.9.1 Small mRNA condensates are pervasive in the absence of stress or stress granules

Using a range of approaches, we discover the existence of pervasive mRNA condensation in cells without stress granule formation, and even in the absence of any discernible stress. Our results illuminate a previously unreported level of molecular organization governed by translation initiation: initiation-blocked transcripts cluster into structures we term translation-initiation-inhibited condensates (TIICs). TIICs can be generated for specific mRNAs by blocking message-specific initiation, or at the transcriptome scale by blocking initiation at any of several stages; they do not require environmental stress for their formation; and they can form when stress granules are either absent or are pharmacologically blocked. This latter result mirrors the persistence of condensates of poly(A)-binding protein when stress granules are blocked [Wallace et al., 2015]. In short, TIICs are not stress granules.

In our experiments, we make no attempt to isolate stress granules or their associated transcriptomes. Given that a range of stress conditions—physiological stresses such as 42°C heat shock and 5% ethanol, and the less-physiologically relevant but widely used 0.5% sodium azide—do not produce stress granules in our hands, but do produce considerable RNA condensation, considerable biology could be overlooked by focusing only on SG-forming conditions. We show that mRNA condensation, and specifically TIIC formation, precedes and potentiates stress granule formation, and we confirm by single-molecule FISH that stress-induced transcripts escape from stress granules. Overall, our results support a model in which stress-associated inhibition of translation initiation causes formation of TIICs which, under intense stress, further assemble into stress granules by separate processes.

3.9.2 mRNA condensation in cells is not primarily driven by ribosome-free RNA

Stress granules have long been thought to form after translation inhibition and ribosome runoff, exposing ribosome-free RNA which serves as platform for new intermolecular interactions, whether directly between RNAs or mediated by RNA-binding proteins [Jain and Vale, 2017, Khong et al., 2017b, Ripin and Parker, 2021, Van Treeck et al., 2018]. The profound effect of mRNA length in promoting apparent SG enrichment and in promoting RNA phase separation, with or without additional protein factors such as G3BP1, has provided a biophysical basis for the role of ribosome-free RNA: condensation of RNA due to multivalent RNA-mediated interactions would naturally be promoted by longer, and thus at least on average higher-valency, RNAs.

However, our results contradict the ribosome-free RNA model for condensation in multiple ways. First, we find that RNA length has little effect on stress-induced mRNA condensation once the effects of length on sedimentation, particularly for non-stress controls, are properly accounted for. Second, by comparing two abundant, similar-length, similarly ribosome-free mRNAs in budding yeast—GCN4 and *HAC1*—we show that only one, *HAC1*, undergoes condensation. This condensation is reversed under conditions which release the *HAC1*-specific blockade in translation initiation, and synthetic versions of both mRNAs reproduce the behavior of these native transcripts. Third, the translation elongation inhibitor cycloheximide, which freezes ribosomes on mRNAs, blocks stress granule formation but does not block mRNA condensation. This latter result is particularly problematic for models of stress granules in which ribosome-free mRNA is required for earlier stages of mRNA condensation.

Specific proposals have suggested that condensation mediated by intermolecular RNA-RNA interactions will occur when the RNA chaperone capacity of cells is exceeded, such as

during stress responses [Ripin and Parker, 2021]. A prediction of this model is that formation of such condensates will not be possible in cells with ample RNA chaperone capacity. This prediction is contradicted by our results demonstrating the formation of TIICs of specific mRNA species, both *HAC1* and synthetic constructs, in otherwise unstressed cells, with no evidence of more widespread condensation. Notably, recent work suggests that a single stalled ribosome suffices to inhibit mRNA recruitment to stress granules [Fedorovskiy et al., 2023], consistent with a model in which ribosomes act as inhibitory signals for stress granule recruitment, rather than as a physical impediment to RNA-sequence-mediated recruitment. Such a model is entirely consistent with our results showing that CHX blocks stress granule formation but not TIIC formation.

Moreover, our data are inconsistent with phase separation of RNA. Phase separation of biological molecules occurs above a critical concentration, resulting in formation of a dense phase; many RNA granules are thought to form in this way [Putnam et al., 2023]. We see no evidence for a critical concentration, either of specific RNAs or of bulk RNA. Indeed, higher-expression (and therefore higher-concentration) mRNAs are less likely to be found in TIICs (Figure 3.10A), and induction of transcripts correlates with their exclusion from condensates (Figure ??A), observations which go directly opposite the predictions of an RNA phase-separation model.

Altogether, we find no evidence supporting a role for ribosome-free RNA as a primary causal factor for mRNA condensation. Our results do not rule out an additional role for RNA-RNA interactions in stabilizing RNA-protein condensates once formed, which might explain some of the observed length-dependence in other datasets.

In contrast to length, we find a profound effect of translation initiation on condensation, supporting a model in which initiation and condensation compete. Such a model is conceptually similar to a translation-factor protection model proposed to regulate mRNA decay [Chan et al., 2018]. In essence, active translation initiation, focused on the 5' end of the mRNA,

physically blocks condensation, perhaps by blocking binding of a condensate-promoting factor (Figure 3.13E). Once initiated ribosomes proceed into the body of the message, the 5' end is no longer blocked and condensation can proceed. The strong connection between initiation and condensation is another possible explanation for previously observed correlations between granule association and transcript length in well-controlled studies, as transcript length itself negatively correlates with initiation rate [Arava et al., 2003, Weinberg et al., 2016].

What factors(s) cause condensation? While our data do not indicate a particular factor, they do appear to rule out a substantial number of potential individual candidates and narrow the search. Consider a provisional model in which a condensation factor targets (or is integral to) protein complexes formed at certain stages of initiation, such the model in mammalian systems in which stalled 48S preinitiation complexes serve as the seed of stress granules [Panas et al., 2016]. Depleting the condensation factor should inhibit condensation and solubilize mRNAs. Under this model, we can rule out initiation factors whose depletion promotes condensation (eIF2α, eIF4E, eIF4G, eIF4A, eIF3b, eIF5) as condensation factors, and by the same logic, rule out direct binding of a condensation factor to these proteins. Moreover, these initiation factors regulate early steps in both mRNA activation (eIF4E/G/A = eIF4F) and 48S preinitiation complex formation (eIF2α, eIF3b, eIF5), suggesting that neither associated protein complex either contains or is the target of a condensation factor.

Instead, our results are consistent with a model in which the condensation factor targets the mRNA cap directly, and scanning-complex assembly (eIF4F/mRNA/43S PIC) is the step at which the cap becomes blocked—thereby blocking condensation—until initiation is complete (Figure 3.13E). Disruption of either mRNA activation or 48S PIC formation blocks assembly of the scanning complex. Activation of mRNA by binding of eIF4F, including cap binding by eIF4E, is insufficient in this model to fully block cap if not followed by 43S recruitment, perhaps due to other proteins capable of destabilizing this interaction [Vilela

et al., 2000].

The single case where we observe strong initiation inhibition with no apparent condensation, depletion of eIF5B (compare to similar inhibition by eIF4A depletion which induces substantial condensation), fits this model: eIF5B regulates an initiation step (60S subunit joining) which occurs after scanning complex assembly, such that its depletion disrupts initiation without exposing the cap and promoting TIIC formation [Wang et al., 2019b].

The cap-dependent condensation model naturally implicates other proteins which bind the cap, including nuclear cap-binding proteins and decapping proteins. Suppression of stress granules by preventing phosphorylation of the decapping protein Dcp2, a major component of P-bodies, [Yoon et al., 2010] hints at a potential role for the latter. Indeed, while TIICs differ from P-bodies in that their formation is not blocked by cycloheximide, they otherwise share the properties of being associated with poorly translated mRNAs and being precursors to stress granules [Hubstenberger et al., 2017]. Another similarity is that yeast P-body foci are not visible in the absence of stress, but oligomeric assemblies of P-body components are nevertheless detectable [Rao and Parker, 2017]. This raises the possibility that the TIICs we observe are associated with at least part of the complex interaction network that leads to P-body formation.

3.9.3   How do newly synthesized mRNAs escape condensation?

Similar to the molecular determinants of TIIC formation, the specific determinants of escape from stress-induced condensation remain unknown. Our transcriptomic and reporter assays both show that transcripts transcribed during stress escape condensation regardless of sequence-encoded mRNA features or regulation by particular transcription factors. Timing of expression, in turn, suggests that these new transcripts are marked in some way before or during nuclear export, and that this mark blocks condensation while permitting trans-

lation initiation. Translation is not required for exclusion of new transcripts, because even when translation is fully inhibited by depletion of eIF3b, newly transcribed transcripts still escape. What might this condensation-inhibiting mark be? Possibilities include an mRNA modification such as methylation (or its stress-induced absence), changes in polyadenylation, or addition or subtraction of a protein factor. Nuclear cap-binding proteins, for example, could be stabilized in the cytoplasm during stress instead of being exchanged during a pioneer round of translation. Indeed, prior work suggests these proteins can support active translation during stress [Garre et al., 2012]. Our study provides a range of new reagents which might be employed in the search for this putative anti-condensation mark. However, the main contribution of our study on this front is clarifying how the mark is made: not by mRNA features or promoters or transcription factors, but by when an mRNA is produced.

While timing plays an important role in regulating escape from condensation, during stress this effect is layered with the competition between translation initiation and condensation. We show that a pre-induced but well-translated *HSP26* reporter is better protected against condensation than a poorly-translated *PMU1* reporter. This effect is also seen transcriptome-wide, as even transcripts whose abundance decreases during stress escape condensation if they are well-translated. These results support the model above in which mRNA condensation is driven by a condensation factor whose binding is in competition with the initiation machinery.

3.9.4 What are the functions of mRNA condensation?

In light of our results, an accounting of the cellular function of mRNA condensation must contend with three facts: the presence of condensation in unstressed cells, the strong causal link to translation initiation inhibition, and the exclusion of stress-induced messages. The latter result argues strongly against any simple mRNA-feature-based biophysical model

of RNA condensation, such as those invoking mRNA length, since we have shown that the timing of expression is decisive for mRNA recruitment. Exclusion of new messages and condensation of older messages also strongly favors an adaptive interpretation: stress-induced mRNA condensation helps cells rapidly redirect translational activity to transcripts most relevant to the cell's current situation.

We hypothesize that mRNA condensation provides cells with useful regulatory control over the translationally active transcriptome through a simple mechanism: preventing reinitiation of ribosomes on translationally stalled mRNAs by sequestering their 5' ends in a condensate. Condensation (which competes with decapping and potentially other processes in addition to reinitiation [Chan et al., 2018]) preserves these mRNAs for short-term retrieval by dispersal factors including molecular chaperones. Blocking reinitiation is crucial for redirecting translational activity, and separable from another effect which we do not explore but which is implied: protection of mRNAs from degradation [Escalante and Gasch, 2021, Hubstenberger et al., 2017, Moon et al., 2019], which would otherwise be another mechanism to prevent reinitiation.

Stress enhances both effects of condensation, prevention of reinitiation and protection, through widespread inhibition of translation initiation and consequent TIIC formation, condensation of additional RNA-binding proteins and related factors. Chaperones responsible for dispersing TIICs under basal conditions are titrated away to these stress-induced condensates. Chaperone titration slows TIIC dispersal, keeping ribosomes free to initiate on the stream of uncondensed transcripts emerging from the nucleus, and thus focusing the cell's translational activity on newly synthesized transcripts for an interval. This interval of translational focus ends when chaperones—whose genes, many under the transcriptional control of Hsf1, are powerfully induced by stress—become sufficiently abundant to disperse stress-induced condensates and TIICs back to pre-stress levels.

Multiple aspects of this condensation/dispersal model have been previously established:

formation of reversible condensates during stress, many of which are stress-granule proteins [Cherkasov et al., 2015, Jain et al., 2016, Wallace et al., 2015]; colocalization of Hsf1-regulon chaperones with stress-induced condensates [Cherkasov et al., 2013, Wallace et al., 2015]; the requirement for these chaperones for efficient condensate dispersal *in vivo* and *in vitro* [Cherkasov et al., 2013, Yoo et al., 2022]; and titration of chaperones from inhibitory binding of Hsf1 to stress-induced substrates, activating transcription [Krakowiak et al., 2018, Zheng et al., 2016]. Here, we have uncovered the key regulatory steps linking translation initiation, condensation, and selective translation. Many testable predictions flow from the synthesis of these observations into a regulatory model, perhaps most importantly the potential chaperone-mediated aspects of dispersal under basal conditions and recovery, which we have not addressed here.

No part of this regulatory model requires formation of visible stress granules or any similar so-called membraneless organelles; small clusters which depend on chaperones for dispersal, as with poly(A)-binding protein, suffice. Our work here clarifies problems for understanding the function and formation of stress granules per se. What is the function, if any, of gathering smaller condensates into large cytosolic foci? How are stress granules built from TIICs and other stress-induced condensates? How does the presence of ribosomes on mRNA prevent stress granules without preventing mRNA condensation? To what extent are these separable stages in assembling TIICs, other protein and RNA condensates, and stress granules conserved over evolutionary time? Many of these remain grand challenges in stress granule biology[Glauninger et al., 2022]. But separating mRNA condensation from stress granule formation is, in a sense, a smaller step than the other advance reported here: separating mRNA condensation from stress itself, and revealing a new layer of molecular organization in unstressed cells, one which extends even to the intensely studied central regulator of a major stress response. How TIICs form, dissolve, influence regulation, and so on outside of stress—how these previously unseen structures carry out previously unseeable

activities—now must become a focus.

3.10   Supplementary Text

3.10.1   A model of free mRNP sedimentation

Let be the length of an mRNA under consideration. We seek the functional form of $pSup(L)$, the proportion in the supernatant after centrifugation, which will depend on many factors. Several of these are experimental and we assume they do not change across samples or mRNAs, such as the spin speed ω, the sample height h, the spin time s, and the viscosity η. Terminal velocity for a particle with mass m and hydration radius r_0 is:

$$v_t(m, r_0) = \frac{m\omega^2 r}{6\pi\eta r_0} = \left(\frac{m}{r_0}\right)(\frac{\omega^2 r}{6\pi\eta}) \qquad (3.1)$$

We assume that both mass m and hydration radius r_0 scale consistently with length L on average. In the case of mass, we assume proportional scaling: a constant (average) molecular weight per unit length deriving from nucleotides and bound proteins. In the case of hydration radius, our scaling assumption is consistent with standard approaches [Yoffe et al., 2008], for the radius of gyration R_g scales as L^χ for naked ssRNA due to secondary structure. The hydration radius r_0 will be proportional to R_g assuming a constant density. The scaling relationship will also depend on the geometry of the vessel.

Assuming a constant mass per nucleotide and protein binding per unit length, the mass of an mRNP scales linearly with L. Therefore, the leading term above will tend to scale with L:

$$\frac{m}{r_0} = (c_1 L)^\chi \qquad (3.2)$$

with proportionality constant c_1 taking care of the specific conversion factors (e.g. the

83

molecular weight per nucleotide) and with χ summarizing the scaling.

Then the proportion of the particle species remaining in the supernatant is the proportion of the tube which is more than $v_t s$ from the bottom. That is: $v_t s$ from the bottom. That is:

$$pSup(m, r_0, h, s) = \begin{cases} 0 & v_t(m, r_0)s \geq h \\ 1 - \frac{v_t(m, r_0)s}{h} & 0 \leq v_t(m, r_0)s < h \end{cases} \qquad (3.3)$$

We can then summarize the dependencies with two constants, as follows.

$$\begin{aligned} pSup(L) &= 1 - \frac{v_t(m, r_0)s}{h} \\ &= 1 - (\frac{m}{r_0})(\frac{\omega^2 r}{6\pi\eta}) \\ &= 1 - c_2(c_1 L)^\chi \\ &= 1 - \beta L^\chi \end{aligned}$$

That is, two parameters should be sufficient to describe the average behavior of free (un-clustered) mRNAs of length . A simple test of this model arises from a particular prediction: by rearranging, we see that

$$\log(1 - pSup(L)) = \log(\beta) + \chi \log(L) \qquad (3.4)$$

which predicts a linear relationship between $log(1 - pSup(L))$ and $logL$. Indeed, our data show this relationship (Figure S1B).

3.10.2 A model of mRNP clustering

To model between-mRNP interactions and their effect on *pSup*, we consider two kinds of interactions, both assumed to be Poisson-distributed with rates which vary across conditions and potentially across transcripts.

The first interaction type is between nucleotides, including direct RNA-RNA interactions and interactions mediated by proteins but dependent on nucleotide content; these are expected to be length-dependent. Consequently, we model them by a per-nucleotide interaction rate v, such that the probability that an mRNP has k nucleotide-dependent interactions is

$$\Pr(k) = (\nu L)^k e^{-\nu L}/k! \tag{3.5}$$

The second interaction type is between molecules and is independent of sequence length, including interactions mediated by the 5' cap or the 3' end. We model these as a per-molecule interaction rate such that the probability that an mRNP has such interactions is

$$\Pr(m) = \frac{\mu^m e^{-\mu}}{m!} \tag{3.6}$$

These rates permit us to model the probability that an mRNP of a given length engages in interactions with other mRNPs, which may have varying lengths/sizes and may themselves also engage in additional interactions, making prediction of sedimentation highly complex. To proceed analytically, we make a simplifying assumption: that under the conditions we study, most mRNP clusters are sufficiently large to sediment completely (). Under this assumption, the observed proportion in the supernatant for an mRNA of length is given by the free-mRNP pSup multiplied by the probability that the mRNP is free. The latter probability is equal to the probability of per-nucleotide interactions and per-molecule interactions. Together, we have

$$pSup(L) = (1 - \beta L^{\chi})e^{-(\mu + \nu L)} \tag{3.7}$$

The mean behavior of transcripts in any particular experiment, in this model, can be derived from only four fitted parameters β, χ, μ, ν and the lengths of all transcripts. Fits of this model are shown in Fig. 1G, where the no-stress sample is modeled with no clustering ($\mu = 0, \nu = 0$) and stress samples are modeled with clustering (solid lines) and also in comparison to curves where the per-molecule interaction rate is zero ($\mu = 0$; dashed lines).

3.10.3 Bounds on condensate sizes

How can we put bounds on the average size of condensates, given an observed value of $pSup$? Any $pSup$ value can be realized in a range of ways, bounded by two extremes. At one extreme, the molecular population is homogeneous (all molecules of a particular type are in condensates of the same size), and all clusters have the same probability of remaining in the supernatant, which is $pSup$. At the other extreme, the molecular population is heterogeneous, with each species of condensate having some proportion in the supernatant $pSup_i$ and proportion of the molecular population q_i. Order the indices i such that the lightest species (monomers) has $i = 1$ and all condensates are ordered by their size (and hence in the descending order of their $pSup$) up to n.

First, if $n = 2$, it is clear that the observed $pSup \leq pSup_2$, simply because the average of two numbers is greater than or equal to the smaller of the two numbers.

Second, if we define the average of the condensates' $pSup$'s as $pSup_{cond}$, we have

$$pSup_{cond} = \frac{1}{1 - q_1} \sum_{i>1}^{n} q_i pSup_i$$

So that

$$pSup = q_1 pSup_1 + (1 - q_1)pSup_{cond}$$

which establishes $pSup \leq pSup_{cond}$ such that in general, $pSup$ is an upper bound on the average condensate size.

3.10.4   Alternatives to condensation

We considered the possibility changes in mRNA length during stress, either due to splicing or changes in polyadenylation, explain these solubility changes. Fewer than 5% of yeast genes contain introns, so splicing cannot account for the transcriptome-scale effects we observe. Polyadenylation yields poly(A) tails of only 50 nucleotides on average (3% of the median transcript length) which, in high-expression genes, grow slightly shorter upon heat stress [Tudek et al. 2021], not longer as would be required to decrease pSup during stress.

What about an increase in mRNP mass due to changes in protein binding? While formally possible, this would not plausibly increase free mRNP sizes by more than tenfold as we observe during severe stress. We provisionally conclude that changes in the physical size of otherwise free mRNPs cannot account for apparent sedimentation changes.

What about stress-induced binding to a large sedimentable structure, such as the ER, which has been argued to be the site of substantial protein synthesis of cytosolic proteins [Reid and Nicchitta 2015]? While we cannot rule all possibilities out, our data suggest this is not the case. Most importantly, substantial transcriptome-wide mRNA clustering occurs while poly(A)+ mRNA appears diffuse and primarily cytosolic (42°C, Fig. 1B/C), inconsistent with localization to the ER or another structure. Once clusters become visually resolvable—i.e., stress granules form—these are well-known to be distinct structures.

3.10.5   Simulation of complex condensation

To assess whether assumed effects produce observed phenomena, we turned to a detailed simulation of condensation and sedimentation (available along with other analytical code; see "Data and code availability" section in the main manuscript). Direct simulation of interactions, consequent formation of condensates in a fully heterogeneous population, and sedimentation of these heterogeneous condensates according to sedimentation theory by the model above, yields the same trends as in Fig. 1G (Fig. S1D,E). Fig. S1E shows a qualitatively excellent reproduction of the major trends in the biological heat-shock data (Fig. 1D), using only one parameter which varies during stress: the rate of interaction per molecule, which can arise e.g. through interactions mediated by the 5' or 3' ends of transcripts (see main text). Importantly, the simulation does not invoke a key assumption used in the analytical model above, which is that all condensates sediment completely.

3.11   Data and code availability

All raw sequencing data generated for this project have been deposited in GEO under accession code: [pending]. All other data and code is deposited at `https://github.com/j abard89/RNA_Condensation_2024/` or available upon request.

3.12   Methods

3.12.1   Cell growth and stress conditions

Unless otherwise noted, the BY4741 strain of Saccharomyces cerevisiae was used in experiments. All experiments were done with at least two biological replicates, starting from growth. Cells were grown at 30°C in synthetic complete dextrose media (SCD) for at least 12 hours to OD600 = 0.4 before being exposed to stress. Temperature stresses for sedi-

mentation experiments were completed by centrifuging the culture and exposing the yeast pellet to either 42°C or 46°C water baths. Control cells were placed inside a 30°C incubator. Cycloheximide treated cells were pre-treated for 10 minutes with 100 μg/mL cycloheximide (Sigma #C7698-5G) before heat shock. Azide stresses were completed at either 0.5% w/v or 0.8% w/v for 30 min in SCD adjusted to pH 6.8 with NaOH. Azide was added from a 10% w/v sodium azide stock in water. Mock treatments were completed by adding pure water at the same volume to cultures. Ethanol stresses were completed by resuspending centrifuged cell pellets in SCD made with either 5%, 7.5%, 10%, or 15% ethanol for 15 min. Control cells were mock treated by resuspending in normal SCD. DTT treated cells were treated with 10 mM DTT for 15 minutes prior to harvesting. Temperature stresses for polysome sequencing and for tet-inducible reporter experiments were done by growing 250 mL of yeast in SCD overnight to OD600 = 0.4, collecting yeast via vacuum filtration onto a 0.45 μm filter (Cytiva 60206), putting the filter in 125 mL of pre-warmed media and incubating in a temperature controlled shaking water bath or incubator. After the indicated time, samples were harvested again via vacuum filtration and immediately scraped into liquid nitrogen.

Yeast transformations were performed either using a standard lithium acetate transformation or Zymo Frozen-EZ Yeast Transformation II Kit (Zymo #T2001) before plating on appropriate selection media79. Clones were verified by colony PCR and Sanger sequencing.

3.12.2   Generation of spike-in RNA

In-vitro transcribed (IVT) RNA or purified Schizosaccharomyces pombe total RNA was used as spike-ins where noted. The IVT RNA was produced by first amplifying a linear DNA fragment encoding NanoLuc using Q5 polymerase (NEB #M0494S), and purifying the DNA using an NEB clean and concentrate kit . The RNA was then made using a T7 Highscribe kit (NEB #E2040S), treated with DNase I (NEB #M0303L) and purified using

an NEB clean and concentrate kit (NEB #T2030). For the S. pombe RNA, fission yeast (FY527) was grown in YES media (5 g/L yeast extract, 30 g/L glucose, 225 mg/L adenine, histidine, leucine, uracil and lysine hydrochloride) at 32°C until OD600 = 0.5, harvested by centrifugation (3 minutes at 2500 g), resuspended in Trizol, and lysed by vortexing with 0.5 mm zirconia glass beads before extracting RNA using Zymo Direct-zol kits (Zymo #R2072).

3.12.3   Fractionation-by-Sedimentation-sequencing (Sed-seq)

Biochemical fractionation was completed similarly to Wallace et al. (Wallace et al. 2015), with the major exception that 20,000 g for 10 min was used rather than the original 100,000 g for 20 min. In short, 50 mL cultures of treated yeast were harvested by centrifugation at 3000 g for 5 minutes, then resuspended in 100 μL of soluble protein buffer (SPB: 20 mM HEPES, pH 7.4, 140 mM KCl, 2 mM EDTA, 0.1 mM TCEP, 1:200 protease inhibitor (Millipore #539136), 1:1000 SUPERase•In RNase Inhibitor (Invitrogen #AM2696)), and flash frozen in liquid nitrogen as a pellet in a 2 mL Eppendorf Safe-Lock tube (Eppendorf #0030123620) with a 7 mm steel ball (Retsch #05.368.0035). The cells were then lysed using a Retsch MM400 for 5x90s at 30 Hz, chilling in liquid nitrogen between each shaking repeat. The lysed cells were resuspended in 600 μL of SPB, and 100 μL of total sample was transferred to 300 μL of Trizol LS (Invitrogen #10296010). For the S. pombe spike-in experiment, purified S. pombe total RNA was added to the lysate immediately after resuspension in SPB. The remainder was centrifuged for 30 seconds at 3000 g, and 300 μL of clarified lysate was transferred to a new 1.5 mL tube. This was then centrifuged for 10 minutes at 20,000 g. A 100 μL supernatant sample was transferred to 300 μL of Trizol LS, and 400 μL of SPB was added to the pellet as a wash. After another spin at 20,000 g for 10 minutes, the supernatant was removed and the pellet was resuspended by vortexing for 15 minutes in 300 μL of Trizol LS and 100 μL of water. If required, 1 ng of spike-in transcript

was added to each sample at this step before RNA was isolated using Zymo Direct-Zol RNA extraction columns (Zymo #R2052), and RNA integrity was assessed by the appearance of two sharp rRNA bands on a 1% agarose gel and quantified using the absorbance at 260 nm.

3.12.4 RNA quantification by RT-qPCR

Reverse transcription for qPCR was either performed using gene-specific reverse priming with the iScript™ Select cDNA Synthesis Kit (Bio-Rad #1708897) or using NEB LunaScript RT SuperMix kit (NEB #E3010L). In both cases, manufacturer protocols were followed using an input of 2.5 ng of RNA per μL of reaction. For gene-specific priming, the reverse primer was used at 5 μM. The IDT Primetime gene expression master mix (IDT #1055771) was used for quantitative PCR on a Bio-Rad CFX384 instrument with Taqman probes (1.5 μM for primers; 600 nM probe). For samples with spike-ins, abundances were calculated relative to the spike-in abundance using the $\Delta\Delta$Cq method.

3.12.5 Polysome collection and analysis

Around 100 mg of frozen yeast that was collected by vacuum filtration was transferred to a pre-chilled 2 ml Eppendorf "Safe-Lock" tube. Cells were lysed with a pre-chilled 7 mM stainless steel ball (Retsch #05.368.0035) by 5x90sx30Hz pulses in a Retsch MM100 mixer mill, chilling in liquid nitrogen (LN2) between pulses. Sample was resuspended in 10:1 (v/w) polysome lysis buffer (20 mM HEPES-KOH (pH 7.4), 100 mM KCl, 5 mM MgCl2, 200 μg/mL heparin (Sigma #H3149), 1% triton X-100, 0.5 mM TCEP (Goldbio #TCEP25), 100 μg/mL cycloheximide (Sigma #C7698-5G), 20 U/ml SUPERase•In (Invitrogen #AM2696), 1:200 Millipore protease inhibitor IV #539136). The lysate was clarified by centrifugation at 3000 g for 30 s, and the clarified lysate was transferred to new tube and aliquots were flash frozen in LN2.

A 10–50%continuous sucrose gradient in polysome gradient buffer (5 mM HEPES-KOH (pH 7.4), 140 mM KCl, 5 mM MgCl2, 100 μg/ml cycloheximide, 10 U/ml SUPERase•In, 0.5 mM TCEP) was prepared in SW 28.1 tubes (Seton #7042) using a Biocomp Gradient Master and allowed to cool to 4°C. Clarified lysate (200 μL) was loaded on top of the gradient, and gradients were spun in a SW28.1 rotor at 27,500 rpm for 3.5 hr at 4°C. Gradients were fractionated into 0.6mL fractions using a Biocomp Piston Gradient Fractionator with UV monitoring at 254 nm, and fractions were flash frozen in LN2. UV traces were normalized to the total signal starting with the 40S peak.

The samples were generated by pooling 50 μL of each fraction from the free fraction (before the monosome peak) and either separately pooling the fractions with 3+ ribosomes bound and the mono/di-some fractions (for the heat shock experiments), or by combining all ribosome-bound fractions together (azide and ethanol stresses). The spike-in (50 ng of S. pombe total RNA) was then added to each pooled sample. RNA was purified via ethanol precipitation (final concentrations of 0.3 M sodium acetate pH 5.2, 0.3 μg/mL glycoblue (Invitrogen #AM9516), and 70%ethanol) at -20°C overnight followed by centrifugation at 4°C for 30 minutes at 21,000 g. The pellet was washed with 1 mL of 70%ethanol before being resuspended in water. The purified RNA was then treated with Dnase I (NEB) before purifying again using an NEB RNA clean and concentrate kit (NEB #T2030).

3.12.6   Sucrose cushion ribosome occupancy analysis

The ribosome occupancy (fraction of mRNA bound to ribosome) for the induction re-porters was measured by spinning lysate through a sucrose cushion. Around 100 mg of frozen yeast was transferred to a pre-chilled 2 ml Eppendorf "Safe-Lok" tube. Cells were lysed with a pre-chilled 7 mM stainless steel ball (Retsch #05.368.0035) by 5x90sx30Hz pulses in a Retsch MM100 mixer mill, chilling in liquid nitrogen (LN2) between pulses. Sample was re-

suspended in 10:1 (v/w) polysome lysis buffer (20 mM HEPES-KOH (pH 7.4), 100 mM KCl, 5 mM MgCl2, 200 μg/mL heparin (Sigma #H3149), 1% triton X-100, 0.5 mM TCEP (Gold-bio #TCEP25), 100 μg/mL cycloheximide (Sigma #C7698-5G), 20 U/ml SUPERase•In (Invitrogen #AM2696), 1:200 Millipore protease inhibitor IV #539136). The lysate was clarified by centrifugation at 3000 g for 30 s, and 500 μL clarified lysate was transferred to a new tube.

At this point the sample was split into +/- EDTA samples. For the +EDTA samples, 6 μL of 0.5 M EDTA (pH 8 in water) was added to 150 μL of clarified lysate and incubated on ice for 10 minutes. Then 100 μL of both samples (+/- EDTA) was gently added on top of 900 μL of matching sucrose cushion (5 mM HEPES-KOH (pH 7.4), 140 mM KCl, 5 mM MgCl2, 100 μg/ml cycloheximide, 10 U/ml SUPERase•In, 0.5 mM TCEP, 20%sucrose w/v, +/- 20 mM EDTA) and centrifuged for 60 minutes at 100,000 g in a TLA55 rotor (Beckman-Coulter) at 4°C. The top 250 μL of supernatant was removed as the supernatant sample and 100 μL of this was mixed with 300 μL Trizol LS. The remaining supernatant was discarded before resuspending the pellet in 100 μL water + 300 μL Trizol LS (pellet is 10x relative to supernatant). To the pellet 1 ng of spike-in RNA was added, but only 0.1 ng was added to the supernatant.

RNA was purified from the supernatant and pellet samples using Zymo Direct-Zol kits, then the abundances of target RNAs were quantified via qPCR as above. Ribosome occupancies were calculated by calculating the percentage of each transcript in the pellet, after correcting for the pelleting observed in the presence of EDTA (this separates EDTA-sensitive polysomes in the pellet from EDTA-insensitive condensates). RNA sequencing

In general, DNase I treated RNA was prepared for sequencing using rRNA depletion (Illumina RiboZero (Illumina #MRZY1306) or Qiagen FastSelect (Qiagen #334215) followed by NEB NEBNext Ultra II (NEB #E7760) or Illumina TruSeq library preparation and Illumina platform sequencing. Specific methods for library preparation, sequencing and

initial data analysis are described below and the method used for each sample is indicated in Table S4.

3.12.7 Sequencing analysis

Genome references

Saccharomyces cerevisiae reference genome files (S288C_reference_genome_R64-3-1_20210421) were downloaded from the Saccharomyces Genome Database (SGD)80. Schizosaccharomyces pombe reference genome files were downloaded from PomBase81. When appropriate (see Table S4), the sequences of the NanoLuc spike-in or the mCherry and Clover reporters were included in the genome and transcriptome files for mapping.

Group A (see Table S4):

Sequencing libraries were prepared by the University of Chicago Genomics Facility from DNase I treated RNA using Illumina RiboZero (Illumina #MRZY1306) and Illumina TruSeq library prep kits. Single end 50 bp sequencing was performed on an Illumina HiSeq 4000 sequencer.

Sequencing reads were trimmed using TrimGalore (v0.6.10, `https://github.com/Fel ixKrueger/TrimGalore`) using default settings (e.g. `trim_galore -gzip -fastqc_args '-outdir fastqc/' -j 4 -o trimmed -basename FW32 EW_FW32_R1.fastq.gz`). They were mapped using STAR v2.7.10b82 (e.g. `STAR -outSAMtype BAM Unsorted -readFilesCommand gunzip -c -sjdbGTFfile saccharomyces_cerevisiae_R64-3-1_20210421_nofasta_geneid.gff -sjdbGTFtagExonParentTranscript Parent -sjdbGTFfeatureExon CDS -sjdbGTFtagExonParentGene gene_id -runThreadN 4 -alignMatesGapMax 20000 -limitBAMsortRAM 1445804817 -genomeDir`

```
STAR_saccharomyces_cerevisiae_R64-3-1_20210421_allchrom -outFileNamePrefix mapped_reads/
-readFilesIn trimmed/FW32_trimmed.fq.gz).
```
To generate estimated counts and tran-
script per million (TPM) values, sequencing reads were mapped to the yeast transcriptome
using kallisto v0.48.083 (e.g. `kallisto quant -i Scerevisiae_orf_coding_all_Scerevisiae_rna_cod`
```
-o kallisto_quant/FW32 -single -l 200 -s 1 -rf-stranded -bootstrap-samples=50
-t 1 trimmed/FW32_trimmed.fq.gz).
```

Group B (see Table S4):

Sequencing libraries were prepared by from DNase I treated RNA using Qiagen FastSelect
(Qiagen #334215), NEBNext Multiplex Oligos (UMI Adaptor RNA Set 1, NEB #E7335L)
and NEBnext Ultra II Directional RNA library prep kits (NEB #E7760L). Paired end 200
bp sequencing with additional reads for dual 8/8 indices plus the 11nt UMI after the i7 index
was performed on an Illumina NovaSeq 6000 at the University of Chicago Genomics Facility.

The unique molecular indices (UMIs) were extracted from fastq R2 using Umi-Tools
v1.1.484 and stored in fastq R1 and R3 (e.g. `umi_tools extract -bc-pattern=XXXXXXXXNNNNNNNNNNN`
```
-I ADJB1SHG02_S2_R2_001.fastq.gz -read2-in=ADJB1SHG02_S2_R1_001.fastq.gz -read2-out=labe
```
Sequencing reads were then trimmed using TrimGalore (v0.6.10, `https://github.com`
`/FelixKrueger/TrimGalore`) using default settings (e.g. `trim_galore -paired -gzip`
```
-fastqc_args '-outdir fastqc/' -j 4 -o trimmed -basename HG002 labeled_fastq/HG002/HG002
labeled_fastq/HG002/HG002_R3.umi.fastq).
```
They were mapped using STAR v2.7.10b82
(e.g. `STAR -outSAMtype BAM Unsorted -readFilesCommand gunzip -c`
```
-sjdbGTFfile spike_saccharomyces_cerevisiae_R64-3-1_20210421_geneid.gff3
-sjdbGTFtagExonParentTranscript Parent -sjdbGTFfeatureExon CDS
-sjdbGTFtagExonParentGene gene_id -runThreadN 4 -alignMatesGapMax 20000 -limitBAMsortRAM
1445804817
```

```
-genomeDir STAR_spike_saccharomyces_cerevisiae_R64-3-1_20210421
-outFileNamePrefix mapped_reads/HG002/HG002_ -readFilesIn
trimmed/HG002_val_1.fq.gz trimmed/HG002_val_2.fq.gz).
```
Umi-Tools was then used again to deduplicate the reads (e.g. `umi_tools dedup -stdin=mapped_reads/HG002/HG002_Aligned_Sor`
```
-chimeric-pairs=discard -unpaired-reads=discard -spliced-is-unique -paired -S
mapped_reads/HG002/HG002_Aligned.sortedByCoord.dedup.out.bam).
```
The reads were split again into fastq files using samtools v1.16.185, and then estimated counts and TPMs were generated using kallisto v0.48.083 (e.g. `kallisto quant -i spike_Scerevisiae_orf_coding_all_S`
```
-o kallisto_quant/HG002 -rf-stranded -bootstrap-samples=50 -t 1 mapped_reads/HG002/HG002
mapped_reads/HG002/HG002_Aligned_dedup_R3.fastq.gz).
```

Group C (see Table S4):

Sequencing libraries were prepared by the University of Chicago Genomics Facility from DNase I treated RNA using Qiagen FastSelect (Qiagen #334215) and Illumina Stranded mRNA Prep (Illumina #20020595) kits. Paired end 200 bp sequencing was performed on an Illumina NovaSeq 6000.

Sequencing reads were trimmed using TrimGalore (v0.6.10, `https://github.com/Fel` `ixKrueger/TrimGalore`) using default settings (e.g. 'trim_galore –paired –fastqc_args '–outdir fastqc/' -j 4 -o trimmed –basename F02 AD-JB-F02_S44_R1_001.fastq.gz AD-JB-F02_S44_R2_001.fastq.gz'). They were mapped using STAR v2.7.10b82 (e.g. 'STAR –outSAMtype BAM Unsorted –readFilesCommand gunzip -c –sjdbGTFfile spike_saccharomyces_cerevisiae_ 3-1_20210421_geneid.gff3 –sjdbGTFtagExonParentTranscript Parent –sjdbGTFfeatureExon CDS –sjdbGTFtagExonParentGene gene_id –runThreadN 4 –alignMatesGapMax 20000 – limitBAMsortRAM 1445804817 –genomeDir STAR_spike_saccharomyces_cerevisiae_R64-3-1_20210421 –outFileNamePrefix mapped_reads/F02/F02_ –readFilesIn trimmed/F02_val_1.fq.gz

trimmed/F02_val_2.fq.gz'). The estimated counts and TPMs were generated using kallisto v0.48.083 (e.g. 'kallisto quant -i spike_Scerevisiae_orf_coding_all_Scerevisiae_rna_coding.fasta.idx -o kallisto_quant/F02 –fr-stranded –bootstrap-samples=50 -t 1 trimmed/F02_val_1.fq.gz trimmed/F02_val_2.fq.gz').

3.12.8   Calculation of pSup

Public code for calculating pSup from sequencing data is available here: `https://gith ub.com/jabard89/sedseqquant`. The statistical model used to estimate the proportion in supernatant (pSup) was based on that used in Wallace et al. (2015) 25. For each fractionated sample, the number of counts of mRNA within each fraction—total (T), supernatant (S), and pellet (P)—were extracted from RNA-sequencing data (see ["Sequencing Analysis" section above]). While mRNAs are expected to obey conservation of mass in the original fractionated lysate (Ti =Si + Pi for mRNA species i), this assumption does not hold in the ratios of abundances directly inferred from the data. Instead, for a particular experiment, Ti = SSi + PPi where we refer to the per-experiment constants S and P as mixing ratios which reflect differential processing and measurement of individual fractions. In order to estimate mixing ratios, and thus recover the original stoichiometry, we assume conservation of mass for each mRNA in the sample, and then estimate the mixing ratios under this constraint using a Bayesian model 86. We assume negative binomial noise for each count measurement, and log-normal underlying distribution of mRNA abundance. Specifically, we model counts as follows:

$$\log(T_i) \sim \text{NB}(\log(S_i + P_i),)$$

97

where

$$T_i = \text{measured abundance of mRNA } i,$$

$$S_i = \text{measured abundance in supernatant of mRNA } i,$$

$$P_i = \text{measured abundance in pellet of mRNA } i,$$

$$S = \text{mixing ratio of supernatant sample},$$

$$P = \text{mixing ratio of pellet sample}.$$

With the following priors:

$$S \sim \text{Cauchy}(0, 3),$$

$$P \sim \text{Cauchy}(0, 3).$$

We implemented the model above in R using the probabilistic programming language STAN, accessed using the rstan package 87,88 and used all mRNA with counts> 20 to estimate mixing ratios for each sample. These mixing ratios were then used to calculate the pSup for mRNA i: pSupi=SSiSSi+PPi.

3.12.9 Other bioinformatic analyses

Transcript features

Transcript features were extracted from Saccharomyces Genome Database (SGD)(Cherry et al. 2012). Targets of HSF1 and MSN2/4 were based off those reported in Pincus et al. 201840 and Solis et al. 201641. Transcript UTR lengths were taken as the median value reported by long read transcript sequencing in Pelechano et al. 201389, or, when no data was reported, the median UTR length in yeast was used as the default. Pombe transcript

lengths, including the lengths of the UTRs, was taken from PomBase81.

Transcript abundance

The transcript abundance is reported as the geometric mean of the TPM value for two biological replicates, estimated by kallisto analysis of the Total fraction for each sample. Changes in transcript abundance were calculated using DeSeq290.

sedScore calculation

In order to calculate sedScores, the pSup for each transcript was converted to a log-odds scale, and transcripts were arranged by their length (including UTRs), and then binned into groups of 100. For each transcript in the bin, the standard deviation from the mean within the bin was used to calculate a Z-score. Individual Z-scores from two biological replicates were calculated and then averaged together for the final reported sedScore.

Ribosome occupancy

Because Polysome-seq data was collected with spike-in values for each fraction (Total, Free, Mono/Poly), it is possible to calculate the absolute ribosome occupancy (% of a transcript which is bound to at least one ribosome) for each transcript. This value is calculated by normalizing transcript abundance for each fraction (TPMs output by kallisto) to the median abundance of the spike-in transcripts. All S. pombe spike-in transcripts with more than 100 estimated counts were used to calculate the spike-in abundance. The ribosome occupancy is then calculated as abundancebound/(abundancebound + abundancefree).

Ribosome association

In stressed samples, it is possible that condensed RNA pellets to the bottom of the sucrose gradient, making it difficult to calculate the absolute ribosome occupancy. Thus, for stressed samples, we calculate a "ribosome association" score which is TPMrib. bound/TPMTotal(Ristau et al. 2022). This metric is similar to "translation efficiency" scores calculated for ribosome profiling studies50. The change in ribosome association upon stress was calculated using DeSeq290, similar to reported methods for calculating changes in translation efficiency using DeSeq2 91.

RNA structure analysis

The sequence for the 5' UTR + the first 20 nucleotides of the CDS was extracted using the 5' UTR lengths described above from Pelechano et al. 201389. The folding energy for each UTR was then calculated using RNAFold from the ViennaRNA package92. Because the folding energy correlates directly with length, a normalized structure score was calculated for each transcript by dividing the calculated folding free energy by the length of the UTR.

3.12.10   Induction reporters

Reporters for pulsed induction were generated by Gibson assembly of gene fragments with a TET-inducible promoter designed for tight control of induction levels 93. Assembly pieces were derived either from gene fragments ordered from IDT or Twist Biosciences or from PCR amplification of other plasmids. Fragments were assembled into backbones generated by golden gate cloning using protocols and plasmids from the Yeast Toolkit 94, and the plasmids were sequenced by overlapped Sanger sequencing. Plasmids were linearized with NotI prior to transformation.

The PMU1 reporter contains the 5' UTR and 3' UTR of the native PMU1 gene and

the CDS is a fusion of the PMU1 CDS with nanoluciferase-PEST95. The HSP26 reporter contains the 5' UTR and 3' UTR of the native HSP26 gene, but the CDS is a fusion of the TPI1 CDS and nanoluciferase-PEST. The TPI1 fusion was used to avoid potential artifacts caused by a large pre-induction of HSP26 molecular chaperone and because TPI1 is well translated during stress and of a similar length (645 nt for HSP26 vs 745 nt for TPI1). Reporters were integrated at the HO locus using hygromycin selection in a strain of yeast containing a C-terminal auxin tag on Sui2, along with the inducible TIR1 ligase at the LEU locus, and the TetR protein at the his locus (see Table S1 for full genotype).

For induction of reporters concurrently with stress, 1 μM anhydrotetracycline (aTC, Cayman #CAYM-10009542-500) was added from a 10 mM stock prepared in DMSO at the beginning of the stress. For pre-induced samples, 0.1 μM aTC was added to yeast in SCD at OD600 = 0.2 and samples were incubated at 30°C for 45 minutes. Samples were then either washed 3x with SCD via centrifugation, or 1x via vacuum filtration before resuspending in prewarmed SCD. Stress was then initiated 30 minutes after washing had begun to ensure complete shutoff of reporter transcription. Samples were then fractionated as described above either using the Sed-Seq protocol to calculate pSup or the sucrose cushion fractionation to calculate ribosome occupancy.

3.12.11   Engineering solubility reporters

Solubility reporters were engineered using the Yeast Toolkit [Lee et al., 2015] (see Table S1 and S2). Variable 5'UTRs were engineered depending on the construct and genetically integrated in front of two copies of Clover, all driven by the constitutive TPI1 promoter and with the TPI1 3' UTR. Each reporter construct also had a copy of mCherry with a TPI1 promoter, 5'UTR and 3'UTR. This construct was inserted into the Leu2 locus with leucine selection.

Steady state protein levels were measured using flow cytometry by normalizing the Clover signal to the mCherry signal in each cell. Data was analyzed with a custom script using FlowCytometryTools in python and then exported and plotted in R. The standard Sed-seq protocol was used to measure the condensation behavior of each strain. Steady state mRNA levels were extracted from the Total sample of the Sed-seq experiment and translation efficiency was calculated as the steady state protein level divided by steady state RNA level.

3.12.12   Auxin-mediated depletions

Auxin induced degron depletions were adapted from the approach in Mendoza-Ochoa et al. [2019]. In short, the endogenous protein of interest was genetically engineered to contain the degron tag in a strain of yeast in which a β-estradiol inducible TIR1 ligase had been genetically integrated at the LEU locus. Some of the strains contained the original Oryza sativa TIR1 (OsTIR1), while others used a variant engineered for more specificity OsTIR1(F74G) 49 as indicated in Table S1. The auxin-FLAG degrons were installed at either the 5´ or 3´ end of genes using CRISPR plasmids from the yeast toolkit. A PCR-generated DNA template was co-transformed with a Cas9 and gRNA containing URA3 selectable plasmid as previously described 94,96. The CRISPR integrations were verified by PCR and Sanger sequencing and the URA3 plasmid was removed by selecting for colonies which did not grow on URA plates.

For depletion experiments, yeast were grown at 30°C in YPD to OD600 = 0.1. To induce TIR1 ligase, 5 μM β-estradiol (10 mM stock in DMSO) or an equivalent volume of DMSO (for mock treatment) was added to each culture and they were incubated for 75 minutes. To induce degradation, either 100 μM of Indole-3-acetic acid sodium salt (Sigma #I5148, 250 mM stock in DMSO) or 5 μM of 5-Ph-IAA (Medchemexpress #HY-134653, 5 mM stock in DMSO) was added. After 2 hours of auxin exposure, cells were temperature treated and

then harvested and fractionated as normal.

3.12.13   Radiolabeling quantification of translation

Yeast cells were cultured overnight in YPD until they reached an OD600 = 0.1. Auxin-inducible yeast strains were then treated with beta-estradiol and auxin, as detailed above, then translation was measured following a published protocol97. After a 1.5-hour depletion period, 1 mL of sample was transferred to 1.5mL tubes, then 1 μCi/mL of mixed 35S-L-methionine and 35S-L-cysteine media were added to each sample (Perkin-Elmer EasyTag #NEG772002MC). Samples were incubated for 30 minutes at 30°C with shaking (15 minutes for heat shocks), then cells were treated with 200 μL of 50%trichloroacetic acid (TCA), chilled on ice for 10 minutes, heated at 70°C for 20 minutes, and cooled again for 10 minutes. The samples were subsequently collected on glass microfiber filters (Sigma #WHA1823025) loaded onto a vacuum manifold (Millipore #XX2702550), washed with 3x 5 mL 5%TCA and 2x 5mL 95%ethanol, and air-dried for at least 12 hours at room temperature. Filters were then immersed in scintillation fluid (Perkin Elmer #6013179), and radioactivity levels were quantified in "counts per minute" through liquid scintillation counting on a Tri-Carb machine.

3.12.14   Western blotting

Western blots were performed as described in a published protocol98. For each sample, 1mL of yeast culture was spun down at 2500 g for 2 minutes, and the pellet was resuspended in 50 μL of 100 mM NaOH. The samples were incubated for 5 minutes at RT, spun at 20,000g for 1min, and resuspended in 50 μL of 1x Laemmli buffer (Bio-rad #1610737) with 5%β-mercaptoethanol. Samples were then boiled for 3 minutes, clarified at 20,000 g for 2 minutes and 15 μL was loaded onto a 4-20%tris-glycine SDS-PAGE gel (Biorad #5671094).

Proteins were then transferred to nitrocellulose (Sigma #10600001) using a wet transfer apparatus (Bio-rad #1704070). The membrane was blocked for 1 hour with 5%milk in TBST buffer, then incubated rocking overnight at 4°C with 1:3000 dilution of anti-FLAG antibody (Sigma #F1804) and 1:10,000 dilution of anti-PGK1 antibody (Invitrogen #459250) in 5%milk solution. Westerns were visualized using 1:20,000 dilutions of fluorophore conjugated secondaries (Licor #926-32212 and #925-68073) and visualized on a Licor Odyssey CLx. Band intensities were quantified in ImageJ and normalized to PGK1 signal.

3.12.15 Fluorescence microscopy and stress granule quantification

Standard confocal microscopy was completed as in Wallace et al. [2015], generally using Pab1-Clover as the SG marker unless otherwise noted. Cells were grown to log-phase as previously described. 1mL of cells were transferred to 1.5mL Eppendorf tubes. For heat stress, cells were shocked in a heat block, spun down in a microfuge, and 950 uL of supernatant were removed. For azide stress, 10%(w/v) azide or water was added directly to the 1mL of cells to proper dilution of aizde. For ethanol stress, cells were spun down in microfuge and resuspended in media with appropriate amounts of ethanol. 1.5 uL of treated cells were then placed on a glass slide and imaged immediately. For AID treatment, cells were treated as previously described, and were imaged immediately after a 2 hour exposure to Auxin. For cycloheximide treatment, cells were exposed to 100 ug/mL of cycloheximide for 10 minutes, stressed for 10 minutes, and then imaged immediately. Cells were imaged on an Olympus DSU spinning disc confocal microscope using a 100x 1.45 TIFM oil objective (PlanApo) and the FITC filter cube for the Clover fluorophore in Z-stacks. Representative images are maximum projections of the collected z-stacks. Maximum projection images of the cells were used to quantify the number of stress granules per cell using CellProfiler.

3.12.16   Single-molecule fluorescence in situ hybridization (smFISH)

Custom Stellaris® RNA FISH Probes were designed against SSB1, SSA4, HSP104, and ADD66 by utilizing the Stellaris® RNA FISH Probe Designer (Biosearch Technologies, Inc., Petaluma, CA) available online at `www.biosearchtech.com/stellarisdesigner` (Table S3). Each Stellaris FISH Probe set was labeled with Quasar670 (Biosearch Technologies, Inc.). smFISH was done as previously described.[99,100] Yeast cultures were grown to an OD of 0.3-0.4 in SCD, spun down at 3k g for 3 min. Cells were then suspended into 4 mL of culture and Oregon Green HaloTag reagent (Promega #G2801) was added to a final concentration of 2 μM. Cells were then resuspended and split into final cultures of 25 mL. Cells were then spun again at 3000 g for 3 min, and 23 mL were removed, such that 2 mL of media remained. Cells were then stressed as stated before. 19.85 mL of pre-warmed media was then added to each Falcon tube, and 3.15 mL of 4% paraformaldehyde (Electron Microscopy Services #15714) was immediately added. Cells were incubated at room temperature for 45 min at room temperature, gently rocking. Cells were spun down at 4°C and washed with ice-cold buffer B. Cells were resuspended into 1 mL of Buffer B (1.2 M sorbitol, 100 mM KHPO$_4$, pH = 7.5) then transferred to a 12-well plate. Cells were crosslinked in a Spectrolinker UV Crosslinker at a wavelength of 254 nm by exposure to 100 mJ/cm^2 twice with 1 min break in between.[101] Cells were pelleted for 3 min at 2000 rpm and then resuspended into spheroplast buffer (1.2 M sorbitol, 100 mM KHPO$_4$, pH = 7.5, 20 mM ribonucleoside-vanadyl complex (NEB #S1402S), 20 mM β-mercaptoethanol). 25 U/OD of lyticase (Sigma #L2524-10KU) were added to each sample. Cell digestion was performed at 30°C and was monitored using a benchtop phase contrast microscope, such that cells were about 50-70% digested. Digestion was stopped by spinning cells at 4°C for 3 min at 2000 rpm and two washes twice in ice-cold buffer B and resuspended in 1 mL Buffer B. 250 μl of cells were placed onto a poly-L-lysine coated coverslip and incubated at 4°C for 1 hr. Cells were washed with 2 mL of Buffer B and

then stored in ice-cold 70% ethanol for at least 3 hours. Coverslips were rehydrated in 2x SSC and then washed twice in pre-hybridization buffer (2x SSC + 5% formamide (Sigma #344206-100ML-M)) for 5 minutes each. smFISH probes were concurrently prepared. A mixture of 0.125 μL of 25 μM smFISH probes, and 2.5 μL of 10 mg/mL yeast tRNA (Thermo #AM7119) and 2.5 μL of 10 mg/mL salmon sperm DNA was dehydrated in a SpeedVac at 45°C. The dried pellet was rehydrated and resuspended in 25 μL hybridization mix (10% formamide, 2×SSC, 1 mg/mL BSA, 10 mM ribonucleoside–vanadyl complex (Thermo #15632011) and 5 mM NaHPO$_4$, pH 7.5) and boiled at 95°C for 2 min. 18 μL of resuspended probes were spotted onto a piece of Parafilm and coverslips were placed cell-side down into hybridization mixture. Hybridization occurred at 37°C for 3 hours. Coverslips were then washed at 37°C for 15 min in 2x SSC + 5% formamide, then in 2x SSC buffer, then 1xSSC buffer. They were then submerged in 100% ethanol, dried, and then mounted into ProLong Gold antifade with DAPI (Thermo P36941).

3.12.17   smFISH image acquisition and analysis

smFISH images were taken on a Nikon TiE microscope with a CFI HP TIRF objective (100x, NA 1.49, Nikon), and an EMCCD (Andor, iXon Ultra 888). Nikon TiE epifluorescent microscope. Samples were excited using the 647nm laser (Cobolt MLD) (15-20 mW for 200-300ms), poly-A FISH was imaged using the 561nm laser (Coherent Obis) (15-20 mW for 200-300ms), and Pab1-Halotag signal was imaged with a 488nm laser (Cobolt MLD) (10-15 mW for 200-300 ms), and DAPI (CL2000, Crystal Laser) (5-10 mW for 100 ms). Imaging of the nucleus was done using the 405nm laser and DIC images were taken as well. Z-stacks of 21 planes, 2uM thick were obtained. Images were analyzed using FISH-quant 102. Briefly, RNA spots were identified using big fish. For the smFISH colocalization analysis, RNA spot intensities were normalized by dividing by the mean intensity of each cell. For each RNA

spot, the mean Pab1 intensity in a 3x3 pixel square around the centroid was calculated. The Pab1 intensity was then measured for 100 random locations in the cell in 3x3 pixel locations. Finally, a distribution was calculated for both the random Pab1 signal and the Pab1 signal that corresponds to a RNA spot. The Z-score of the mean intensity of the Pab1 signal in a RNA spot compared to the Pab1 signal in a random spot was compared, and this is termed the 'colocalization score'. Each Z-score is calculated independently for each cell, and the average shown is for every cell.

3.12.18   Simulation of mRNA condensation

The underlying biophysical model for pSup in the absence of condensation is $pSup(g) = 1\text{-}Lg$ for a mRNA transcript encoded by gene g, of length Lg. In conditions where there is mRNA condensation, governed by parameter per-transcript and per-nucleotide, the model is: $pSup(g) = (1\text{-}Lg)\, e^{-(+Lg)}$. These models were fitted to sedimentation on the log-odds(pSup) scale, i.e. approximating the log-odds sedScore as normally distributed. Non-linear least squares fits were performed using the nls function in R. See supplemental text for details.

3.12.19   Statistical analyses

Unless otherwise stated, all experiments were performed as at least two biological replicates. The mean or geometric mean value (for log-distributed transcript abundance data) was calculated from the replicates.

Unless otherwise noted, all correlation values are reported as Spearman's rank correlation coefficient. Significance tests for comparing groups of data points were performed using a Wilcoxon rank-sum test, with a Bonferroni correction when comparing multiple groups (*P < 0.05, **P < 0.01, ***P < 0.001). 'N.S.' denotes not significant (P ≥ 0.05).

Table 3.1: Yeast strains used in this study

Yeast Strain	Description	Genotype	Source
BY4741	background strain S288C	MATa ura3Δ0 leu2Δ0 his3Δ1 met15Δ0	(Brachmann et al. 1998)
BY4742	background strain S288C	MATα ura3Δ0 leu2Δ0 his3Δ1 lys2Δ0	(Brachmann et al. 1998)
yJB001	Pab1-Halotag	MATa ura3Δ0 leu2Δ0 his3Δ1 met15Δ0 pab1::PAB1-HaloTag	This manuscript
yAER020	Pab1-Clover	MATα ura3Δ0 leu2Δ0 his3Δ1 lys2Δ0 pab1::PAB1-Clover pTEF-KanMX	(Wallace et al. 2015)
yJB42 (eIF3b)	PRT1-AID*-3xflag+pZTRL	MATα ura3Δ0 leu2::pZ4EV-OsTIR1_Z4EV-ATF_LEU2 his3Δ1 lys2Δ0 PRT1::PRT1-AID*-3xflag	This manuscript
yHG55 (eIF4b)	AID*-TIF3-3xflag+pZTRL	MATα ura3Δ0 leu2::pZ4EV-OsTIR1_Z4EV-ATF_LEU2 his3Δ1 lys2Δ0 TIF3::TIF3-AID*-3xflag	This manuscript

Yeast Strain	Description	Genotype	Source
yHG38 (eIF4E)	CDC33-AID*-3xflag+pZTRL	MATα ura3Δ0 leu2::pZ4EV-OsTIR1_Z4EV-ATF_LEU2 his3Δ1 lys2Δ0 CDC33::CDC33-AID*-3xflag	This manuscript
yHG72 (eIF4A)	TIF1-AID*-3xflag+pZTRL	MATα ura3Δ0 leu2::pZ4EV-OsTIR1_Z4EV-ATF_LEU2 his3Δ1 lys2Δ0 TIF1::TIF1-AID*-3xflag tif2Δ::KANMX	This manuscript
yJB143 (eIF2α)	SUI2-AID-3xFlag + pJB773	MATα ura3Δ0 leu2::pZ4EV-OsTIR1F74G_Z4EV-ATF_LEU2 his3Δ1 lys2Δ0 SUI2::SUI2-AID*-3xflag	This manuscript

Table 3.1: (Continued from previous page)

Yeast Strain	Description	Genotype	Source
yJB147 (eIf5)	TIF5-AID-3xFlag + pJB773	MATα ura3Δ0 leu2::pZ4EV-OsTIR1F74G_Z4EV-ATF_LEU2 his3Δ1 lys2Δ0 TIF5::TIF5-AID*-3xflag	This manuscript
yJB148 (eIF5B)	AID*-FUN12-3xFlag + pJB773	MATα ura3Δ0 leu2::pZ4EV-OsTIR1F74G_Z4EV-ATF_LEU2 his3Δ1 lys2Δ0 FUN12::AID-FUN12*-3xflag	This manuscript
yJB262 (eIF4G)	TIF4631-AID*-3xFLAG+pJB773	MATα ura3Δ0 leu2::pZ4EV-OsTIR1F74G_Z4EV-ATF_LEU2 his3Δ1 lys2Δ0 TIF4631::TIF4631-AID*-3xFLAG tif4632Δ::KANMX	This manuscript
Pbp1-GFP	Pbp1-GFP	MATa his3Δ1 leu2Δ0 met15Δ0 ura3Δ0 pbp1::Pbp1-GFP	(Huh et al. 2003)

Table 3.1: (Continued from previous page)

Yeast Strain	Description	Genotype	Source
yJB265	yJB42+Pab1-Clover	MATα ura3Δ0 leu2::pZ4EV-OsTIR1_Z4EV-ATF_LEU2 his3Δ1 lys2Δ0 PRT1::PRT1-AID*-3xflag pab1::PAB1-Clover	This manuscript
yHG005	Weakest hairpin	MATa ura3Δ0 his3Δ1 met15Δ0 leu2::LEU2_5'weakest hairpin-cds2xClover-3'TPI1_5'TPI1-cdsmCherry-3'TPI1	This manuscript
yHG006	Weak hairpin	MATa ura3Δ0 his3Δ1 met15Δ0 leu2::LEU2_5'weak hairpin-cds2xClover-3'TPI1_5'TPI1-cdsmCherry-3'TPI1	This manuscript

Table 3.1: (Continued from previous page)

Yeast Strain	Description	Genotype	Source
yHG007	Medium hairpin	MATa ura3Δ0 his3Δ1 met15Δ0 leu2::LEU2_5'medium hairpin-cds2xClover-3'TPI1_5'TPI1-cdsmCherry-3'TPI1	This manuscript
yHG008	Strongest hairpin	MATa ura3Δ0 his3Δ1 met15Δ0 leu2::LEU2_5'strongest hairpin-cds2xClover-3'TPI1_5'TPI1-cdsmCherry-3'TPI1	This manuscript
yHG010	No hairpin	MATa ura3Δ0 his3Δ1 met15Δ0 leu2::LEU2_5'no hairpin-cds2xClover-3'TPI1_5'TPI1-cdsmCherry-3'TPI1	This manuscript

Yeast Strain	Description	Genotype	Source
yHG026	GCN4 reporter	MATa ura3Δ0 his3Δ1 met15Δ0 leu2::LEU2_5'GCN4-cds2xClover-3'TPI1_5'TPI1-cdsmCherry-3'TPI1	This manuscript
yHG027	GCN4 5xmut	MATa ura3Δ0 his3Δ1 met15Δ0 leu2::LEU2_5'GCN4(5xmut)-cds2xClover-3'TPI1_5'TPI1-cdsmCherry-3'TPI1	This manuscript

Table 3.2: Plasmids used in the study

Plasmid	Description	Source
pV1382	Cas9 editing	(Vyas et al. 2018)
pZTRL	Inducible OsTIR1	(Mendoza-Ochoa et al. 2019)
pJB773	OsTIR1F74G leu2 int leu	This manuscript
FRP2371	TETO system	(Azizoglu, Brent, and Rudolf 2021)
pyHG005	Weakest hairpin	This manuscript
pyHG006	Weak hairpin	This manuscript
pyHG007	Medium harpin	This manuscript
pyHG008	Strongest hairpin	This manuscript
pyHG010	No hairpin	This manuscript
pyHG026	GCN4 reporter	This manuscript
pyHG027	GCN4 5xmut	This manuscript
pJB801	Tet inducible PMU1 reporter	This manuscript
pJB805	Tet inducible HSP26 reporter	This manuscript

Table 3.3: smFISH probes used in this study

Gene	Number	Sequence	Dye
SSA4	1	cacatgaataggttgtacct	Quasar 670
SSA4	2	tcaaccctatcgtttgcaaa	Quasar 670
SSA4	3	acataagaaggcgtcgttct	Quasar 670
SSA4	4	agcctttctgtgtcagtaaa	Quasar 670
SSA4	5	tattatgtgggttcatcgca	Quasar 670
SSA4	6	ggatcatcgaatttacgtcc	Quasar 670
SSA4	7	taatgcttagcatcgttcgt	Quasar 670
SSA4	8	cccttgtcaatcactttgaa	Quasar 670
SSA4	9	tctttgtctcgcctttatat	Quasar 670
SSA4	10	ataggctggaaccgttacta	Quasar 670
SSA4	11	gattgtaccggcatcttttg	Quasar 670
SSA4	12	tacgaagaacgttcaagccc	Quasar 670
SSA4	13	gcagctgtaggttcattaat	Quasar 670
SSA4	14	ttctgcgatttcttgtccag	Quasar 670
SSA4	15	aaagatcaagacgttgtgct	Quasar 670
SSA4	16	ccttcatctatggatagcag	Quasar 670
SSA4	17	agaaagttaaccagcctact	Quasar 670
SSA4	18	ttttcttttgaactcctcgg	Quasar 670
SSA4	19	ggttagttgttagatccttt	Quasar 670
SSA4	20	tccttaacctccttagggac	Quasar 670
SSA4	21	tttctatagatgtctgagca	Quasar 670
SSA4	22	aattcttcaaatcttgccct	Quasar 670
SSA4	23	atcagccaaaactttttcca	Quasar 670

Table 3.3: (Continued from previous page)

Gene	Number	Sequence	Dye
SSA4	24	accagtttttgtactttttgg	Quasar 670
SSA4	25	cctcatcagggttaatcgaa	Quasar 670
SSA4	26	ctgtacggcagcaccataag	Quasar 670
SSA4	27	actggtcacccgttaagatg	Quasar 670
SSA4	28	cagtaaatcttgggtcgtcg	Quasar 670
SSA4	29	ataatggtgcaacatccagc	Quasar 670
SSA4	30	tttttttgttgggatagtcga	Quasar 670
SSA4	31	gtaggtggaaaacacttccg	Quasar 670
SSA4	32	tttcaccctcaaaaacttgt	Quasar 670
SSA4	33	caactcaaatttacccagta	Quasar 670
SSA4	34	tcaacggcagatacgttcag	Quasar 670
SSA4	35	tcttcccttatcgttagtaa	Quasar 670
SSA4	36	aacttttctgcctcagcaac	Quasar 670
SSA4	37	gattcttagcttgaacacgt	Quasar 670
SSA4	38	gtaaacgcgtacgattctag	Quasar 670
SSA4	39	ttcgctcacagaatttttca	Quasar 670
SSA4	40	ccaccttctccttgaagtta	Quasar 670
SSA4	41	aatttcctggcatcctcttc	Quasar 670
SSA4	42	atttatagcatcttgggcgg	Quasar 670
SSA4	43	ccgcttgcgaagcatctaac	Quasar 670
SSA4	44	ataatggggtttgcaacacc	Quasar 670
SSA4	45	ctgcagctccgtaaaattta	Quasar 670
SSB1	1	taccgatagcaccttggaaa	Quasar 670

Gene	Number	Sequence	Dye
SSB1	2	tttcttgggttcaaagcagc	Quasar 670
SSB1	3	gtcgtcgaatcttctaccaa	Quasar 670
SSB1	4	gtcgataaccttgaaaggcc	Quasar 670
SSB1	5	tcttggtttcttccaagtat	Quasar 670
SSB1	6	agcggaaatttcttgtgggg	Quasar 670
SSB1	7	accaatcttagcttcagcaa	Quasar 670
SSB1	8	ggttcgttgatgatacgcaa	Quasar 670
SSB1	9	cacctagaccgtaagcaata	Quasar 670
SSB1	10	aacatgtctttccttttcgg	Quasar 670
SSB1	11	accagcaatgtgcaacaagg	Quasar 670
SSB1	12	gtgttaccggaagtagattt	Quasar 670
SSB1	13	agtgttccaacaagttggtg	Quasar 670
SSB1	14	ttcttcttgaattcagcctt	Quasar 670
SSB1	15	atcgtcggagatgtccaaac	Quasar 670
SSB1	16	aaggttctcttagctctttc	Quasar 670
SSB1	17	acggtagtttgagtgacaga	Quasar 670
SSB1	18	ggattcgaaatcttcaccgt	Quasar 670
SSB1	19	aacaatgcggcgttcaagtc	Quasar 670
SSB1	20	cttagagatcttagcatcct	Quasar 670
SSB1	21	ccaaccaagacaacttcgtc	Quasar 670
SSB1	22	tccaattgcttaccgtcaaa	Quasar 670
SSB1	23	acaacaagtccttggtttcg	Quasar 670
SSB1	24	gttcttctcttgatggttgg	Quasar 670

Gene	Number	Sequence	Dye
SSB1	25	actgggaattgaacggtggt	Quasar 670
SSB1	26	tgggatgttcttcaagtcga	Quasar 670
SSB1	27	atagcttccaagactggttc	Quasar 670
SSB1	28	accgttagcatcaacttcga	Quasar 670
SSB1	29	cgacggcagtaaccttcaag	Quasar 670
SSB1	30	gaagacttaccggtagactt	Quasar 670
SSB1	31	agacaagactgggtcagtga	Quasar 670
SSB1	32	gacttggaacctctcttcaa	Quasar 670
SSB1	33	tcgatttgcaaagcagccaa	Quasar 670
SSB1	34	aacgagaagacatggccttg	Quasar 670
HSP104	1	taggtaagggactgatccat	Quasar 670
HSP104	2	caggttgctgttgaggaatt	Quasar 670
HSP104	3	cccaaagcataacttggagt	Quasar 670
HSP104	4	ttgaatcttagcagcgtctt	Quasar 670
HSP104	5	gcgctataaatgagtccttc	Quasar 670
HSP104	6	tggcctcaatatctacttga	Quasar 670
HSP104	7	accacgaagttcaagagctt	Quasar 670
HSP104	8	ccacgagagtcaattctagt	Quasar 670
HSP104	9	tccaaaggtgtgttcgtatc	Quasar 670
HSP104	10	cctgctcagtcatatcaatg	Quasar 670
HSP104	11	agggtcaagtttaccttgac	Quasar 670
HSP104	12	tcttatttcttcttcacggc	Quasar 670
HSP104	13	acctggctcaccaattaaac	Quasar 670

Table 3.3: (Continued from previous page)

Gene	Number	Sequence	Dye
HSP104	14	ttagcgccttgtaagatagt	Quasar 670
HSP104	15	aatgcggccaaatctagact	Quasar 670
HSP104	16	cttcaagatgttagcagcgt	Quasar 670
HSP104	17	tcaattggcctctggacaaa	Quasar 670
HSP104	18	cttctttcaaaggcaccatc	Quasar 670
HSP104	19	cactgtttgtctcacacttg	Quasar 670
HSP104	20	gttgcagacctctcaatatg	Quasar 670
HSP104	21	actaaggcgctatccagaat	Quasar 670
HSP104	22	aacgcttggctaattgagca	Quasar 670
HSP104	23	ctggcaatcttctatatggc	Quasar 670
HSP104	24	tcttctggcttagaatctct	Quasar 670
HSP104	25	catcttcatctctctctaga	Quasar 670
HSP104	26	ctatctttagtggtggagtc	Quasar 670
HSP104	27	tgcaatgaagcttccttctg	Quasar 670
HSP104	28	gttgtcttagaggttccaat	Quasar 670
HSP104	29	tttgatatctgggatggcga	Quasar 670
HSP104	30	accacattttggatcatgga	Quasar 670
HSP104	31	atcttgcagctgtttcagaa	Quasar 670
HSP104	32	cccacgacttcagatgataa	Quasar 670
HSP104	33	acggcattggaaacagcttt	Quasar 670
HSP104	34	ccttggattagctaaacctg	Quasar 670
HSP104	35	tagccaattcagtttttaccg	Quasar 670
HSP104	36	aatcgaccctgatcatcatg	Quasar 670

Table 3.3: (Continued from previous page)

Gene	Number	Sequence	Dye
HSP104	37	acttagagaccgcatacttc	Quasar 670
HSP104	38	ttcatcgtacccgacataac	Quasar 670
HSP104	39	cggagtatggtttgtattgc	Quasar 670
HSP104	40	gtaattctaccgtcatccaa	Quasar 670
HSP104	41	ttggaacagtcgatcgtctt	Quasar 670
HSP104	42	aaatgttgcctaacagcacc	Quasar 670
HSP104	43	tttgctcgaatctctcttca	Quasar 670
HSP104	44	ggcctcttgagttaaattca	Quasar 670
HSP104	45	cccatatcatcggaataacc	Quasar 670
HSP104	46	tctttaagatccttagtgcc	Quasar 670
HSP104	47	cgagatttacccttcttcaa	Quasar 670
HSP104	48	tagtagcttcgtgatttggt	Quasar 670
ADD66	1	gtatgttcctttgggttttg	Quasar 670
ADD66	2	tactaatggcaacaccaggc	Quasar 670
ADD66	3	attgtggtatattccctacg	Quasar 670
ADD66	4	ttcagcagccagtcaatact	Quasar 670
ADD66	5	ttcccattcatttgcttgtg	Quasar 670
ADD66	6	tcgaatctaacgcctccaaa	Quasar 670
ADD66	7	cccacaaattccactaggta	Quasar 670
ADD66	8	atcctctggtctgtctaatg	Quasar 670
ADD66	9	tctttatatagcgagtcgct	Quasar 670
ADD66	10	caaagcgctgctatacttca	Quasar 670
ADD66	11	cctcgcttcttattgtagaa	Quasar 670

Gene	Number	Sequence	Dye
ADD66	12	ttcgttgctgtatggcaaaa	Quasar 670
ADD66	13	tagttaacggacacgagtgg	Quasar 670
ADD66	14	cggcaagatgatctctacga	Quasar 670
ADD66	15	ccgatatattatacttgctc	Quasar 670
ADD66	16	agagagtcccaaatgcatat	Quasar 670
ADD66	17	attttcatcctccattgcat	Quasar 670
ADD66	18	cctgtggacgtacaatcaca	Quasar 670
ADD66	19	aactctccgagcgaatatac	Quasar 670
ADD66	20	ctcagcttcatcgtcgaaat	Quasar 670
ADD66	21	tcgtttagatggaggttcga	Quasar 670
ADD66	22	gttattgaccatcgactctt	Quasar 670
ADD66	23	tcttggaaactggtaggagt	Quasar 670
ADD66	24	tcggctgatcaacggatatc	Quasar 670
ADD66	25	cgacgcattcagtatttgga	Quasar 670
ADD66	26	taatgctgcggagggcttta	Quasar 670
ADD66	27	attggccaaacaactacagt	Quasar 670
ADD66	28	gaatctaatgagttgtcccc	Quasar 670
ADD66	29	ggcgcgttttgataactttt	Quasar 670
ADD66	30	ggcctgacaaactttacaat	Quasar 670
ADD66	31	gtatgcaccttgccatgata	Quasar 670
ADD66	32	aatttatctcttgcatccgc	Quasar 670
ADD66	33	tacttctcggtttcaattgt	Quasar 670
ADD66	34	gtggctatatatgcacttgt	Quasar 670

Table 3.3: (Continued from previous page)

Gene	Number	Sequence	Dye
oligodT	1	tttttttttttttttttttt	Quasar 570

CHAPTER 4

POLY-A BINDING PROTEIN 1 CONDENSATION DOES NOT REGULATE TRANSLATION OF HEAT SHOCK TRANSCRIPTS DURING RECOVERY

This chapter includes contributions from Dr. Chris Katanski (original 5'UTR analysis), Dr. Haneul Yoo (DLS data of O.para Pab1), and Dr. Jared Bard (Polysome sequencing data).

4.1 Introduction

Cells across the tree of life encounter elevated temperatures, from single-celled organisms living in the wild, to pathogens infecting warm-blooded hosts, to mammalian cells experiencing fever. When cells experience heat shock, they launch an archetypal response that is both adaptive and reversible: global translation is attenuated, while heat shock transcripts, largely encoding molecular chaperones, are induced and translated [Verghese et al., 2012]. Heat also induces intracellular protein aggregates, which had long been thought to be the result of a misfolding catastrophe that results from heat-destabilized proteins [Vabulas et al., 2010]. However, recent work has suggested that these are reversible assemblies that form through a biomolecular condensation process such as phase separation, meaning they consist of folded proteins concentrated without fixed stoichiometry or structure, rather than typical misfolding and aggregation [Riback et al., 2017, Wallace et al., 2015, Iserman et al., 2020, Lyon et al., 2020]. Biomolecular condensation may thus be another adaptive intracellular change that occurs alongside the transcriptional and translational responses. Yet it is unclear how biomolecular condensation promotes survival.

Previous work in the Drummond lab identified a list of proteins that form condensates

during heat shock in yeast, noting that many essential proteins involved in cap-dependent translation form condensates and raising the possibility that biomolecular condensation is involved in translational regulation during heat shock [Wallace et al., 2015]. Biomolecular condensation may help explain the currently unresolved question of how molecular chaperones are translated in spite of global translational attenuation. Furthermore, the significance of A-rich 5'UTRs found heat-induced transcripts is unknown [Lindquist and Petersen, 1990]. Perhaps biomolecular condensation and the unique sequence features of molecular chaperone transcripts together promote a stress-specific mode of translation.

Poly(A) binding protein (Pab1) is a protein that connects biomolecular condensation, A-rich 5'UTRs, molecular chaperones, and cell survival during heat shock. Pab1, which binds poly(A) mRNA, forms reversible heat-induced condensates by phase separation in budding yeast. Pab1 condensation is adaptive during heat shock, as disrupting its condensation behavior results in growth defects at high temperatures [Riback et al., 2017]. Here, it was proposed that Pab1 acts as a translational repressor of heat shock transcripts, and that condensation regulates this function; this hypothesis was the result of several compelling observations about Pab1 and heat shock transcripts.

First, Pab1 is a known translational repressor. Although Pab1 is best known for binding 3' poly(A) tails of mRNA and helping mRNAs circularize, Pab1 also acts as a translational repressor for transcripts that have A-rich 5'UTRs, such as its own transcript [Kini et al., 2016, Kahvejian et al., 2001, Xia et al., 2011]. Pab1 regulates its own translation through an autoregulatory circuit: at high concentrations, Pab1 binds its own 5'UTR to block new translation [de Melo Neto et al., 1995, Wu and Bag, 1998, Bag and Wu, 1996].

Second, Pab1's condensation disrupts its ability to bind mRNA. Pab1 does not bind mRNA when is condensed [Riback et al., 2017, Yoo et al., 2022].

Third, heat shock-induced transcripts have A-rich 5'UTRs bound by Pab1 in the absence of stress. These 5'UTRs have similar A-richness to PAB1, and they are similarly enriched

for Pab1 binding at their 5'UTRs in vivo [Tuck and Tollervey, 2013], suggesting that Pab1 may also repress translation of these transcripts.

Finally, the same molecular chaperones that have A-rich 5'UTRs, such as Ssa4 and Hsp104, disperse Pab1 [Cherkasov et al., 2013]. This dispersal of Pab1 coincides with the resumption of growth in cells, suggesting that the dispersal of Pab1 condensates may lead Pab1 to bind mRNA, redirecting ribosomal capacity away from the no longer needed molecular chaperones [Cherkasov et al., 2013].
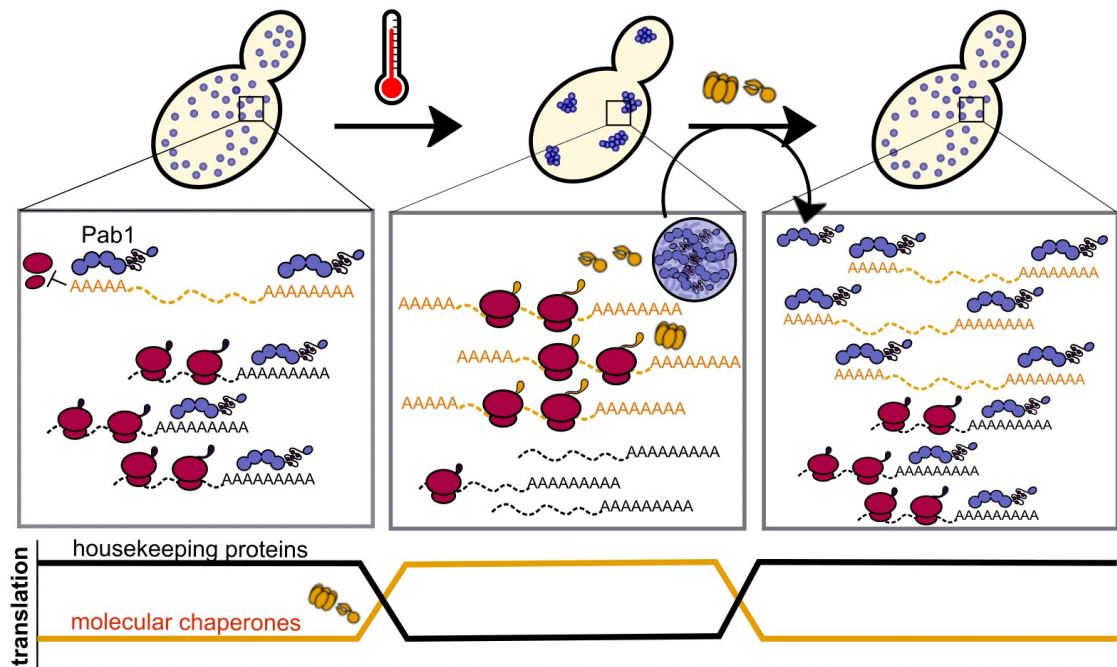
Figure 4.1: **Model of Pab1 condensation regulating translation during stress and recovery**

Together, these details led us to the following model where Pab1 condensation modulates its activity as a translational repressor, regulating the production of molecular chaperones with A-rich 5'UTRs (Figure 4.1). When the cell is exposed to heat, Pab1 autonomously forms condensates and no longer binds mRNA. Thus Pab1 is sequestered and A-rich 5'UTRs

124

are exposed, allowing maximal translation of heat shock transcripts. However, when the stress is removed and the cells recover, Pab1 is dispersed by the newly translated molecular chaperones. Now solubilized Pab1 then represses the highly abundant heat shock transcripts by binding to their 5'UTRs. This allows the cell to quickly shift from translating chaperones to translating metabolic and growth-related proteins, promoting fitness. In the case of sustained heat stress, this circuit could help maintain an equilibrium level of molecular chaperones.

This model presents a compelling view of biomolecular condensation as a mechanism by which cells sense and respond to changes in their external environments. To test this model, we isolated specific steps of the model using *in vitro* and *in vivo* systems. However, we found that although there was strong circumstantial evidence backing up the proposed model, the implications of the model ultimately did not hold.

4.2   Pab1 binds to A-rich 5'UTRs found in stress transcripts

Generally, transcripts that are induced during stress tend to have more A nucleotides in their 5'UTRs compared to other transcripts, although the role of these A-rich UTRs is unclear. This trend is seen clearly in a comparison of the *SSA4* and *SSA2* transcripts—paralogous HSP70s— as *SSA4* is induced during stress and contains long tracts of A nucleotides, while *SSA2* is constitutively expressed and lacks such long stretches of As (Figure 4.2A). Notably, the *PAB1* transcript itself also features an A-rich 5'UTR, suggesting an autoregulatory function. When compared to the rest of the transcriptome, *SSA4* and *PAB1* have 5'UTRs that are significantly more A-rich (Figure 4.2B). Previous studies using Crosslinking Immunoprecipitation-Sequencing (CLIP-Seq) have shown that Pab1 binds directly to the *PAB1* 5'UTR and the *SSA4* 5'UTR but not to the *SSA2* 5'UTR (Figure 4.2C), which aligns clearly with the enrichment of As found there. A global analysis of this data indicates

that, in general, transcripts encoding molecular chaperones that are induced during stress tend to have increased Pab1 binding in their 5'UTRs (Figure 4.2D). The presence of these A-rich 5'UTRs, combined with evidence of direct Pab1 binding, supports the model of Pab1 binding to and regulating translation of these transcripts.
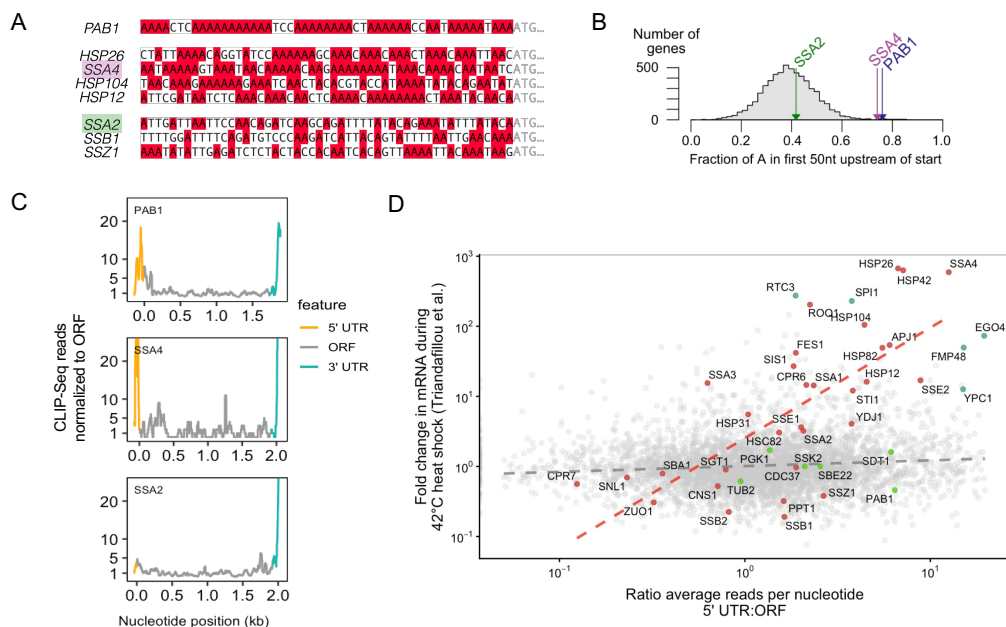

Figure 4.2: **Heat shock transcripts have A-rich 5'UTRs which can be bound by Pab1** (A) Heat shock induced transcripts tend to be more A-rich and have longer A-tracts than constitutive transcripts. *PAB1* is an exception, which is very A-rich. (B) *SSA4* and *PAB1* transcripts are significantly more A-rich compared to 5'UTRs across the transcriptome. *SSA4* is a about average. (C) CLIP-Seq data taken from [Tuck and Tollervey, 2013], originally analyzed by Dr. Chris Katanski. The yellow shows Pab1 enrichment at the 5'UTR for *PAB1* and *SSA4* transcripts, but not for *SSA2*. The teal shows that there is Pab1 enrichment in the 3'UTR for all transcripts. This would be expected given the poly-A tail attached to mRNAs. (D) mRNA abundance change vs. Pab1 binding to the 5'UTR. The dotted red line shows a relationship between Pab1 binding and the chaperones that are induced most during heat shock.

4.3 Pab1 can repress translational activity *in vitro*, depending on its condensation state

Given the circumstantial evidence that Pab1 can regulate its own translation, we sought to see if we could see Pab1 regulate translation *in vitro*. To do this, we established an *in vitro* translation assay in *S. cerevisiae* lysate to measure how 5'UTRs affect translation. To test the hypothesis that Pab1 can represses transcripts with A-rich 5'UTRs, we designed nanoluciferase mRNA constructs with 5'UTRs from the following transcripts: *SSA4, SSA2, EGO4, EGO2, HSP104,*, and *SEC18* (Figure 4.3A). These six transcripts belong to two pairs, each with a control transcript. *SSA4* and *HSP104* have A-rich 5'UTRs, are enriched for Pab1 at their 5'UTRs, and encode molecular chaperones necessary for Pab1 dispersal. *SSA2* is a control for *SSA4*, as it is a paralog of *SSA4* that both does not contain an A-rich 5'UTR and does not get induced during heat shock. *EGO2* is a control for *EGO4* as these are paralogs that arose in the whole genome duplication, but *EGO4* has a long A-tract. Similarly, *SEC18* is a control for *HSP104* as it encodes a constitutively expressed AAA+ ATPase but does not have an A-rich 5'UTR. We inserted the 5'UTRs of these transcripts in front of a gene encoding nanoluciferase with an endogenous constant 3'UTR and a poly-A tail.

To measure the effect of soluble Pab1 on translation, we added the nanoluciferase mRNA constructs to translationally active yeast lysate, with and without additional purified Pab1 (Figure 4.3A). The data suggest that Pab1 can specifically repress the constructs that have endogenous A-rich 5'UTRs (Figure 4.3B). *SSA4* is significantly translational repressed compared to *SSA2*, and the same holds for the *EGO4/EGO2* pair and the *HSP104/SEC18* pair. We next wanted to test whether the adition of pre-condensed Pab1 would diminish this affect, as we expect condensed Pab1 to have a diminished ability to bind to transcripts. Indeed, ddition of condensed Pab1, in contrast, did not repress the translation A-rich 5'UTR

transcripts. This data supports the proposed model by demonstrating that Pab1 can regulate the translation of heat-shock transcripts in a 5'UTR dependent way, while condensation eliminates this effect.

Figure 4.3: **Monomeric Pab1 can repress translation *in vitro* while condensed Pab1 does not** (A) Schematic of IVT assay. Briefly, 5'UTRs of interest were engineered in front of a nanoluciferase coding sequence. mRNA was made via in vitro transcription, and then added to translationally active yeast lysate. Purified Pab1 was added to a final concentration of 5μM. Luminesence is used as a readout for amount of translation. (B) Left: Monomeric Pab1 can repress translation, and represses translation of transcripts with A-rich 5'UTR more than other transcripts. Right: Condensed Pab1 is much worse than monomeric Pab1 at repression translation. (C) Some of the 5'UTRs and scrambled 5'UTRs added in front of nanoluciferase. (D) More IVT data, comparing scrambled 5'UTRs, as well as *HSP12* and *HSP26*.

Next, we were curious how important the composition vs. the primary sequence of the A-rich 5'UTR is for translational repression via Pab1. To do this, we constructed scrambled 5'UTR sequences of the *SSA4* and *EGO4* transcripts, which have the same nucleotide composition but in a different order, with as few As in a row as possible (Figure 4.3C). In-

terestingly, the *SSA4_scram* 5'UTR showed a similar amount of repression to the WT *SSA4* 5'UTR, but the *EGO4_scram* transcript was basically not repressed at all while the WT *EGO4* was extremely repressed (Figure 4.3D). We also tested the 5'UTRs of *HSP12* and *HSP26* transcripts, as they are both heat-induced transcripts. *HSP26* was translationally repressed by Pab1, while *HSP12* was not, even though both transcripts are relatively A-rich and contain A-tracts. *HSP12* 5'UTR has a tract of eight As in a row, so it is a puzzling result that Pab1 did not repress, or likely even bind, this transcript.

Altogether, this data suggest that Pab1 binding to the 5'UTR is likely more complicated than just binding to the 5'UTR and sterically blocking translation initiation. There may be more specificity than expected, or there may be contributions from certain sequence features that can regulate Pab1 binding.

4.4   Pab1 is not more repressed than average at 30°C *in vivo*

To follow up on the *in vitro* results, we wanted to see to what extent Pab1 binding *in vivo* was correlated with translational repression. To do this, we compared the Pab1 CLIP-Seq data with a measure of translational repression through Polysome profiling-Sequencing (Poly-Seq). Through Poly-Seq, we can assess how much a given transcript is enriched in a polysome fraction vs. not in polysomes, using the metric "occupancy odds". The higher the occupancy odds, the more highly translated a transcript is. When we compared the extent of Pab1 binding to the 5'UTRs and transcriptome-wide occupancy odds at 30°C, we were expecting to see a strong correlation between Pab1 binding and translational repression. Surprisingly, there was essentially no relationship between these two measurements (Figure 4.4A). Even chaperones with enriched Pab1 binding seen by CLIP-Seq still had relatively high occupancy odds, suggesting they were getting actively translated. The *PAB1* transcript itself, which showed highly enriched Pab1 binding at its 5'UTR, showed a high occupancy

odds and no translational repression. In other words, the strong effect we had seen *in vitro* did not seem to be recapitulated *in vivo*.
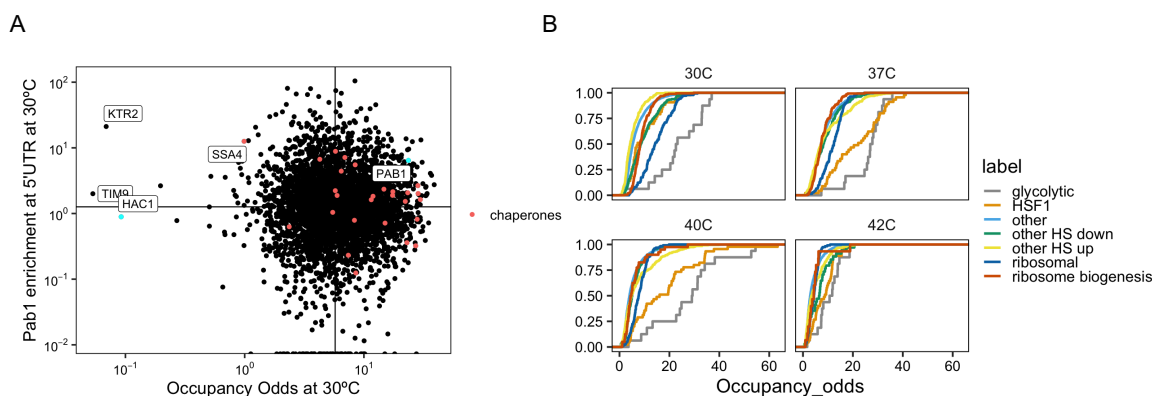

Figure 4.4: **No clear evidence that Pab1 represses translation *in vivo*** (A) Comparing CLIP-Seq Pab1 data at 5'UTRs to the Poly-Seq data which measures translation via occupancy odds. There is not a strong relationship, and Pab1 itself shows high binding but not translational repression. (B) Occupancy odds data showing how different groups of transcripts change translation at different temperatures.

Just looking at the occupancy odds of Hsf1 target transcripts, we would have expected them to be translated worse on average than most other transcripts, if Pab1 was causing translational repression (Figure 4.4B). Polysome profiling at 30°C showed that the Hsf1 targets were not translationally repressed. The data at higher stressful temperatures, including 37°C, 40°C, and 42°C, show that Hsf1 targets shift more into polysomes. This happens at temperatures before we see signicant Pab1 condensation, and could be simply explained by the fact that there are now more transcripts available for translation.

The finding that Pab1 binding does not correlate with translational repression is a significant challenge to the model of Pab1 functional condensation. Particularly notable is that the *PAB1* transcript itself seems to be both highly bound by Pab1 and translationally repressed,

which is inconsistent with our proposed model.

However, perhaps Pab1's functionality does not play a role predominantly during heat shock, but more during recovery. After heat shock, there are a high number of heat shock transcripts around that cell no longer needs to actively translate. For example, the rate of production of molecular chaperones can decrease during recovery. Pab1 translational repression might not be clearly seen during non-stress conditions or immediately after heat shock, as there might not be enough transcripts and/or monomeric Pab1 to show the effect. To test this, we decided to specifically look at how stress induced transcripts were being translationally regulated during recovery from stress.

4.5 Heat shock transcripts are still in polysomes after 20 minutes, even though translation has mostly recovered by that point

To look at how transcripts are regulated during recovery from stress, we returned again to polysome profiling, this time with qPCR as a read-out rather than sequencing. We performed polysome profiling on cells with the following treatments: 30°C, 42°C (20 min stress), 42°C (20 min stress + 20 min recovery at 30°C), 46°C (20 min stress), and 46°C (20min stress + 20 min recovery at 30°C) (Figure 4.5A). We noted that for 42°C stress, the polysomes profiles show that after 20min of recovery, the polysomes are almost fully restored to the 30°C unstressed level. However, for 46°C stress, the polysome profiles remain mostly the same after 20min.

Since there were clear differences in the 42°C profiles before and after recovery, we decided to explore how different transcripts behaved. We tested some heat shock transcripts and some housekeeping transcripts, predicting that HS transcripts shift to being repressed during recovery, while housekeeping transcripts would shift to being translated during recovery. However, the poly-qPCR data show that both housekeeping and heat shock transcripts are
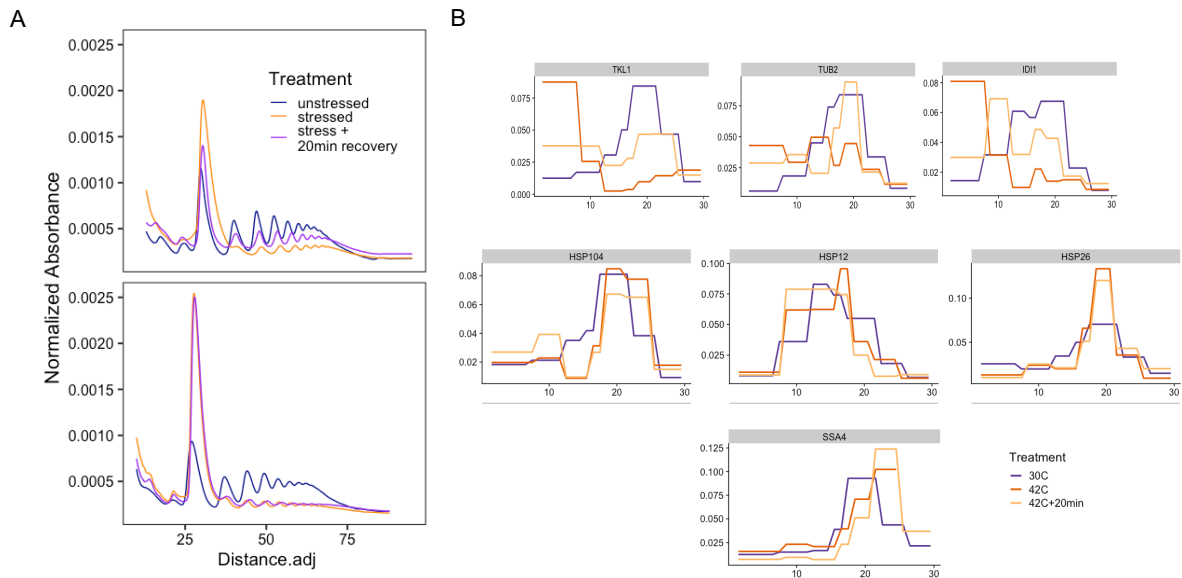
Figure 4.5: **Heat shock and housekeeping transcripts are both translated during recovery** (A) Top: Polysome profiles at 42°C Bottom: Polysome profiles at 46°C. Translation recovers after a 42° C after 20 minutes, but polysomes are still collapsed after 20 minutes after 46°C stress. (B) Poly-qPCR data. X-axis is different fractions, Y-axis is qPCR signal of each probe. TKL1, IDI1, TUB2 are all in polysomes after 20min stress, along with HSP104, HSP12, SSA4, and HSP26.

still enriched in polysomes after 20 minutes of recovery (Figure 4.5B). This suggests that the heat shock transcripts are not being translationally repressed within this time frame, although the cells have recovered enough such that translation of housekeeping transcripts has resumed.

4.6 Pab1 is not leading to specific degradation of transcripts

If Pab1 is not directly binding and repressing translation, we wondered if it might be promoting specific degradation of HS transcripts. To test this we did a qPCR time-course on the following heat shock transcripts *HSP104, HSP12, HSP26, SSA4*, as well as the house-keeping transcripts *PAB1, IDI1, TKL1* and *TUB2*. We looked at the transcript levels during stress and recovery in both haploid and diploid cells. In diploids, we found that transcript levels are relatively stable within the first 20 minutes of recovery; we were not seeing specific, rapid degradation of HS transcripts (Figure 4.6A). In haploid cells, we did see more rapid degradation of HS transcripts (Figure 4.6B); however, this would not explain the polysome profiling from Figure 4.5.
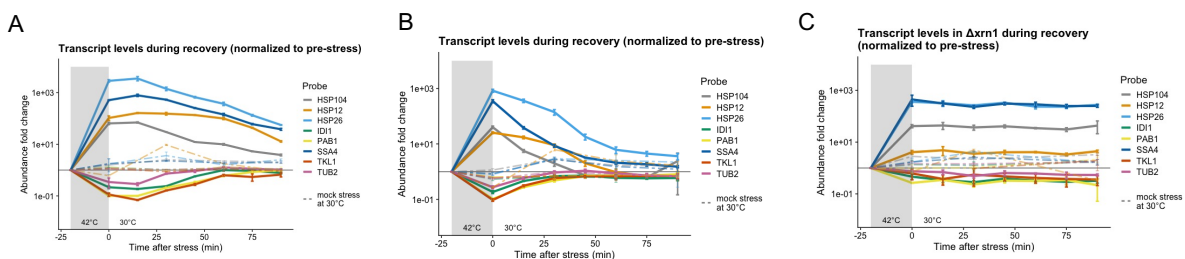

Figure 4.6: **Xrn1 is responsible for RNA degradation during heat stress and recovery** (A) Diploid yeast cells were stressed at 42°C for 20 minutes, then let recover for 90 minutes, with time points taken every 15 minutes. Heat shock transcripts were induced as expected, and then degrade slowly over time. Overall, the transcripts are relatively stable in the short term after stress. (B) Haploid cells were given the same treatment as in A. Transcripts degrade faster. (C) Same treatment done in Δ*xrn1* cells. Transcript levels are stable because Xrn1 is not present to degrade them.

We also looked at a transcript level time-course in a an $\Delta xrn1$ strain, to see how much of the transcript degradation is due to the Xrn1 exonuclease. Surprisingly, in this strain, the transcript level was extremely stable up until 1 hour of recovery, with the overall level barely moving (Figure 4.6C). This aligns with a finding that Xrn1 is the main exonuclease responsible for transcript degradation during heat stress [Bresson et al., 2020].

4.7 Translation rate follows degradation rate, with no specific difference for an A-rich 5'UTR

Given the rapid degradation of HS transcripts in haploids, we asked whether Pab1 might be leading to that degradation, perhaps by recruiting Xrn1. To test this, we created translation reporters that had various 5'UTRs but with the CDS for a nanoluciferase-PEST protein that leads to rapid degradation of the Nanoluc protein. This means we can use luminescence as a readout for a close to real-time translational level, or at least, a real time protein level readout. We compared a translational reporter that had a SSA4 5'UTR, which we know to be extremely A-rich with Pab1 binding at the 5'UTR. We compared this to a translational reporter with the 5'UTR of the glycolytic protein Tkl1, which is a housekeeping gene without an A-rich 5'UTR (Figure 4.7A).

When we did the time course that looked at luminescence level over 90 minutes, we saw that the translational reporters with the *SSA4* 5'UTR were induced during stress and then degraded over time. The reporters with the *TKL1* 5'UTR were stable over time. This suggests that the protein level predominantly follows degradation rate, with no specific difference for an A-rich 5'UTR (Figure 4.7B).
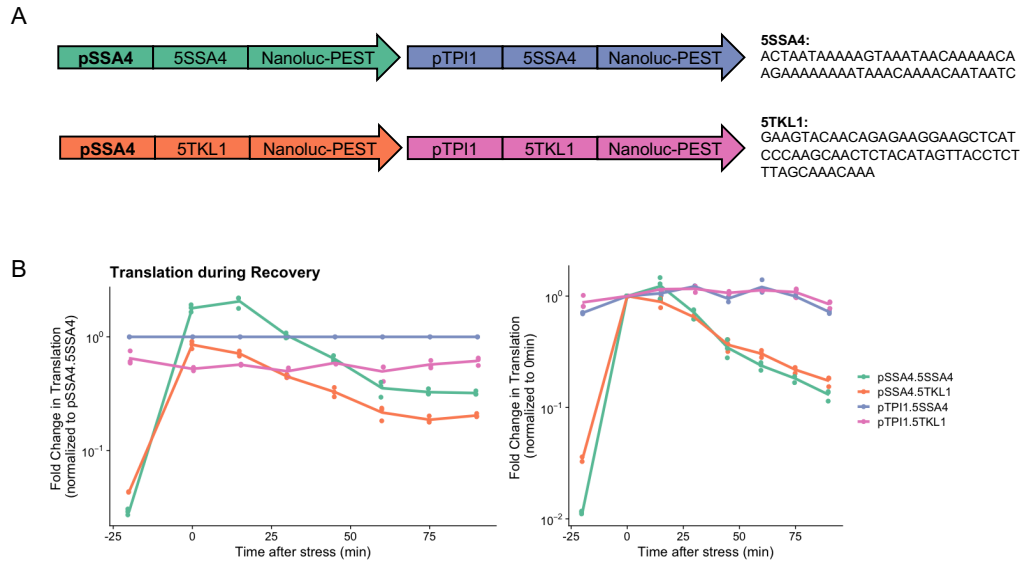
Figure 4.7: **A-rich 5'UTR does not lead to a different rate of degradation during recovery** (A) Different constructs used in this experiment, which match the colors in B. Green and orange have SSA4 promoters but green has a SSA4 5'UTR and orange has a TKL1 5'UTR. Purple and pink have TPI1 promoters (not induced during stress), but purple has a SSA4 5'UTR and pink has the TKL1 5'UTR (B) Left: the constructs with the pSSA4 are induced during stress, and then degrade. Constructs with pTPI1 are relatively stable. There is not significant difference between having the SSA4 5'UTR and the TKL1 5'UTR in terms of degradation rate.

4.8 Thermophilic Pab1 swap does not not affect production of molecular chaperones during stress

As a final test for our original model, we wanted to test what would happen in cells that were heat shocked but in which Pab1 was unable to condensed. To get this condition, we used yeast cells that had their WT Pab1 copies swapped for the Pab1 from a thermophilic yeast strain, *Ogataea parapolymorpha*. The O. parapolymorpha Pab1 does not condense until a much later temperature, 5°C warmer than S. cerevisiae (Figure 4.8A). Thus, the S. cerevisiae yeast with the O.parapolymorpha Pab1 swap will experience heat stress at 42°C but will not have Pab1 condense, providing the condition we need to look at how Pab1 condensation affects chaperone production and translation during stress.

To compare strains, we used cells that had Ssa4-Clover and used flow cytometry where we could measure green fluorescence as a readout for chaperone induction. We compared both diploid cells and haploid cells, that have WT Pab1 and O.para Pab1, at 30°C, 42°C, and 46°C (Figure 4.8B). Overall, we saw no significant difference in SSA4 levels during recovery for haploids or diploids with WT Pab1 or O.para Pab1at 42°C (Figure 4.8C). At 46°C, yCGT040 (OpPab1 + SSA4-Clover) shows a faster induction of Ssa4-Clover, and a very slightly lower amount. We would have expected in cells that did not have Pab1 that condensed during stress, that we would have seen less Ssa4-Clover produced during heat shock. However, the data for all four strains was extremely similar, suggesting that the amount of Ssa4 does not depend on whether Pab1 is condensed or not, strongly challenging our initial proposed model.
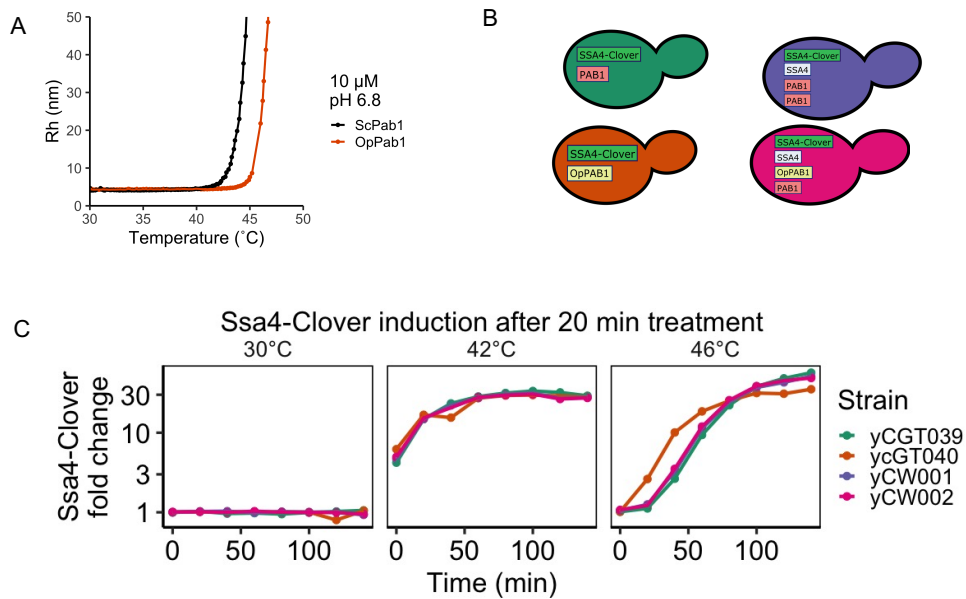
Figure 4.8: **Thermophilic Pab1 swap does not affect the production of *SSA4*** (A) Data (from Haneul Yoo) showing that O.para Pab1 has a higher condensation threshold than S. cerevisiae Pab1. (B) The different strains of yeast used in this experiment, matching the colors in C. Green ScPab1 + Ssa4-Clover. Orange has OpPab1 + SSA4-Clover. Purple is a diploid with 1 copy of Ssa4-Clover, 1 untagged Ssa4, and two copies of wtPab1. Pink has 1 copy of Ssa4-Clover and 1 copy of opPab1. (C) Ssa4 levels are essentially identical between the four yeast strains at 42°C. At 46°C, yCGT040(orange) has slightly earlier SSA4 clover induction

4.9 Discussion

Based on our previous work and other circumstantial evidence, we developed a convincing model of how Pab1's condensation state could be regulating translation of transcripts with A-rich 5'UTRs during stress and recovery. However, after a series of careful experiments, we were not able to come up with sufficient evidence to support this model.

The *in vitro* evidence from the IVT experiments is still incredibly compelling. The fact that adding in Pab1 to cell lysate can strongly affect that lead to specific translational repression of transcripts is extremely interesting, and is in line with previous *in vitro* findings of Pab1 regulating its own transcript. Additionally, the fact that heat-shocked Pab1 could not recapitulate the translational repression is strong evidence that condensed Pab1 is not able to bind RNA during stress, still leaving the possibility that heat shock could be regulating Pab1's ability to bind RNA through its condensation state.

However, all the the experiments done *in vivo* have not supported a model where Pab1 condensation state regulates translation of heat transcripts or chaperone production in a way or timescale that is physiologically crucial for cell recovery. For 42°C heat stress, after 20 minutes, 50% of Pab1 is no longer in the condensed state. Assuming that condensed Pab1 does not bind RNA, 20 minutes of recovery would leave plenty of free Pab1 that could bind RNA and repress translation. However, at 20 minutes of recovery, heat shock transcripts are still found in polysomes and likely being translated, along with housekeeping genes. HS transcript levels are still high and are relatively stable, so Pab1 is likely not leading to immediate specific degradation. The physiological findings found from the results are summarized Table 1.

The fact that we could not find convincing evidence for Pab1 binding leading to translational repression is extremely problematic for the proposed model, essentially killing it. The difference between *in vitro* and *in vivo* data is notable. It is possible that the *in vivo* results
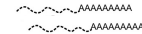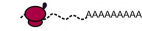
42ºC heat shock	0min	15-20min	60min	90min
Pab1	• In pellet • Pab1 bound to transcripts?	• 50% resolubilized	• >90% resolubilized	• Soluble
HS transcript level	• Transcript levels high (induced)	• Peak transcript level • New transcription has slowed	• ~10-fold decrease in transcript levels	• Continued, steady decrease • (exception: HSP12)
HS transcript translation state	• HS transcripts enriched in polysomes • Peak level of translation	• Transcripts enriched in polysomes • Active translation, close to peak level	• Translation levels decreasing	• Translation levels stabilized
Housekeeping transcripts	• Transcript levels lower than pre-stress levels	• Levels are stable or decreasing	• Transcript levels restored to pre-stress levels	• Transcript levels at pre-stress levels
Housekeeping transcript translation state	• Polysome collapse • Transcripts enriched in free fraction, shifted out of polysomes	• Shifted back into polysome fraction	• Polysomes restored	• Polysomes restored
Cell growth	• Stalled	• Stalled	• Growth restarts	• Growing

Figure 4.9: **Summary of findings during stress and recovery**

are the result of translational repression, and we'd see much higher amounts of translation if we did the same experiment in a strain with Pab1. However, we did not see clear differences in translation of even Pab1 between stress and non-stress conditions, nor any change during stress when with the thermophilic Pab1 swap, so it is perhaps unlikely.

Is it worth it to move forward, leaving this model behind? Yes, given the robust phenotype showing that Pab1 condensation is adaptive and playing an important role, at least in long term growth and survival during stress [Riback et al., 2017]. Further investigation is necessary, likely without constraints that come from testing a specific model. As the essential function of Pab1 still remains unknown, it is possible that uncovering the functional role of condensation will point toward other functions of Pab1. The essential function of Pab1 remains unknown. Condensation might be regulating some aspect of nuclear export, or might be regulating the translation of a different set of transcripts. It might be a subtle effect that is only really noticeable during stressful situations. The strength of the phenotype should motivate future study, knowing that this process is likely physiologically important for cell survival during stress.

CHAPTER 5

DISCUSSION

The question I was always hoping to tackle during my PhD was the function of stress-induced biomolecular condensation. However, the two main projects I worked on did not quite lead me in that direction. The Pab1 project asked the function question, but led me to one way condensation *wasn't* functioning. The RNA condensation project focused on an initial and thorough characterization of stress-induced condensates, emphasizing that what we care about might not always be what we can see or measure.

So, to me the most exciting next steps are the ones that bring us closer to answering the question of function. What happens when stress-induced biomolecular condensation is totally broken? How do we get to the point where we understand it well enough to totally break it? On the protein side, I think we are close and there are ways to break in a controlled fashion– perhaps a more comprehensive swap of thermophilic proteins would answer some questions about important stress-induced protein condensation [Iserman et al., 2020, Keyport Kik et al., 2023]. And the RNA work has many promising next steps, although step one is certainly to identify the protein factor that drives RNA condensation. With that information, it will hopefully be straightforward to prevent stress-induced RNA condensation and look for an adaptive phenotype in cells.

Finding an adaptive phenotype and function would be convenient, because the inconvenient question about stress-induced condensation that still remains is are these structures actually important? Or are the ways we study these condensates, especially the initial experiments which make them appear bright and beautiful, leading us to the biased assumption that they must be important and essential? In Chapters 2 and 3 we discuss how our techniques might bias us to assume that granules are large because they perform roles that require a large size, and that in fact many proposed roles could be performed by many small

things instead of one large thing. But do they even have to be doing anything? Or might they be just a beautiful side effect[Mateju and Chao, 2022]? To bring it back to the sun analogy, might they be sunspots? Perhaps, and without a definitive function, they still may be. These questions floated in the air when I first started, and although certain functions have been found and suggested over time, it doesn't seem that the field has coalesced around framing principles of how cells, and biology, would rely on the phenomenon of biomolecular condensation.

Regardless, from a biophysical standpoint, it is still fascinating that biomolecules can form condensates. Sometimes indistinguishable from unfolded gunk, somewhere between monomer and misfolded aggregate, sit these droplets, gels, granules, foci, clusters, speckles, assemblies, bodies, and whatever new names will be invented in the coming years. Some of them are liquids, some solids, some can even hold gas [Kroschwald et al., 2018, Riback et al., 2017, Wang et al., 2019a]. They're reversible [Wallace et al., 2015, Yoo et al., 2022]. They're everywhere, from bacteria to plants to humans [Pattanayak et al., 2020, Basalla et al., 2023, Solis-Miranda et al., 2023, Field et al., 2023], inside nuclei and cytoplasms [Cho et al., 2018, Ali et al., 2023, Keber et al., 2024]. Perhaps they are everywhere because we have not quite figured out how to properly categorize them. But maybe the way they are ubiquitous and conserved and just, cool, is enough to make them worth studying. At the very least, it makes them worth the delight of sitting at a microscope and seeing how the smooth diffuse signal has gathered into a bright spot.

There is always more work to be done, but this thesis has described a small corner of the mysterious and surprising world of biomolecular condensation. It's easy to wish it was a little less mysterious and surprising, but uncovering the unexpected brings its own set of joys, like a particularly difficult puzzle or particularly clever plot twist, and it's about the process [Yoo et al., 2019]. The fundamental questions remain open, but the future of these questions is bright like, one might say, a fluorescently-labeled condensate.

REFERENCES

Rachy Abraham, Debra Hauer, Robert Lyle McPherson, Age Utt, Ilsa T Kirby, Michael S Cohen, Andres Merits, Anthony K L Leung, and Diane E Griffin. ADP-ribosyl-binding and hydrolase activities of the alphavirus nsp3 macrodomain are critical for initiation of virus replication. *Proc. Natl. Acad. Sci. U. S. A.*, 115(44):E10457–E10466, October 2018.

Daniel Ackerman and M Celeste Simon. Hypoxia, lipids, and cancer: surviving the harsh tumor microenvironment. *Trends Cell Biol.*, 24(8):472–478, August 2014.

Adva Aizer, Alon Kalo, Pinhas Kafri, Amit Shraga, Rakefet Ben-Yishay, Avi Jacob, Noa Kinor, and Yaron Shav-Tal. Quantifying mRNA targeting to P bodies in living human cells reveals a dual role in mRNA decay and storage, 2014.

Azat Akhmetov, Jon M Laurent, Jimmy Gollihar, Elizabeth C Gardner, Riddhiman K Garge, Andrew D Ellington, Aashiq H Kachroo, and Edward M Marcotte. Single-step precision genome editing in yeast using CRISPR-Cas9. 8(6), 2018.

Ivan Akhrymuk, Ilya Frolov, and Elena I Frolova. Sindbis virus infection causes cell death by nsP2-Induced transcriptional shutoff or by nsP3-Dependent translational shutoff. *J. Virol.*, 92(23), December 2018.

Simon Alberti and Serena Carra. Quality control of membraneless organelles. *J. Mol. Biol.*, 430(23):4711–4729, November 2018.

Simon Alberti and Anthony A Hyman. Biomolecular condensates at the nexus of cellular stress, protein aggregation disease and ageing. *Nat. Rev. Mol. Cell Biol.*, 22(3):196–213, March 2021.

Asif Ali, Rania Garde, Olivia C Schaffer, Jared A M Bard, Kabir Husain, Samantha Keyport Kik, Kathleen A Davis, Sofia Luengo-Woods, Maya G Igarashi, D Allan Drummond,

Allison H Squires, and David Pincus. Adaptive preservation of orphan ribosomal proteins in chaperone-dispersed condensates. *Nat. Cell Biol.*, 25(11):1691–1703, November 2023.

P Anderson and N Kedersha. Stressful initiations. 115(Pt 16):3227–3234, 2002.

Paul Anderson, Nancy Kedersha, and Pavel Ivanov. Stress granules, p-bodies and cancer. *Biochim. Biophys. Acta*, 1849(7):861–870, July 2015.

Y Arava, F E Boas, P O Brown, and D Herschlag. Dissecting eukaryotic translation and its control by ribosome density mapping. *Nucleic Acids Res.*, 33(8):2421–2432, 2005.

Yoav Arava, Yulei Wang, John D Storey, Chih Long Liu, Patrick O Brown, and Daniel Herschlag. Genome-wide analysis of mRNA translation profiles in saccharomyces cerevisiae. 100(7):3889–3894, 2003.

Kyoko Arimoto, Hiroyuki Fukuda, Shinobu Imajoh-Ohmi, Haruo Saito, and Mutsuhiro Takekawa. Formation of stress granules inhibits apoptosis by suppressing stress-responsive MAPK pathways. *Nat. Cell Biol.*, 10(11):1324–1332, November 2008.

Stella Aronov, Saray Dover-Biterman, Edith Suss-Toby, Michael Shmoish, Lea Duek, and Mordechai Choder. Pheromone-encoding mRNA is transported to the yeast mating projection by specific RNP granules. *J. Cell Biol.*, 209(6):829–842, June 2015.

Joshua A Arribere, Jennifer A Doudna, and Wendy V Gilbert. Reconsidering movement of eukaryotic mRNAs between polysomes and P bodies. *Mol. Cell*, 44(5):745–758, December 2011.

Anaïs Aulas, Marta M Fay, Shawn M Lyons, Christopher A Achorn, Nancy Kedersha, Paul Anderson, and Pavel Ivanov. Stress-specific differences in assembly and composition of stress granules and related foci. *J. Cell Sci.*, 130(5):927–937, March 2017.

Asli Azizoglu, Roger Brent, and Fabian Rudolf. A precisely adjustable, variation-suppressed eukaryotic transcriptional controller to enable genetic discovery. 10, 2021.

Jnanankur Bag and Jun Wu. Translational control of Poly(A)-Binding protein expression, 1996.

Salman F Banani, Hyun O Lee, Anthony A Hyman, and Michael K Rosen. Biomolecular condensates: organizers of cellular biochemistry. *Nat. Rev. Mol. Cell Biol.*, February 2017.

Joseph L Basalla, Claudia A Mak, Jordan A Byrne, Maria Ghalmi, Y Hoang, and Anthony G Vecchiarelli. Dissecting the phase separation and oligomerization activities of the carboxysome positioning protein McdB. *Elife*, 12, September 2023.

Kyle Begovich and James E Wilhelm. An in vitro assembly system identifies roles for RNA nucleation and ATP in yeast stress granule formation. *Mol. Cell*, July 2020.

Giulia Biancon, Poorval Joshi, Joshua T Zimmer, Torben Hunck, Yimeng Gao, Mark D Lessard, Edward Courchaine, Andrew E S Barentine, Martin Machyna, Valentina Botti, Ashley Qin, Rana Gbyli, Amisha Patel, Yuanbin Song, Lea Kiefer, Gabriella Viero, Nils Neuenkirchen, Haifan Lin, Joerg Bewersdorf, Matthew D Simon, Karla M Neugebauer, Toma Tebaldi, and Stephanie Halene. Precision analysis of mutant U2AF1 activity reveals deployment of stress granules in myeloid malignancies. *Mol. Cell*, 82(6):1107–1122.e7, March 2022.

Nadine Bley, Marcell Lederer, Birgit Pfalz, Claudia Reinke, Tommy Fuchs, Markus Glaß, Birgit Möller, and Stefan Hüttelmaier. Stress granules are dispensable for mRNA stabilization during cellular stress. *Nucleic Acids Res.*, 43(4):e26, February 2015.

G Blobel. Isolation of a 5S RNA-protein complex from mammalian ribosomes. 68(8):1881–1885, 1971.

Steven Boeynaems, Simon Alberti, Nicolas L Fawzi, Tanja Mittag, Magdalini Polymenidou, Frederic Rousseau, Joost Schymkowitz, James Shorter, Benjamin Wolozin, Ludo Van Den Bosch, Peter Tompa, and Monika Fuxreiter. Protein phase separation: A new phase in cell biology. *Trends Cell Biol.*, 28(6):420–435, June 2018.

Daryl A Bosco, Nathan Lemay, Hae Kyung Ko, Hongru Zhou, Chris Burke, Thomas J Kwiatkowski, Jr, Peter Sapp, Diane McKenna-Yasek, Robert H Brown, Jr, and Lawrence J Hayward. Mutant FUS proteins that cause amyotrophic lateral sclerosis incorporate into stress granules. *Hum. Mol. Genet.*, 19(21):4160–4175, November 2010.

Ouissame Bounedjah, Bénédicte Desforges, Ting-Di Wu, Catherine Pioche-Durieu, Sergio Marco, Loic Hamon, Patrick A Curmi, Jean-Luc Guerquin-Kern, Olivier Piétrement, and David Pastré. Free mRNA in excess upon polysome dissociation is a scaffold for protein multimerization to form stress granules. *Nucleic Acids Res.*, 42(13):8678–8691, July 2014.

Clifford P Brangwynne. Phase transitions and size scaling of membrane-less organelles. *J. Cell Biol.*, 203(6):875–881, December 2013.

Nicolas L Bray, Harold Pimentel, Páll Melsted, and Lior Pachter. Near-optimal probabilistic RNA-seq quantification. 34(5):525–527, 2016.

Stefan Bresson, Vadim Shchepachev, Christos Spanos, Tomasz W Turowski, Juri Rappsilber, and David Tollervey. Stress-Induced translation inhibition through rapid displacement of scanning initiation factors. *Mol. Cell*, 0(0), October 2020.

J Ross Buchan and Roy Parker. Eukaryotic stress granules: the ins and outs of translation. *Mol. Cell*, 36(6):932–941, December 2009.

J Ross Buchan, Denise Muhlrad, and Roy Parker. P bodies promote stress granule assembly in saccharomyces cerevisiae. *J. Cell Biol.*, 183(3):441–455, November 2008.

146

J Ross Buchan, Je-Hyun Yoon, and Roy Parker. Stress-specific composition, assembly and kinetics of stress granules in saccharomyces cerevisiae. *J. Cell Sci.*, 124(Pt 2):228–239, January 2011.

J Ross Buchan, Regina-Maria Kolaitis, J Paul Taylor, and Roy Parker. Eukaryotic stress granules are cleared by autophagy and Cdc48/VCP function. *Cell*, 153(7):1461–1474, June 2013.

Hannah M Burgess and Ian Mohr. Defining the role of stress granules in innate immune suppression by the herpes simplex virus 1 endoribonuclease VHS. *J. Virol.*, 92(15), August 2018.

Danae Campos-Melo, Zachary C E Hawley, Cristian A Droppelmann, and Michael J Strong. The integral role of RNA in stress granule formation and function. *Front Cell Dev Biol*, 9:621779, May 2021.

Leon Y Chan, Christopher F Mugler, Stephanie Heinrich, Pascal Vallotton, and Karsten Weis. Non-invasive measurement of mRNA decay reveals translation initiation as the major determinant of mRNA stability. 7, 2018.

Valeria Cherkasov, Sarah Hofmann, Silke Druffel-Augustin, Axel Mogk, Jens Tyedmers, Georg Stoecklin, and Bernd Bukau. Coordination of translational control and protein homeostasis during severe heat stress. *Curr. Biol.*, 23(24):2452–2462, December 2013.

Valeria Cherkasov, Tomas Grousl, Patrick Theer, Yevhen Vainshtein, Christine Gläßer, Cyril Mongis, Günter Kramer, Georg Stoecklin, Michael Knop, Axel Mogk, and Bernd Bukau. Systemic control of protein synthesis through sequestration of translation and ribosome biogenesis factors during severe heat stress. *FEBS Lett.*, October 2015.

J Michael Cherry, Eurie L Hong, Craig Amundsen, Rama Balakrishnan, Gail Binkley, Esther T Chan, Karen R Christie, Maria C Costanzo, Selina S Dwight, Stacia R Engel, Dianna G Fisk, Jodi E Hirschman, Benjamin C Hitz, Kalpana Karra, Cynthia J Krieger, Stuart R Miyasato, Rob S Nash, Julie Park, Marek S Skrzypek, Matt Simison, Shuai Weng, and Edith D Wong. Saccharomyces genome database: the genomics resource of budding yeast. 40(Database issue):D700–5, 2012.

Won-Ki Cho, Jan-Hendrik Spille, Micca Hecht, Choongman Lee, Charles Li, Valentin Grube, and Ibrahim I Cisse. Mediator and RNA polymerase II clusters associate in transcription-dependent condensates. *Science*, 361(6400):412–415, July 2018.

Sonia Chothani, Eleonora Adami, John F Ouyang, Sivakumar Viswanathan, Norbert Hubner, Stuart A Cook, Sebastian Schafer, and Owen J L Rackham. deltaTE: Detection of translationally regulated genes by integrative analysis of ribo-seq and RNA-seq data. 129 (1):e108, 2019.

Hanna J Clarke, Joseph E Chambers, Elizabeth Liniker, and Stefan J Marciniak. Endoplasmic reticulum stress in malignancy. *Cancer Cell*, 25(5):563–573, May 2014.

N C Collier, J Heuser, M A Levy, and M J Schlesinger. Ultrastructural and biochemical analysis of the stress granule in chicken embryo fibroblasts. 106(4):1131–1139, 1988.

J S Cox and P Walter. A novel mechanism for regulating activity of a transcription factor that controls the unfolded protein response. 87(3):391–404, 1996.

Yongjun Dang, Nancy Kedersha, Woon-Kai Low, Daniel Romo, Myriam Gorospe, Randal Kaufman, Paul Anderson, and Jun O Liu. Eukaryotic initiation factor 2alpha-independent pathway of stress granule induction by the natural product pateamine a. *J. Biol. Chem.*, 281(43):32870–32878, October 2006.

O P de Melo Neto, N Standart, and C Martins de Sa. Autoregulation of poly(a)-binding protein synthesis in vitro. *Nucleic Acids Res.*, 23(12):2198–2205, June 1995.

Carolyn J Decker and Roy Parker. P-bodies and stress granules: possible roles in the control of translation and mRNA degradation. *Cold Spring Harb. Perspect. Biol.*, 4(9):a012286, September 2012.

Alexander Dobin, Carrie A Davis, Felix Schlesinger, Jorg Drenkow, Chris Zaleski, Sonali Jha, Philippe Batut, Mark Chaisson, and Thomas R Gingeras. STAR: ultrafast universal RNA-seq aligner. 29(1):15–21, 2013.

L Duret and D Mouchiroud. Expression pattern and, surprisingly, gene length shape codon usage in caenorhabditis, drosophila, and arabidopsis. *Proc. Natl. Acad. Sci. U. S. A.*, 96 (8):4482–4487, 1999.

Nina Eiermann, Katharina Haneke, Zhaozhi Sun, Georg Stoecklin, and Alessia Ruggieri. Dance with the devil: Stress granules and signaling in antiviral responses. *Viruses*, 12(9), September 2020.

Nina Eiermann, Georg Stoecklin, and Bogdan Jovanovic. Mitochondrial inhibition by sodium azide induces assembly of eIF2α Phosphorylation-Independent stress granules in mammalian cells. 23(10):5600, 2022.

Leah E Escalante and Audrey P Gasch. The role of stress-activated RNA-protein granules in surviving adversity. *RNA*, April 2021.

Ana Eulalio, Isabelle Behm-Ansmant, Daniel Schweizer, and Elisa Izaurralde. P-body formation is a consequence, not the cause, of RNA-mediated gene silencing. *Mol. Cell. Biol.*, 27(11):3970–3981, June 2007.

Natalie G Farny, Nancy L Kedersha, and Pamela A Silver. Metazoan stress granule assembly is mediated by P-eIF2alpha-dependent and -independent mechanisms. *RNA*, 15(10):1814–1821, October 2009.

Artem G Fedorovskiy, Anton V Burakov, Ilya M Terenin, Dmitry A Bykov, Kseniya A Lashkevich, Vladimir I Popenko, Nadezhda E Makarova, Ivan I Sorokin, Anastasia P Sukhinina, Vladimir S Prassolov, Pavel V Ivanov, and Sergey E Dmitriev. A solitary stalled 80S ribosome prevents mRNA recruitment to stress granules. 88(11):1786–1799, 2023.

A M Femino, F S Fay, K Fogarty, and R H Singer. Visualization of single RNA transcripts in situ. 280(5363):585–590, 1998.

Sterling Field, Geng-Jen Jang, Caroline Dean, Lucia C Strader, and Seung Y Rhee. Plants use molecular mechanisms mediated by biomolecular condensates to integrate environmental cues with development. *Plant Cell*, 35(9):3173–3186, September 2023.

Marie-Josée Fournier, Cristina Gareau, and Rachid Mazroui. The chemotherapeutic agent bortezomib induces the formation of stress granules. *Cancer Cell Int.*, 10:12, April 2010.

Tobias M Franks and Jens Lykke-Andersen. TTP and BRF proteins nucleate processing body formation to silence mRNAs with AU-rich elements. *Genes Dev.*, 21(6):719–735, March 2007.

Titus M Franzmann, Marcus Jahnel, Andrei Pozniakovsky, Julia Mahamid, Alex S Holehouse, Elisabeth Nüske, Doris Richter, Wolfgang Baumeister, Stephan W Grill, Rohit V Pappu, Anthony A Hyman, and Simon Alberti. Phase separation of a yeast prion protein promotes cellular fitness. 359(6371):eaao5654, 2018.

Brian D Freibaum, James Messing, Peiguo Yang, Hong Joo Kim, and J Paul Taylor. High-fidelity reconstitution of stress granules and nucleoli in mammalian cellular lysate. *J. Cell Biol.*, 220(3), March 2021.

Ken Fujimura, Atsuo T Sasaki, and Paul Anderson. Selenite targets eIF4E-binding protein-1 to inhibit translation initiation and induce the assembly of non-canonical stress granules. *Nucleic Acids Res.*, 40(16):8099–8110, September 2012.

Jozsef Gal, Lisha Kuang, Kelly R Barnett, Brian Z Zhu, Susannah C Shissler, Konstantin V Korotkov, Lawrence J Hayward, Edward J Kasarskis, and Haining Zhu. ALS mutant SOD1 interacts with G3BP1 and affects stress granule dynamics. *Acta Neuropathol.*, 132 (4):563–576, October 2016.

Xiaomeng Gao, Li Jiang, Yanling Gong, Xiaobing Chen, Meidan Ying, Hong Zhu, Qiaojun He, Bo Yang, and Ji Cao. Stress granule: A promising target for cancer treatment. *Br. J. Pharmacol.*, 176(23):4421–4433, December 2019.

Elena Garre, Lorena Romero-Santacreu, Nikki De Clercq, Nati Blasco-Angulo, Per Sunnerhagen, and Paula Alepuz. Yeast mRNA cap-binding protein Cbc1/Sto1 is necessary for the rapid reprogramming of translation after hyperosmotic shock. 23(1):137–150, 2012.

R Daniel Gietz and Robin A Woods. Transformation of yeast by lithium acetate/single-stranded carrier DNA/polyethylene glycol method. 350:87–96, 2002.

Hendrik Glauninger, Caitlin J Wong Hickernell, Jared A M Bard, and D Allan Drummond. Stressful steps: Progress and challenges in understanding stress-induced mRNA condensation and accumulation in stress granules. 82(14):2544–2556, 2022.

Edward Gomes and James Shorter. The molecular language of membraneless organelles. *J. Biol. Chem.*, 294(18):7115–7127, May 2019.

Chiara Gorrini, Isaac S Harris, and Tak W Mak. Modulation of oxidative stress as an anticancer strategy. *Nat. Rev. Drug Discov.*, 12(12):931–947, December 2013.

T Grousl, P Ivanov, I Frydlova, P Vasicova, F Janda, J Vojtova, K Malinska, I Malcova, L Novakova, D Janoskova, L Valasek, and J Hasek. Robust heat shock induces eIF2alpha-phosphorylation-independent assembly of stress granules containing eIF3 and 40S ribosomal subunits in budding yeast, saccharomyces cerevisiae. *J. Cell Sci.*, 122(Pt 12):2078–2088, 2009.

T Grousl, P Ivanov, I Malcova, P Pompach, I Frydlova, R Slaba, L Senohrabkova, L Novakova, and J Hasek. Heat shock-induced accumulation of translation elongation and termination factors precedes assembly of stress granules in s. cerevisiae. *PLoS One*, 8(2): e57083, 2013.

Jordina Guillén-Boixet, Andrii Kopach, Alex S Holehouse, Sina Wittmann, Marcus Jahnel, Raimund Schlüßler, Kyoohyun Kim, Irmela R E A Trussina, Jie Wang, Daniel Mateju, Ina Poser, Shovamayee Maharana, Martine Ruer-Gruß, Doris Richter, Xiaojie Zhang, Young-Tae Chang, Jochen Guck, Alf Honigmann, Julia Mahamid, Anthony A Hyman, Rohit V Pappu, Simon Alberti, and Titus M Franzmann. RNA-Induced conformational switching and clustering of G3BP drive stress granule assembly by condensation. *Cell*, 181(2):346–361.e17, April 2020.

Lin Guo and James Shorter. It's raining liquids: RNA tunes viscoelasticity and dynamics of membraneless organelles. *Mol. Cell*, 60(2):189–192, October 2015.

Anna R Guzikowski, Yang S Chen, and Brian M Zid. Stress-induced mRNP granules: Form and function of processing bodies and stress granules. *Wiley Interdiscip. Rev. RNA*, 10 (3):e1524, May 2019.

Youngdae Gwon, Brian A Maxwell, Regina-Maria Kolaitis, Peipei Zhang, Hong Joo Kim, and J Paul Taylor. Ubiquitination of G3BP1 mediates stress granule disassembly in a context-specific manner. *Science*, 372(6549):eabf6548, June 2021.

Tatsuya Hata, Yuki Ishiwata-Kimata, and Yukio Kimata. Induction of the unfolded protein response at high temperature in saccharomyces cerevisiae. 23(3), 2022.

Alan G Hinnebusch. Translational regulation of GCN4 and the general amino acid control of yeast. 59:407–450, 2005.

Sarah Hofmann, Nancy Kedersha, Paul Anderson, and Pavel Ivanov. Molecular mechanisms of stress granule assembly and disassembly. *Biochim. Biophys. Acta Mol. Cell Res.*, 1868 (1):118876, September 2020.

Nathaniel P Hoyle, Lydia M Castelli, Susan G Campbell, Leah E A Holmes, and Mark P Ashe. Stress-dependent relocalization of translationally primed mRNPs to cytoplasmic granules that are kinetically and spatially distinct from p-bodies. 179(1):65–74, 2007.

Arnaud Hubstenberger, Maïté Courel, Marianne Bénard, Sylvie Souquere, Michèle Ernoult-Lange, Racha Chouaib, Zhou Yi, Jean-Baptiste Morlot, Annie Munier, Magali Fradet, Maëlle Daunesse, Edouard Bertrand, Gérard Pierron, Julien Mozziconacci, Michel Kress, and Dominique Weil. P-Body purification reveals the condensation of repressed mRNA regulons. *Mol. Cell*, 68(1):144–157.e5, October 2017.

Anthony A Hyman, Christoph A Weber, and Frank Jülicher. Liquid-liquid phase separation in biology. *Annu. Rev. Cell Dev. Biol.*, 30:39–58, 2014.

Arthur Imbert, Wei Ouyang, Adham Safieddine, Emeline Coleno, Christophe Zimmer, Edouard Bertrand, Thomas Walter, and Florian Mueller. FISH-quant v2: a scalable and modular analysis tool for smFISH image analysis. 2021.

Christiane Iserman, Christine Desroches Altamirano, Ceciel Jegers, Ulrike Friedrich, Taraneh Zarin, Anatol W Fritsch, Matthäus Mittasch, Antonio Domingues, Lena Hersemann, Marcus Jahnel, Doris Richter, Ulf-Peter Guenther, Matthias W Hentze, Alan M Moses, Anthony A Hyman, Günter Kramer, Moritz Kreysing, Titus M Franzmann, and Simon Alberti. Condensation of ded1p promotes a translational switch from housekeeping to stress protein production. *Cell*, 0(0), April 2020.

P A Ivanov, E M Chudinova, and E S Nadezhdina. RNP stress-granule formation is inhibited by microtubule disruption. *Cell Biol. Int.*, 27(3):207–208, 2003a.

P A Ivanov, E M Chudinova, and E S Nadezhdina. Disruption of microtubules inhibits cytoplasmic ribonucleoprotein stress granule formation. *Exp. Cell Res.*, 290(2):227–233, 2003b.

Pavel Ivanov, Nancy Kedersha, and Paul Anderson. Stress granules and processing bodies in translational control. *Cold Spring Harb. Perspect. Biol.*, 11(5), May 2019.

Ankur Jain and Ronald D Vale. RNA phase transitions in repeat expansion disorders. *Nature*, 546(7657):243–247, June 2017.

Saumya Jain, Joshua R Wheeler, Robert W Walters, Anurag Agrawal, Anthony Barsic, and Roy Parker. ATPase-Modulated stress granules contain a diverse proteome and substructure. *Cell*, 164(3):487–498, January 2016.

Aravinth Kumar Jayabalan, Srivathsan Adivarahan, Aakash Koppula, Rachy Abraham, Mona Batish, Daniel Zenklusen, Diane E Griffin, and Anthony K L Leung. Stress granule formation, disassembly, and composition are regulated by alphavirus ADP-ribosylhydrolase activity. *Proc. Natl. Acad. Sci. U. S. A.*, 118(6), February 2021.

154

Christian Kaehler, Jörg Isensee, Tim Hucho, Hans Lehrach, and Sylvia Krobitsch. 5-fluorouracil affects assembly of stress granules based on RNA incorporation. *Nucleic Acids Res.*, 42(10):6436–6447, June 2014.

A Kahvejian, G Roy, and N Sonenberg. The mRNA closed-loop model: the function of PABP and PABP-interacting proteins in mRNA translation. *Cold Spring Harb. Symp. Quant. Biol.*, 66:293–300, 2001.

Kenta Kato, Yosuke Yamamoto, and Shingo Izawa. Severe ethanol stress induces assembly of stress granules in saccharomyces cerevisiae. 28(5):339–347, 2011.

Hiroshi Katoh, Toru Okamoto, Takasuke Fukuhara, Hiroto Kambara, Eiji Morita, Yoshio Mori, Wataru Kamitani, and Yoshiharu Matsuura. Japanese encephalitis virus core protein inhibits stress granule formation through an interaction with caprin-1 and facilitates viral propagation. *J. Virol.*, 87(1):489–502, January 2013.

Felix C Keber, Thao Nguyen, Andrea Mariossi, Clifford P Brangwynne, and Martin Wühr. Evidence for widespread cytoplasmic structuring into mesoscale condensates. *Nat. Cell Biol.*, 26(3):346–352, March 2024.

N Kedersha and P Anderson. Stress granules: sites of mRNA triage that regulate mRNA stability and translatability. *Biochem. Soc. Trans.*, 30(Pt 6):963–969, November 2002.

N Kedersha, M R Cho, W Li, P W Yacono, S Chen, N Gilks, D E Golan, and P Anderson. Dynamic shuttling of TIA-1 accompanies the recruitment of mRNA to mammalian stress granules. *J. Cell Biol.*, 151(6):1257–1268, December 2000.

N L Kedersha, M Gupta, W Li, I Miller, and P Anderson. RNA-binding proteins TIA-1 and TIAR link the phosphorylation of eIF-2 alpha to the assembly of mammalian stress granules. *J. Cell Biol.*, 147(7):1431–1442, December 1999.

Nancy Kedersha and Paul Anderson. Regulation of translation by stress granules and processing bodies. *Prog. Mol. Biol. Transl. Sci.*, 90:155–185, October 2009.

Nancy Kedersha, Samantha Chen, Natalie Gilks, Wei Li, Ira J Miller, Joachim Stahl, and Paul Anderson. Evidence that ternary complex (eIF2-GTP-tRNA(i)(Met))-deficient preinitiation complexes are core constituents of mammalian stress granules. *Mol. Biol. Cell*, 13(1):195–210, January 2002.

Nancy Kedersha, Pavel Ivanov, and Paul Anderson. Stress granules and cell signaling: more than just a passing phase? *Trends Biochem. Sci.*, 38(10):494–506, October 2013.

Nancy Kedersha, Marc D Panas, Christopher A Achorn, Shawn Lyons, Sarah Tisdale, Tyler Hickman, Marshall Thomas, Judy Lieberman, Gerald M McInerney, Pavel Ivanov, and Paul Anderson. G3BP-Caprin1-USP10 complexes mediate stress granule condensation and associate with 40S subunits. *J. Cell Biol.*, 212(7):845–860, March 2016.

Jan Keiten-Schmitz, Kristina Wagner, Tanja Piller, Manuel Kaulich, Simon Alberti, and Stefan Müller. The nuclear SUMO-Targeted ubiquitin quality control network regulates the dynamics of cytoplasmic stress granules. *Mol. Cell*, 79(1):54–67.e7, July 2020.

Samantha Keyport Kik, Dana Christopher, Hendrik Glauninger, Caitlin Wong Hickernell, Jared A M Bard, Michael Ford, Tobin R Sosnick, and D Allan Drummond. An adaptive biomolecular condensation response is conserved across environmentally divergent species. 2023.

Anthony Khong and Roy Parker. The landscape of eukaryotic mRNPs. 26(3):229–239, 2020.

Anthony Khong, Craig H Kerr, Clarence H L Yeung, Kathleen Keatings, Arabinda Nayak, Douglas W Allan, and Eric Jan. Disruption of stress granule formation by the multifunctional cricket paralysis virus 1A protein. *J. Virol.*, 91(5), March 2017a.

Anthony Khong, Tyler Matheny, Saumya Jain, Sarah F Mitchell, Joshua R Wheeler, and Roy Parker. The stress granule transcriptome reveals principles of mRNA accumulation in stress granules. *Mol. Cell*, 68(4):808–820.e5, November 2017b.

Michael A Kiebler and Gary J Bassell. Neuronal RNA granules: movers and makers. *Neuron*, 51(6):685–690, September 2006.

Yukio Kimata, Yuki Ishiwata-Kimata, Seiko Yamada, and Kenji Kohno. Yeast unfolded protein response pathway regulates expression of genes for anti-oxidative stress and for cell surface proteins. 11(1):59–69, 2006.

Hemant K Kini, Ian M Silverman, Xinjun Ji, Brian D Gregory, and Stephen A Liebhaber. Cytoplasmic poly(a) binding protein-1 binds to genomically encoded sequences within mammalian mRNAs, 2016.

Hema Kopalle. *Visualization of membrane-less granules in yeast and mammalian cells using modified fluorescence in-situ hybridization.* PhD thesis, 2019.

Joanna Krakowiak, Xu Zheng, Nikit Patel, Zoë A Feder, Jayamani Anandhakumar, Kendra Valerius, David S Gross, Ahmad S Khalil, and David Pincus. Hsf1 and hsp70 constitute a two-component feedback loop that regulates the yeast heat shock response. 7, 2018.

S Kramer, R Queiroz, L Ellis, H Webb, J D Hoheisel, C Clayton, and M Carrington. Heat shock causes a decrease in polysomes and the appearance of stress granules in trypanosomes independently of eIF2(alpha) phosphorylation at thr169. *J. Cell Sci.*, 121(Pt 18):3002–3014, 2008.

Sonja Kroschwald, Shovamayee Maharana, Daniel Mateju, Liliana Malinovska, Elisabeth Nüske, Ina Poser, Doris Richter, and Simon Alberti. Promiscuous interactions and protein

disaggregases determine the material state of stress-inducible RNP granules. *Elife*, 4: e06807, August 2015.

Sonja Kroschwald, Matthias C Munder, Shovamayee Maharana, Titus M Franzmann, Doris Richter, Martine Ruer, Anthony A Hyman, and Simon Alberti. Different material states of pub1 condensates define distinct modes of stress adaptation and recovery. *Cell Rep.*, 23(11):3327–3339, June 2018.

V V Kushnirov. Rapid and reliable protein extraction from yeast. 16(9):857–860, 2000.

Lok Man John Law, Brandon S Razooky, Melody M H Li, Shihyun You, Andrea Jurado, Charles M Rice, and Margaret R MacDonald. ZAP's stress granule localization is correlated with its antiviral activity and induced by virus replication. *PLoS Pathog.*, 15(5): e1007798, May 2019.

Michael E Lee, William C DeLoache, Bernardo Cervantes, and John E Dueber. A highly characterized yeast toolkit for modular, multipart assembly. 4(9):975–986, 2015.

Heng Li, Bob Handsaker, Alec Wysoker, Tim Fennell, Jue Ruan, Nils Homer, Gabor Marth, Goncalo Abecasis, and Richard Durbin. The sequence Alignment/Map format and SAMtools. 25(16):2078–2079, 2009.

Weihan Li, Anna Maekiniemi, Hanae Sato, Christof Osman, and Robert H Singer. An improved imaging system that corrects MS2-induced RNA destabilization. 19(12):1558–1562, 2022.

Ya-Cheng Liao, Michael S Fernandopulle, Guozhen Wang, Heejun Choi, Ling Hao, Catherine M Drerup, Rajan Patel, Seema Qamar, Jonathon Nixon-Abell, Yi Shen, William Meadows, Michele Vendruscolo, Tuomas P J Knowles, Matthew Nelson, Magdalena A Czekalska, Greta Musteikyte, Mariam A Gachechiladze, Christina A Stephens, H Amalia Pasolli,

Lucy R Forrest, Peter St George-Hyslop, Jennifer Lippincott-Schwartz, and Michael E Ward. RNA granules hitchhike on lysosomes for Long-Distance transport, using annexin A11 as a molecular tether. *Cell*, 179(1):147–164.e20, September 2019.

S Lindquist. Regulation of protein synthesis during heat shock. *Nature*, 293(5830):311–314, September 1981.

S Lindquist and R Petersen. Selective translation and degradation of heat-shock messenger RNAs in drosophila. *Enzyme*, 44(1-4):147–166, 1990.

Inês Lopes, Gulam Altab, Priyanka Raina, and João Pedro de Magalhães. Gene size matters: An analysis of gene length in the human genome. *Front. Genet.*, 12:559998, February 2021.

Ronny Lorenz, Stephan H Bernhart, Christian Höner Zu Siederdissen, Hakim Tafer, Christoph Flamm, Peter F Stadler, and Ivo L Hofacker. ViennaRNA package 2.0. 6:26, 2011.

Michael I Love, Wolfgang Huber, and Simon Anders. Moderated estimation of fold change and dispersion for RNA-seq data with DESeq2. 15(12):550, 2014.

Woon-Kai Low, Yongjun Dang, Tilman Schneider-Poetsch, Zonggao Shi, Nam Song Choi, William C Merrick, Daniel Romo, and Jun O Liu. Inhibition of eukaryotic translation initiation by the marine natural product pateamine a. *Mol. Cell*, 20(5):709–722, December 2005.

Andrew S Lyon, William B Peeples, and Michael K Rosen. A framework for understanding the functions of biomolecular condensates across scales. *Nat. Rev. Mol. Cell Biol.*, November 2020.

Ian R Mackenzie, Alexandra M Nicholson, Mohona Sarkar, James Messing, Maria D Purice, Cyril Pottier, Kavya Annu, Matt Baker, Ralph B Perkerson, Aishe Kurti, Billie J Match-

ett, Tanja Mittag, Jamshid Temirov, Ging-Yuek R Hsiung, Charles Krieger, Melissa E Murray, Masato Kato, John D Fryer, Leonard Petrucelli, Lorne Zinman, Sandra Weintraub, Marsel Mesulam, Julia Keith, Sasha A Zivkovic, Veronica Hirsch-Reinshagen, Raymond P Roos, Stephan Züchner, Neill R Graff-Radford, Ronald C Petersen, Richard J Caselli, Zbigniew K Wszolek, Elizabeth Finger, Carol Lippa, David Lacomis, Heather Stewart, Dennis W Dickson, Hong Joo Kim, Ekaterina Rogaeva, Eileen Bigio, Kevin B Boylan, J Paul Taylor, and Rosa Rademakers. TIA1 mutations in amyotrophic lateral sclerosis and frontotemporal dementia promote phase separation and alter stress granule dynamics. *Neuron*, 95(4):808–816.e9, August 2017.

Hicham Mahboubi and Ursula Stochaj. Cytoplasmic stress granules: Dynamic modulators of cell signaling and disease. *Biochim. Biophys. Acta Mol. Basis Dis.*, 1863(4):884–895, April 2017.

Sebastian Markmiller, Sahar Soltanieh, Kari L Server, Raymond Mak, Wenhao Jin, Mark Y Fang, En-Ching Luo, Florian Krach, Dejun Yang, Anindya Sen, Amit Fulzele, Jacob M Wozniak, David J Gonzalez, Mark W Kankel, Fen-Biao Gao, Eric J Bennett, Eric Lécuyer, and Gene W Yeo. Context-Dependent and Disease-Specific diversity in protein interactions within stress granules. *Cell*, 172(3):590–604.e13, January 2018.

Hagai Marmor-Kollet, Aviad Siany, Nancy Kedersha, Naama Knafo, Natalia Rivkin, Yehuda M Danino, Thomas G Moens, Tsviya Olender, Daoud Sheban, Nir Cohen, Tali Dadosh, Yoseph Addadi, Revital Ravid, Chen Eitan, Beata Toth Cohen, Sarah Hofmann, Claire L Riggs, Vivek M Advani, Adrian Higginbottom, Johnathan Cooper-Knock, Jacob H Hanna, Yifat Merbl, Ludo Van Den Bosch, Paul Anderson, Pavel Ivanov, Tamar Geiger, and Eran Hornstein. Spatiotemporal proteomic analysis of stress granule disas-

sembly using APEX reveals regulation by SUMOylation and links to ALS pathogenesis. *Mol. Cell*, 80(5):876–891.e6, December 2020.

Anna E Masser, Ganapathi Kandasamy, Jayasankar Mohanakrishnan Kaimal, and Claes Andréasson. Luciferase NanoLuc as a reporter for gene expression and protein levels in saccharomyces cerevisiae. 33(5):191–200, 2016.

Daniel Mateju and Jeffrey A Chao. Stress granules: regulators or by-products? *FEBS J.*, 289(2):363–373, January 2022.

Daniel Mateju, Bastian Eichenberger, Franka Voigt, Jan Eglinger, Gregory Roth, and Jeffrey A Chao. Single-Molecule imaging reveals translation of mRNAs localized to stress granules. *Cell*, 183(7):1801–1812.e13, December 2020.

Tyler Matheny, Bhalchandra S Rao, and Roy Parker. Transcriptome-Wide comparison of stress granules and P-Bodies reveals that translation plays a major role in RNA partitioning. *Mol. Cell. Biol.*, 39(24), December 2019.

Tyler Matheny, Briana Van Treeck, Thao Ngoc Huynh, and Roy Parker. RNA partitioning into stress granules is based on the summation of multiple interactions. *RNA*, 27(2): 174–189, February 2021.

Brian A Maxwell, Youngdae Gwon, Ashutosh Mishra, Junmin Peng, Haruko Nakamura, Ke Zhang, Hong Joo Kim, and J Paul Taylor. Ubiquitination is essential for recovery of cellular activities after heat shock. *Science*, 372(6549):eabc3593, June 2021.

Rachid Mazroui, Marc-Etienne Huot, Sandra Tremblay, Christine Filion, Yves Labelle, and Edouard W Khandjian. Trapping of messenger RNA by fragile X mental retardation protein into cytoplasmic granules induces translation repression. 11(24):3007–3017, 2002.

Rachid Mazroui, Rami Sukarieh, Marie-Eve Bordeleau, Randal J Kaufman, Peter Northcote, Junichi Tanaka, Imed Gallouzi, and Jerry Pelletier. Inhibition of ribosome recruitment induces stress granule formation independently of eukaryotic initiation factor 2alpha phosphorylation. *Mol. Biol. Cell*, 17(10):4212–4219, October 2006.

Gonzalo I Mendoza-Ochoa, J David Barrass, Barbara R Terlouw, Isabella E Maudlin, Susana de Lucas, Emanuela Sani, Vahid Aslanzadeh, Jane A E Reid, and Jean D Beggs. A fast and tuneable auxin-inducible degron for depletion of target proteins in budding yeast. 36 (1):75–81, 2019.

Diana M Mitrea and Richard W Kriwacki. Phase separation in biology; functional organization of a higher order. *Cell Commun. Signal.*, 14:1, January 2016.

Tanja Mittag and Rohit V Pappu. A conceptual framework for understanding phase separation and addressing open questions and challenges. 2022.

Amandine Molliex, Jamshid Temirov, Jihun Lee, Maura Coughlin, Anderson P Kanagaraj, Hong Joo Kim, Tanja Mittag, and J Paul Taylor. Phase separation by low complexity domains promotes stress granule assembly and drives pathological fibrillization. *Cell*, 163 (1):123–133, September 2015.

Stephanie L Moon, Tatsuya Morisaki, Anthony Khong, Kenneth Lyon, Roy Parker, and Timothy J Stasevich. Multicolour single-molecule tracking of mRNA interactions with RNP granules. *Nat. Cell Biol.*, 21(2):162–168, February 2019.

Stephanie L Moon, Tatsuya Morisaki, Timothy J Stasevich, and Roy Parker. Coupling of translation quality control and mRNA targeting to stress granules. *J. Cell Biol.*, 219(8), August 2020.

R I Morimoto. Regulation of the heat shock transcriptional response: cross talk between a family of heat shock factors, molecular chaperones, and negative regulators. *Genes Dev.*, 12(24):3788–3796, December 1998.

P P Mueller and A G Hinnebusch. Multiple upstream AUG codons mediate translational control of GCN4. 45(2):201–207, 1986.

Moritz Mühlhofer, Evi Berchtold, Chris G Stratil, Gergely Csaba, Elena Kunold, Nina C Bach, Stephan A Sieber, Martin Haslbeck, Ralf Zimmer, and Johannes Buchner. The heat shock response in yeast maintains protein homeostasis by chaperoning and replenishing proteins. 29(13):4593–4607.e8, 2019.

E S Nadezhdina, A J Lomakin, A A Shpilman, E M Chudinova, and P A Ivanov. Microtubules govern stress granule mobility and dynamics. *Biochim. Biophys. Acta*, 1803(3): 361–371, 2010.

Sim Namkoong, Allison Ho, Yu Mi Woo, Hojoong Kwak, and Jun Hee Lee. Systematic characterization of Stress-Induced RNA granulation. *Mol. Cell*, 70(1):175–187.e8, April 2018.

R D Nolan and H R Arnstein. The dissociation of rabbit reticulocyte ribosomes into subparticles active in protein synthesis. 10(1):96–101, 201969.

L Nover, K D Scharf, and D Neumann. Formation of cytoplasmic heat shock granules in tomato cell cultures and leaves. *Mol. Cell. Biol.*, 3(9):1648–1655, September 1983.

L Nover, K D Scharf, and D Neumann. Cytoplasmic heat shock granules are formed from precursor particles and are associated with a specific set of mRNAs. *Mol. Cell. Biol.*, 9 (3):1298–1308, March 1989.

Alejandro Padrón, Shintaro Iwasaki, and Nicholas T Ingolia. Proximity RNA labeling by APEX-Seq reveals the organization of translation initiation complexes and repressive RNA granules. *Mol. Cell*, 75(4):875–887.e5, August 2019.

Marc D Panas, Pavel Ivanov, and Paul Anderson. Mechanistic insights into mammalian stress granule dynamics. *J. Cell Biol.*, 215(3):313–323, November 2016.

Avinash Patel, Hyun O Lee, Louise Jawerth, Shovamayee Maharana, Marcus Jahnel, Marco Y Hein, Stoyno Stoynov, Julia Mahamid, Shambaditya Saha, Titus M Franzmann, Andrej Pozniakovski, Ina Poser, Nicola Maghelli, Loic A Royer, Martin Weigert, Eugene W Myers, Stephan Grill, David Drechsel, Anthony A Hyman, and Simon Alberti. A Liquid-to-Solid phase transition of the ALS protein FUS accelerated by disease mutation. *Cell*, 162(5):1066–1077, August 2015.

Gopal K Pattanayak, Yi Liao, Edward W J Wallace, Bogdan Budnik, D Allan Drummond, and Michael J Rust. Daily cycles of reversible protein condensation in cyanobacteria. *Cell Rep.*, 32(7):108032, August 2020.

Vicent Pelechano, Wu Wei, and Lars M Steinmetz. Extensive transcriptional heterogeneity revealed by isoform profiling. 497(7447):127–131, 2013.

Sijia Peng, Weiping Li, Yirong Yao, Wenjing Xing, Pilong Li, and Chunlai Chen. Phase separation at the nanoscale quantified by dcFCCS. *Proc. Natl. Acad. Sci. U. S. A.*, 117 (44):27124–27131, November 2020.

David Pincus, Jayamani Anandhakumar, Prathapan Thiru, Michael J Guertin, Alexander M Erkine, and David S Gross. Genetic and epigenetic determinants establish a continuum of hsf1 occupancy and activity across the yeast genome. 29(26):3168–3182, 2018.

Thomas Preiss, Julie Baron-Benhamou, Wilhelm Ansorge, and Matthias W Hentze. Homodirectional changes in transcriptome composition and mRNA translation induced by rapamycin and heat shock. *Nat. Struct. Biol.*, 10(12):1039–1047, December 2003.

David S W Protter and Roy Parker. Principles and properties of stress granules. 26(9): 668–679, 2016.

Kavya Vinayan Pushpalatha and Florence Besse. Local translation in axons: When membraneless RNP granules meet Membrane-Bound organelles. *Front Mol Biosci*, 6:129, November 2019.

Andrea Putnam, Laura Thomas, and Geraldine Seydoux. RNA granules: functional compartments or incidental condensates? 37(9-10):354–376, 2023.

R Core Team. R: A language and environment for statistical computing, 2022.

Samir Rahman and Daniel Zenklusen. Single-molecule resolution fluorescent in situ hybridization (smFISH) in the yeast s. cerevisiae. 1042:33–46, 2013.

Bhalchandra S Rao and Roy Parker. Numerous interactions act redundantly to assemble a tunable size of P bodies in *Saccharomyces cerevisiae*. 114(45):E9569–E9578, 2017.

Lucas C Reineke and Joel R Neilson. Differences between acute and chronic stress granules, and how these differences may impact function in human disease. *Biochem. Pharmacol.*, 162:123–131, April 2019.

Joshua A Riback, Christopher D Katanski, Jamie L Kear-Scott, Evgeny V Pilipenko, Alexandra E Rojek, Tobin R Sosnick, and D Allan Drummond. Stress-Triggered phase separation is an adaptive, evolutionarily tuned response. *Cell*, 168(6):1028–1040.e19, March 2017.

Joshua A Riback, Jorine M Eeftens, Daniel S W Lee, Sofia A Quinodoz, Lien Beckers, Lindsay A Becker, and Clifford P Brangwynne. Viscoelastic RNA entanglement and advective flow underlie nucleolar form and function. January 2022.

Nina Ripin and Roy Parker. Are stress granules the RNA analogs of misfolded protein aggregates? *RNA*, October 2021.

Johannes Ristau, Kathleen Watt, Christian Oertlin, and Ola Larsson. Polysome fractionation for Transcriptome-Wide studies of mRNA translation. 2418:223–241, 2022.

F Ritossa. A new puffing pattern induced by temperature shock and DNP in drosophila. *Experientia*, 18(12):571–573, December 1962.

Christian P Robert and George Casella. *Monte Carlo Statistical Methods*. Springer New York.

Kim M Rutherford, Manuel Lera-Ramírez, and Valerie Wood. PomBase: a global core biodata resource-growth, collaboration, and sustainability. 2024.

Pabitra K Sahoo, Seung Joon Lee, Poonam B Jaiswal, Stefanie Alber, Amar N Kar, Sharmina Miller-Randolph, Elizabeth E Taylor, Terika Smith, Bhagat Singh, Tammy Szu-Yu Ho, Anatoly Urisman, Shreya Chand, Edsel A Pena, Alma L Burlingame, Clifford J Woolf, Mike Fainzilber, Arthur W English, and Jeffery L Twiss. Axonal G3BP1 stress granule protein limits axonal mRNA translation and nerve regeneration. *Nat. Commun.*, 9(1): 3358, August 2018.

Pabitra K Sahoo, Amar N Kar, Nitzan Samra, Marco Terenzio, Priyanka Patel, Seung Joon Lee, Sharmina Miller, Elizabeth Thames, Blake Jones, Riki Kawaguchi, Giovanni Coppola, Mike Fainzilber, and Jeffery L Twiss. A Ca2+-Dependent switch activates axonal casein

kinase 2α translation and drives G3BP1 granule disassembly for axon regeneration. *Curr. Biol.*, 30(24):4882–4895.e6, December 2020.

Parimal Samir, Sannula Kesavardhana, Deanna M Patmore, Sebastien Gingras, R K Subbarao Malireddi, Rajendra Karki, Clifford S Guy, Benoit Briard, David E Place, Anannya Bhattacharya, Bhesh Raj Sharma, Amanda Nourse, Sharon V King, Aaron Pitre, Amanda R Burton, Stephane Pelletier, Richard J Gilbertson, and Thirumala-Devi Kanneganti. DDX3X acts as a live-or-die checkpoint in stressed cells by regulating NLRP3 inflammasome. *Nature*, 573(7775):590–594, September 2019.

Natalia Sanchez de Groot, Alexandros Armaos, Ricardo Graña-Montes, Marion Alriquet, Giulia Calloni, R Martin Vabulas, and Gian Gaetano Tartaglia. RNA structure drives interaction with proteins. *Nat. Commun.*, 10(1):3246, July 2019.

David W Sanders, Nancy Kedersha, Daniel S W Lee, Amy R Strom, Victoria Drake, Joshua A Riback, Dan Bracha, Jorine M Eeftens, Allana Iwanicki, Alicia Wang, Ming-Tzo Wei, Gena Whitney, Shawn M Lyons, Paul Anderson, William M Jacobs, Pavel Ivanov, and Clifford P Brangwynne. Competing Protein-RNA interaction networks control multiphase intracellular organization. *Cell*, 181(2):306–324.e28, April 2020.

Jenifer E Shattuck, Kacy R Paul, Sean M Cascarina, and Eric D Ross. The prion-like protein kinase sky1 is required for efficient stress granule disassembly. *Nat. Commun.*, 10(1):3614, August 2019.

Ujwal Sheth and Roy Parker. Decapping and decay of messenger RNA occur in cytoplasmic processing bodies. *Science*, May 2003.

Nobuyuki Shiina. Liquid- and solid-like RNA granules form through specific scaffold proteins and combine into biphasic granules. *J. Biol. Chem.*, 294(10):3532–3548, March 2019.

167

Tom Smith, Andreas Heger, and Ian Sudbery. UMI-tools: modeling sequencing errors in unique molecular identifiers to improve quantification accuracy. 27(3):491–499, 2017.

Eric J Solís, Jai P Pandey, Xu Zheng, Dexter X Jin, Piyush B Gupta, Edoardo M Airoldi, David Pincus, and Vladimir Denic. Defining the essential function of yeast hsf1 reveals a compact transcriptional program for maintaining eukaryotic proteostasis. 63(1):60–71, 2016.

Jorge Solis-Miranda, Monika Chodasiewicz, Aleksandra Skirycz, Alisdair R Fernie, Panagiotis N Moschou, Peter V Bozhkov, and Emilio Gutierrez-Beltran. Stress-related biomolecular condensates in plants. *Plant Cell*, 35(9):3187–3204, September 2023.

Syam Prakash Somasekharan, Fan Zhang, Neetu Saxena, Jia Ni Huang, I-Chih Kuo, Caitlin Low, Robert Bell, Hans Adomat, Nikolay Stoynov, Leonard Foster, Martin Gleave, and Poul H Sorensen. G3BP1-linked mRNA partitioning supports selective protein synthesis in response to oxidative stress. *Nucleic Acids Res.*, 48(12):6855–6873, July 2020.

Reed Sorenson and Julia Bailey-Serres. Selective mRNA sequestration by OLIGOURIDYLATE-BINDING PROTEIN 1 contributes to translational control during hypoxia in arabidopsis. *Proc. Natl. Acad. Sci. U. S. A.*, 111(6):2373–2378, February 2014.

Stan Development Team. RStan: the R interface to Stan, 2023.

Nadine Stöhr, Marcell Lederer, Claudia Reinke, Sylke Meyer, Mechthild Hatzfeld, Robert H Singer, and Stefan Hüttelmaier. ZBP1 regulates mRNA stability during cellular stress. *J. Cell Biol.*, 175(4):527–534, November 2006.

R V Storti, M P Scott, A Rich, and M L Pardue. Translational control of protein synthesis in response to heat shock in d. melanogaster cells. *Cell*, 22(3):825–834, December 1980.

Devin Tauber, Gabriel Tauber, Anthony Khong, Briana Van Treeck, Jerry Pelletier, and Roy Parker. Modulation of RNA condensation by the DEAD-Box protein eIF4A. *Cell*, 0 (0), January 2020a.

Devin Tauber, Gabriel Tauber, and Roy Parker. Mechanisms and regulation of RNA condensation in RNP granule formation. *Trends Biochem. Sci.*, May 2020b.

Catherine G Triandafillou, Christopher D Katanski, Aaron R Dinner, and D Allan Drummond. Transient intracellular acidification regulates the core transcriptional heat shock response. 9, 2020.

Nien-Pei Tsai and Li-Na Wei. RhoA/ROCK1 signaling regulates stress granule formation and apoptosis. *Cell. Signal.*, 22(4):668–675, April 2010.

Alex Charles Tuck and David Tollervey. A transcriptome-wide atlas of RNP composition reveals diverse classes of mRNAs and lncRNAs. *Cell*, 154(5):996–1009, August 2013.

Agnieszka Tudek, Paweł S Krawczyk, Seweryn Mroczek, Rafał Tomecki, Matti Turtola, Katarzyna Matylla-Kulińska, Torben Heick Jensen, and Andrzej Dziembowski. Global view on the metabolism of RNA poly(a) tails in yeast saccharomyces cerevisiae. 12(1): 4951, 2021.

R Martin Vabulas, Swasti Raychaudhuri, Manajit Hayer-Hartl, and F Ulrich Hartl. Protein folding in the cytoplasm and the heat shock response. *Cold Spring Harb. Perspect. Biol.*, 2(12):a004390, December 2010.

Briana Van Treeck and Roy Parker. Emerging roles for intermolecular RNA-RNA interactions in RNP assemblies. *Cell*, 174(4):791–802, August 2018.

Briana Van Treeck, David S W Protter, Tyler Matheny, Anthony Khong, Christopher D Link, and Roy Parker. RNA self-assembly contributes to stress granule formation and

defining the stress granule transcriptome. *Proc. Natl. Acad. Sci. U. S. A.*, page 201800038, February 2018.

Jacob Verghese, Jennifer Abrams, Yanyu Wang, and Kevin A Morano. Biology of the heat shock response and protein chaperones: budding yeast (saccharomyces cerevisiae) as a model system. *Microbiol. Mol. Biol. Rev.*, 76(2):115–158, June 2012.

C Vilela, C Velasco, M Ptushkina, and J E McCarthy. The eukaryotic mRNA decapping protein dcp1 interacts physically and functionally with the eIF4F translation initiation complex. 19(16):4372–4382, 2000.

Eneko Villanueva, Tom Smith, Mariavittoria Pizzinga, Mohamed Elzek, Rayner M L Queiroz, Robert F Harvey, Lisa M Breckels, Oliver M Crook, Mie Monti, Veronica Dezi, Anne E Willis, and Kathryn S Lilley. System-wide analysis of RNA and protein subcellular localization dynamics. 2023.

Edward W J Wallace, Jamie L Kear-Scott, Evgeny V Pilipenko, Michael H Schwartz, Pawel R Laskowski, Alexandra E Rojek, Christopher D Katanski, Joshua A Riback, Michael F Dion, Alexander M Franks, Edoardo M Airoldi, Tao Pan, Bogdan A Budnik, and D Allan Drummond. Reversible, specific, active aggregates of endogenous proteins assemble upon heat stress. *Cell*, 162(6):1286–1298, September 2015.

Robert W Walters, Denise Muhlrad, Jennifer Garcia, and Roy Parker. Differential effects of ydj1 and sis1 on hsp70-mediated clearance of stress granules in saccharomyces cerevisiae. 21(9):1660–1671, 2015.

H Wang, X Yan, H Aigner, A Bracher, N D Nguyen, W Y Hee, B M Long, G D Price, F U Hartl, and M Hayer-Hartl. Rubisco condensate formation by CcmM in β-carboxysome biogenesis. *Nature*, 566(7742):131–135, February 2019a.

Jinfan Wang, Alex G Johnson, Christopher P Lapointe, Junhong Choi, Arjun Prabhakar, Dong-Hua Chen, Alexey N Petrov, and Joseph D Puglisi. eIF5B gates the transition from translation initiation to elongation. 573(7775):605–608, 2019b.

Tim Weenink, Jelle van der Hilst, Robert M McKiernan, and Tom Ellis. Design of RNA hairpin modules that predictably tune translation in yeast. 3(1):ysy019, 2018.

David E Weinberg, Premal Shah, Stephen W Eichhorn, Jeffrey A Hussmann, Joshua B Plotkin, and David P Bartel. Improved Ribosome-Footprint and mRNA measurements provide insights into dynamics and regulation of yeast translation. *Cell Rep.*, 14(7):1787–1799, February 2016.

Joshua R Wheeler, Tyler Matheny, Saumya Jain, Robert Abrisch, and Roy Parker. Distinct stages in stress granule assembly and disassembly. *Elife*, 5, September 2016.

James P White, Ana Maria Cardenas, Wilfred E Marissen, and Richard E Lloyd. Inhibition of cytoplasmic mRNA stress granule formation by a viral proteinase. *Cell Host Microbe*, 2(5):295–305, November 2007.

Johannes H Wilbertz, Franka Voigt, Ivana Horvathova, Gregory Roth, Yinxiu Zhan, and Jeffrey A Chao. Single-Molecule imaging of mRNA localization and regulation during the integrated stress response. *Mol. Cell*, 73(5):946–958.e7, March 2019.

Jun Wu and Jnanankur Bag. Negative control of the Poly(A)-binding protein mRNA translation is mediated by the adenine-rich region of its 5'-untranslated region, 1998.

Xuhua Xia, Vivian MacKay, Xiaoquan Yao, Jianhua Wu, Fumihito Miura, Takashi Ito, and David R Morris. Translation initiation: a regulatory role for poly(a) tracts in front of the AUG codon in saccharomyces cerevisiae. *Genetics*, 189(2):469–478, October 2011.

Peiguo Yang, Cécile Mathieu, Regina-Maria Kolaitis, Peipei Zhang, James Messing, Ugur Yurtsever, Zemin Yang, Jinjun Wu, Yuxin Li, Qingfei Pan, Jiyang Yu, Erik W Martin, Tanja Mittag, Hong Joo Kim, and J Paul Taylor. G3BP1 is a tunable switch that triggers phase separation to assemble stress granules. *Cell*, 181(2):325–345.e28, April 2020.

Xiaoxue Yang, Yi Shen, Elena Garre, Xinxin Hao, Daniel Krumlinde, Marija Cvijović, Christina Arens, Thomas Nyström, Beidong Liu, and Per Sunnerhagen. Stress Granule-Defective mutants deregulate stress responsive transcripts. *PLoS Genet.*, 10(11):e1004763, November 2014.

Aisha Yesbolatova, Yuichiro Saito, Naomi Kitamoto, Hatsune Makino-Itou, Rieko Ajima, Risako Nakano, Hirofumi Nakaoka, Kosuke Fukui, Kanae Gamo, Yusuke Tominari, Haruki Takeuchi, Yumiko Saga, Ken-Ichiro Hayashi, and Masato T Kanemaki. The auxin-inducible degron 2 technology provides sharp degradation control in yeast, mammalian cells, and mice. 11(1):5701, 2020.

Haneul Yoo, Catherine Triandafillou, and D Allan Drummond. Cellular sensing by phase separation: Using the process, not just the products. *J. Biol. Chem.*, 294(18):7151–7159, May 2019.

Haneul Yoo, Jared A M Bard, Evgeny Pilipenko, and D Allan Drummond. Chaperones directly and efficiently disperse stress-triggered biomolecular condensates. May 2021.

Haneul Yoo, Jared A M Bard, Evgeny V Pilipenko, and D Allan Drummond. Chaperones directly and efficiently disperse stress-triggered biomolecular condensates. 82(4): 741–755.e11, 2022.

J H Yoon, E J Choi, and R Parker. Dcp2 phosphorylation by ste20 modulates stress granule assembly and mRNA decay in saccharomyces cerevisiae. 189(5):813–827, 2010.

Ji-Young Youn, Wade H Dunham, Seo Jung Hong, James D R Knight, Mikhail Bashkurov, Ginny I Chen, Halil Bagci, Bhavisha Rathod, Graham MacLeod, Simon W M Eng, Stéphane Angers, Quaid Morris, Marc Fabian, Jean-François Côté, and Anne-Claude Gingras. High-Density proximity mapping reveals the subcellular organization of mRNA-Associated granules and bodies. *Mol. Cell*, 69(3):517–532.e11, February 2018.

Peipei Zhang, Baochang Fan, Peiguo Yang, Jamshid Temirov, James Messing, Hong Joo Kim, and J Paul Taylor. Chronic optogenetic induction of stress granules is cytotoxic and reveals the evolution of ALS-FTD pathology. *Elife*, 8, March 2019.

Xu Zheng, Joanna Krakowiak, Nikit Patel, Ali Beyzavi, Jideofor Ezike, Ahmad S Khalil, and David Pincus. Dynamic control of hsf1 during heat shock by a chaperone switch and phosphorylation. 5, 2016.

Chuankai Zhou, Brian D Slaughter, Jay R Unruh, Fengli Guo, Zulin Yu, Kristen Mickey, Akshay Narkar, Rhonda Trimble Ross, Melainia McClain, and Rong Li. Organelle-Based aggregation and retention of damaged proteins in asymmetrically dividing cells. 159(3): 530–542, 2014.

Brian M Zid and Erin K O'Shea. Promoter sequences direct cytoplasmic localization and translation of mRNAs during starvation in yeast. *Nature*, 514(7520):117–121, October 2014.